The Dissertation Committee for Claudia Marino Certifies that this is the approved version of the following dissertation:

The role of Hsp60 in Amyloid β toxicity: Relevance to Alzheimer's disease

Committee:

Giulio Taglialatela, PhD Mentor, Chair

Mark Emmett, PhD

Rakez Kayed, PhD

Maria Adelaide Micci, PhD

Christopher Norris, PhD

Dean, Graduate School

The role of Hsp60 in Amyloid β toxicity: Relevance to Alzheimer's disease

by

Claudia Marino, M.S., Ph.D.

Dissertation

Presented to the Faculty of the Graduate School of

The University of Texas Medical Branch

in Partial Fulfillment

of the Requirements

for the Degree of

Doctor of Philosophy

The University of Texas Medical Branch
March, 2019

Dedication

To my wonderful mother, who will always be my inspiration for her hard work, her love

for medicine and her outstanding intelligence.

Acknowledgements

The role of Hsp60 in Amyloid β toxicity: Relevance to Alzheimer's disease

Publication No._____

Claudia Marino, PhD

The University of Texas Medical Branch, 2019

Supervisor: Giulio Taglialatela

Alzheimer's disease (AD) is a devastating neurodegenerative disorder leading to dementia, affecting millions of individuals worldwide. Currently, there are no successful disease-modifying therapies, due to the complexity of biochemical alterations and risk factors leading to AD. One of the earliest alterations leading to AD is the synaptotoxic effect of amyloid beta oligomers (Aβo). These oligomers are formed by the misfolding and subsequent aggregation of Aβ, a cleavage product of the amyloid precursor protein (APP). Furthermore, compelling evidence suggests that an age-related failure of the protein quality control machinery could also contribute to the onset of AD, thus supporting the hypothesis that the main risk factor of late-onset AD is aging. Chaperones are critical components of the protein quality control machinery known to target misfolding proteins and to preserve cellular homeostasis. Here, we focused on the mitochondrial chaperone Hsp60, which is known to protect mitochondria from misfolded proteins. Evidence suggests that Hsp60 directly interacts with APP/Aβ *in vitro*, and this interaction could contribute to protecting mitochondria from Aβ-induced damage. However, weather Hsp60 interacts with Aβo thus preventing the downstream synaptic toxicity is still unknown. In the current work, we aimed to characterize the effect of Hsp60 on Aβ aggregation and if Hsp60- Aβo interaction could reduce the downstream toxic effect of Aβo at the synapses. Using spectroscopy, atomic force microscopy and chromatographic techniques we characterized the effect of Hsp60 on the aggregation pathway of Aβ. We further tested the effect of Hsp60 on naturally secreted Aβo *in vitro* using immunocytochemistry, western blotting, and ELISA. As Aβo are known to bind to the synapses, impair synaptic plasticity and cause synaptic toxicity, we also tested if the interaction between these two proteins contributed to a change of Aβo conformation, thus resulting in a change of downstream toxicity. Overall, our findings support that Hsp60 effectively targets Aβ, thus resulting in protection of Aβo-derived toxicity and propose Hsp60 as an attractive candidate for future therapies aiming in targeting Aβo toxicity.

TABLE OF CONTENTS

List of Tables

List of Figures

List of Abbreviations

7PA2	CHO overexpressing APPswe protein
7PA2/H60	7PA2 overexpressing Hsp60
a.a.	amino acid
a.u.	arbitrary units
Aβ	amyloid beta
aCSF	artificial cerebral spinal fluid
AD	Alzheimer's disease
AFM	atomic force microscopy
AIACUC	Institutional Animal Care and Use Committee
APP	amyloid precursor protein
APOE	apolipoprotein e
BACE1	beta-secretase 1
Bis-ANS	4,4'-dianilino-1,1'-binaphtyl-5,5'-disulfonic acid
CA	*cornu ammonis*
CD	circular Dichroism
CHO	Chinese hamster ovary
CM	conditioned Medium
CSF	cerebral spinal fluid
CT	control
DAPI	4′,6-diamidino-2-phenylindole
DMEM	Dulbecco's modified Eagle Medium
EDTA	ethylenediaminetetraacetic acid
fAD	familial Alzheimer's disease

FBS	fetal bovine serum
fEPSP	field excitatory post-synaptic potential
FV	fiber volley
HBK	HEPES-buffered Krebs-like
HEPES	4-(2-hydroxyethyl)-1-piperazineethanesulfonic acid
HFIP	hexafluoro-2-propanol
HFS	high frequency stimulation
HPLC	high performance liquid chromatography
H	hour or hours
Hsp60	heat shock protein 60
IACUC	Institutional Animal Care and Use Committee
ICC	immunocytochemistry
IDRs	intrinsically disordered regions
IP	immuno-precipitation
I/O	input/output
kDa	Kilo Dalton
LDH	lactate Dehydrogenase
LTP	long-term potentiation
MW	molecular weight
Min.	minutes
MS	mass spectroscopy
NDAN	Non-Demented with Alzheimer's Neuropathology
NFT	neurofibrillary tangles
NMDA	N-methyl-D-aspartate
NMDG	N-methyl-D-glucamine

MRI	magnetic resonance imaging
O	oligomer
PBS	phosphate buffer saline
PET	positron emission tomography
PPF	paired-pulse facilitation
PP50	paired-pulse facilitation
PSD95	post-synaptic density 95
p/s	penicillin/streptomycin
rcf	relative centrifugal force
rpm	revolution per minute
R.T.	retention time
sAD	sporadic Alzheimer's disease
SEC	size exclusion chromatography
TBS-T	Tris buffered saline with Tween 20
ThT	Thioflavin T
USDA	United States Department of Agriculture
WB	western blotting

CHAPTER I. INTRODUCTION

HISTORY AND PATHOPHYSIOLOGY OF ALZHEIMER'S DISEASE

Alzheimer's disease (AD) is a devastating neurodegenerative disorder leading to dementia that was first discovered in the early 1900's by Dr. Aloysius Alzheimer and collaborators [1]. The diagnosis of this first case of an "unusual case of psychiatric illness" in 1906 began a century-long research efforts aiming to elucidate the mechanisms of AD pathogenesis and to design successful disease-modifying therapies [2]. Despite this effort, any such therapies are still lacking [3,4].

The Alzheimer's association reported that around 5.8 million Americans are affected by AD in 2019, with costs nearing 234 billion dollars per year [5,6]. In the USA alone, the number of new cases of AD is projected to increase by 2-fold every year, with 16 million people affected by 2050. This makes AD the most common form of dementia worldwide [6–9]. As a consequence, the need for a resolving cure is of the utmost urgency and it is crucial to characterize the causative biological cascades that allow for the design of successful disease-modifying therapies.

The lesions that characterize AD pathology are intracellular neurofibrillary tangles (NFT) and extracellular amyloid plaques [3,10]. NFT are large intracellular aggregates formed by the accumulation of misfolded and hyperphosphorylated tau protein, a protein of the MAP (microtubule-associated protein) family [11]. Amyloid plaques are large extracellular deposits mainly formed by insoluble fibers of amyloid beta peptides (Aβ) [10]. Aβ peptides are 39-43 residue sequences formed by the cleavage of the amyloid precursor protein (APP) [12]. Both NFT and amyloid plaques begin accumulating years (even decades) before the clinical manifestation of the disease along with key biochemical alterations [13,14].

Recently, it has been revealed that amyloid plaques and NFT lesions correlate only partially to the onset of the disease, as further demonstrated by the cohort of individuals referred to as "non-demented with Alzheimer's neuropathology" (NDAN) [15–19]. These individuals, while they are histopathologically indistinguishable from AD patients, cognitive abilities are entirely preserved. One possible explanation of this phenomenon is that although levels in Aβ are increased in both AD and NDAN groups, the binding of Aβ to post-synaptic termini is dramatically decreased in NDAN compared to AD individuals [16]. This critical discovery suggests the presence of specific mechanisms of resilience in NDAN individuals that protects against AD pathology. This finding also suggests the existence of complex pathways governing the progression of AD pathology [15,18].

As depicted in Figure 1.1, the biomolecular alterations associated with AD begin accumulating long before any clinical symptom occurs. One of the earliest alterations is the accumulation of Aβ pathology, which precedes the accumulation of tau in the cerebral spinal fluid (CSF) (Figure 1.1). Both alterations occur during a pre-symptomatic stage of the disease and therefore before clinical symptoms become manifest [8].
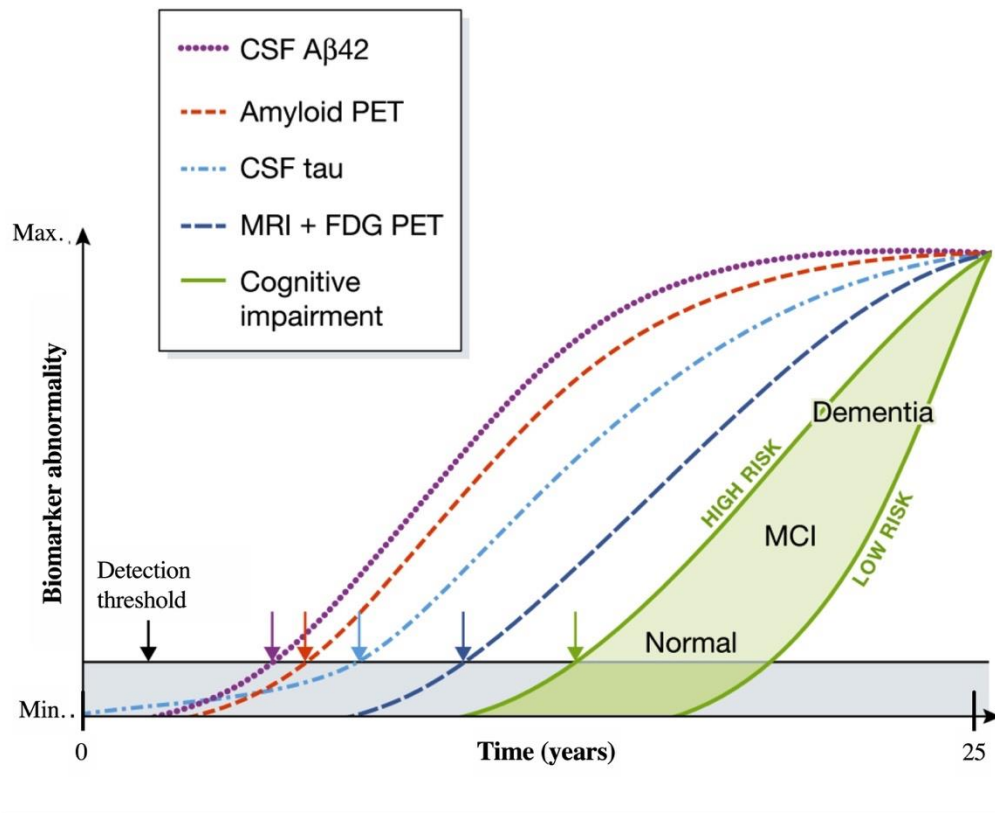
Figure 1.1 Alzheimer's disease progression.

Diagram representing the increase of AD-related biomarkers (biomarker abnormality) over time, expressed in years, during the disease progression from normal cognition to dementia. Data suggesting that up to 25 years before dementia can be diagnosed, the detection of Aβ in the CSF (purple line) or by PET (positron emission tomography) imaging (red line) precedes the detection of tau in the CSF (light blue line), changes in MRI (magnetic resonance imaging) and FDG PET (fluorodeoxyglucose PET) profile (blue line) and cognitive impairment (green line). Adapted from Selkoe & Hardy, 2016 [8].

At later stages of its progression, AD is macroscopically characterized by massive cortex degeneration, affecting the limbic and paralimbic regions, and the frontal-parietal network, along with enlargement of ventricles (Figure1.2) [3,20].
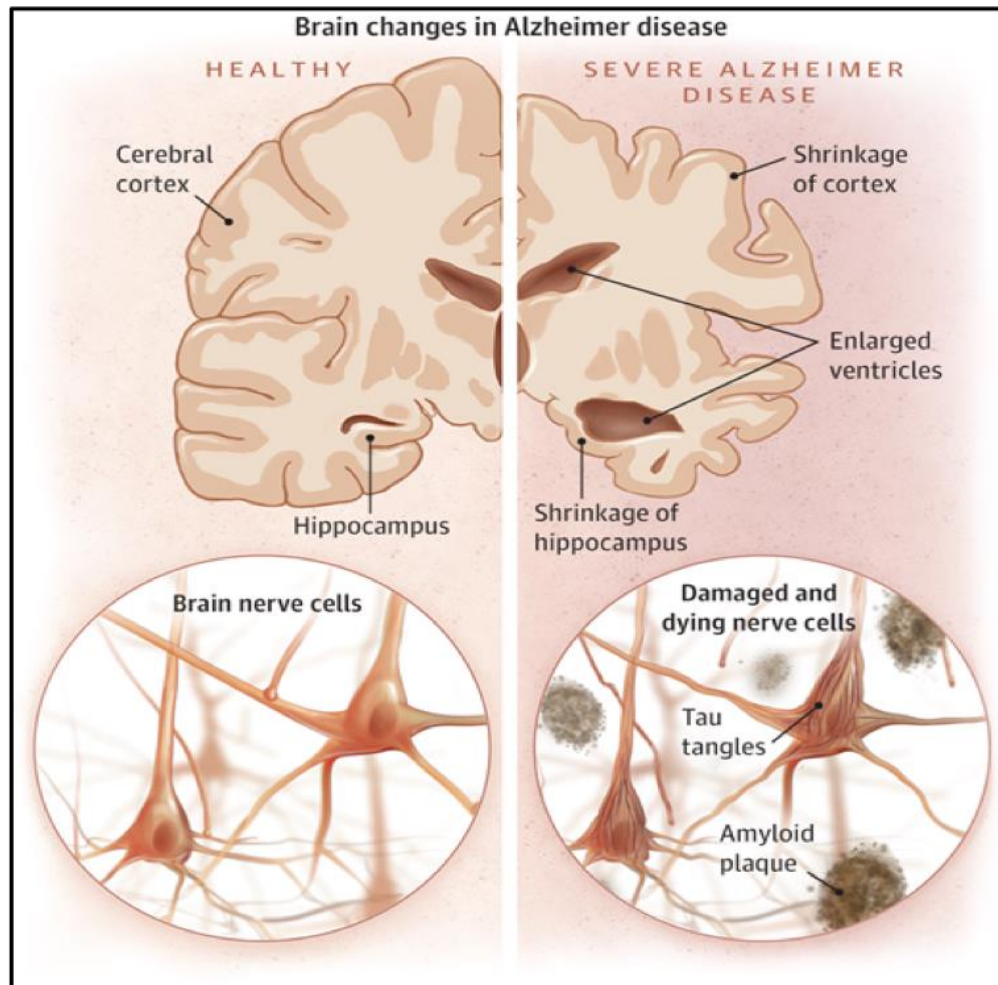
Figure 1.2. Brain changes in AD compared to healthy individuals.

Pictogram of the gross (top) and microscopic (bottom of the figure) changes in AD brains (right panel) compared to a healthy brain (left panel), showing both cortical changes (shrinkage of cortex, enlarged ventricles, shrinkage of hippocampus) and accumulation of Aβ (amyloid plaque) and tau deposits (tau tangles), along with damages and dying nerve cells. Adapted from Musiek 2015 [21].

Considering the most recent Diagnostic and Statistical Manual of Mental Disorders (DSM-IV), a positive diagnosis of Alzheimer's disease is confirmed by the presence of cortical lesions and a definite impairment of short-term memory, along with at least one of the following symptoms: aphasia, apraxia, agnosia, or executive dysfunction. Further, lesions should not be related to any other medical conditions [22]. Despite progress in refining the diagnostic criteria, not only we have not found therapies to reverse AD

symptoms, we have not developed reliable ways to either abrogate or stop progression of the symptoms once they start [23–25].

AD is also characterized by high comorbidity with several other age-related diseases such as cardiovascular diseases, diabetes and age-related changes of the immune system, thus making AD a complex pathology [26–31]. It cannot be excluded that the onset of AD is triggered by a combination of biomolecular alterations, such as aging, protein misfolding, the impairment of protein quality control machinery and oxidative stress, along with several other factors [21,32].

An intriguing hypothesis is that Aβ is responsible for a chain reaction that triggers aberrant protein aggregation, thus overloading and impairing the "protein quality control machinery", which is already generally impaired as age progresses [3,33]. This phenomenon could precede neuronal dysfunction and subsequent neuronal death.

Consequently, understanding the biological cascades responsible for the onset of AD is crucial for the design of successful therapies, and it will contribute to reducing the dramatic impact of Alzheimer's disease to the society [1,34].

CLASSIFICATION OF AD PATHOLOGIES

AD is classified in two main groups: familial and sporadic AD. Familial AD (fAD) is mainly caused by genetic factors and constitutes about 2-4 % of AD cases [20,35]. Interestingly, all mutations associated with the disease are related to the biological cascade controlling either the biosynthesis or the processing of APP [6,36,37]. These include mutations of the APP gene or genes encoding enzymes involved in APP processing, such as presenilin1 and presenilin2. Trisomy 21, the underlying cause of Down syndrome, is another genetic factor contributing to fAD (although, technically not following a frank "familial" recurrence pattern) pathology due to the location of the APP gene on

chromosome 21 [38,39]. Altogether these findings suggest a pivotal role of the APP/Aβ cascade in the pathogenesis of AD pathology [8,40–42].

In contrast to fAD, factors responsible for sporadic AD (sAD) are complex and heterogeneous. The main genetic risk factor correlating with sAD is the presence of the ApoE ε4 gene variant [37]. Recent reports showed that there are other possible genetic contributors to sAD, such as the TREM2, ABCA7, ADAMTS4 and ADAM10 genes. The role of genetic inheritance in sAD is not fully understood [43], and compelling evidence supports the major role of non-genetic factors in the disease onset [44,45].

RISK FACTORS

fAD is mainly triggered by genetic factors, whereas sAD is mostly associated with non-genetic risk factors, with the main genetic risk factor for sAD being the presence of ApoE ε4 allele [1].

Risk factors leading to the onset of fAD are mainly mutations involving APP or enzymes controlling the processing of APP (presenilin1 or 2, BACE1, BACE2 and nicastrin genes). Because APP is located on chromosome 21, individuals with trisomy 21 are at increased risk for AD, as the presence of an extra copy might lead to an increase of APP production and subsequent Aβ accumulation [39]. Subjects affected by Down syndrome usually present significant accumulation of Aβ deposits by the age of 40 [46]. Conversely, several risk factors that are biological, social or environmental are known to contribute to the onset of sAD. Examples of non-genetic risk factors linked to sAD are old age, cardiovascular disorders, type II diabetes, obesity, hypertension, chronic sleep deprivation, Lewy bodies disease, vasculopathies, traumatic brain injury, and many others [47–51].

Aging has a pivotal role in the pathogenesis of sAD [52]. During aging there are several biochemical changes such as oxidative stress, increased inflammation,

mitochondrial dysfunction, and impairment of the ubiquitin-proteasome system and chaperone machinery that facilitates protein misfolding [53,54].

Recent genome-wide association analysis revealed the presence of at least 20 different genes, whose alteration might contribute to a non-Mendelian inheritance of sAD in about 60-70% of AD cases [36,43]. One possible other factor contributing to the onset of sAD is an increase of DNA methylation. This has been suggested as an early alteration leading to AD pathogenesis [36].

The understanding of the correlation between risk factors and the onset of AD is essential, as it can help to predict possible predisposition to contract the disease or it could contribute to characterizing novel biomarkers [47].

THE BIOCHEMISTRY OF THE AMYLOID BETA PEPTIDE

AD has also been classified as a "misfolding disease" [55–57]. The main lesions characterizing AD, amyloid plaques and neurofibrillary tangles, are the product of the misfolding and aggregation of Aβ and tau protein respectively [10]. Both proteins from a naïve conformation can be induced into an "aggregation-prone" conformation. This can trigger an aggregation cascade and precipitation of insoluble aggregates [58–60].

FAD can be caused either by overexpression, mutations of the APP gene or by mutations of genes encoding for some of the enzymes involved in APP processing. There is consensus that Aβ may play a key role in the early pathological mechanisms of the disease, although its contribution to later symptomatic stages of AD dominated by tau toxicity remains controversial [8].

Aβ peptides are 36 to 43 amino acids (a. a.) long peptides that are produced by the cleavage of the APP, an ubiquitous type-I oriented transmembrane protein constituted by 695 residues [61–63]. Aβ peptides are released as a result of a two-step cleavage of the APP protein, operated by β- and γ-secretases. This latter mechanism of "pro-

amyloidogenic pathway" is opposite to a "non-amyloidogenic pathway" of APP processing operated by α- and γ-secretase, as summarized by the schematic in Figure 1.3.

In the pro-amyloidogenic pathway (Figure 1.3.B), APP is first cleaved by the β-secretase complex (BACE1) into C99 and APPsβ fragments and releases Aβ peptide upon γ-secretase cleavage in the extracellular fluids [26,64]. The accumulation of Aβ is facilitated by an alteration of the balance between amyloid production and amyloid clearance, thus leading to the accumulation of neurotoxic species [65]. The non-amyloidogenic processing of APP is characterized by a cascade that does not produce Aβ peptides, as the cleavage of APP by α-secretase is in the middle of the Aβ sequence (Figure 1.3.A). Notably, the first cleavage by α-secretase generates APPsα and C83 fragments. C83 fragment is further processed by γ-secretase into p3 and C59 fragments that are not able to aggregate [65].
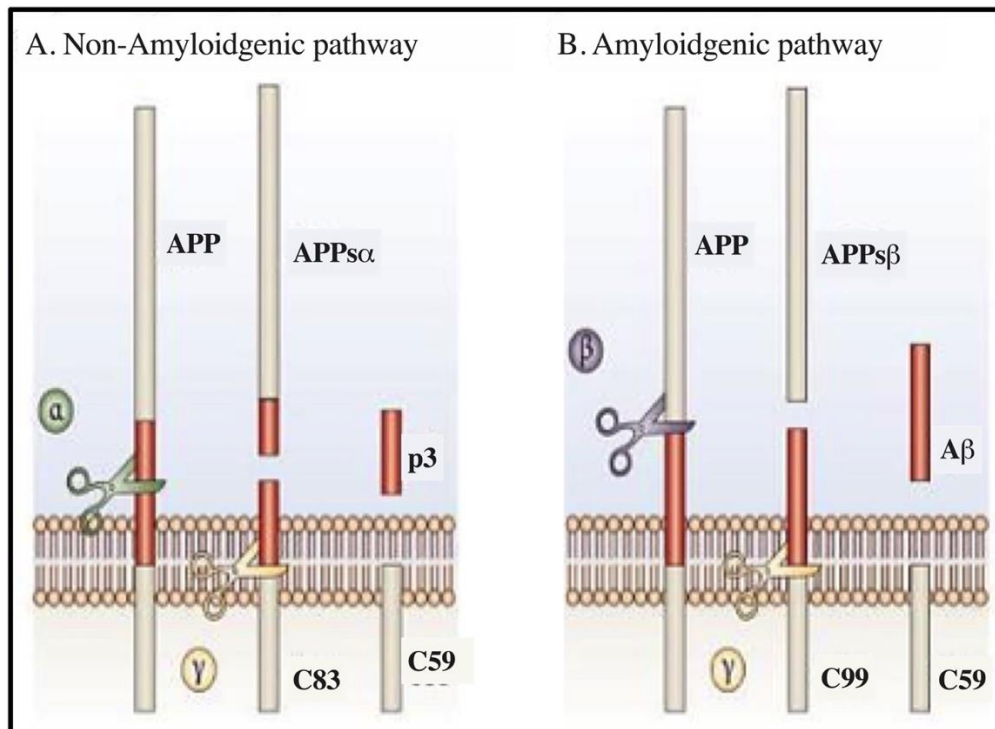
Figure 1.3. The amyloid cascade.

A. Diagram representing the non-amyloidogenic pathway of the transmembrane protein APP controlled by α- and γ- secretases, which produces APP fragments not prone to

25

aggregate: C83, C59 and p3. B. Diagram representing the amyloidogenic pathway of APP controlled by β- and γ- secretases, which lead to the extracellular release of the Aβ peptide, along with C99 and C59 fragments [26].

Aβ peptide is characterized by an amorphous and highly disorganized structure that makes the peptide prone to aggregate [66,67]. The most abundant forms of human Aβ are Aβ$_{1-40}$ and Aβ$_{1-42}$. Particularly, Aβ$_{1-42}$ is the most aggressive form for its increased pro-amyloidogenic propensity caused by the two a. a. isoleucine and alanine at its C-terminus [68].

Despite Aβ$_{1-40}$ is the most abundant form of Aβ in the brain, it has been reported as a less toxic peptide [69]. For both peptides, the aggregation kinetic is characterized by a slow nucleation where small oligomers are formed (referred to as seeds). This constitutes the rate limiting factor of the whole reaction, and is followed by a fast elongation step, leading to the formation of well-organized fibers [42]. Figure 1.4 summarizes the steps of Aβ aggregation from a monomeric to a mature fibril structure.
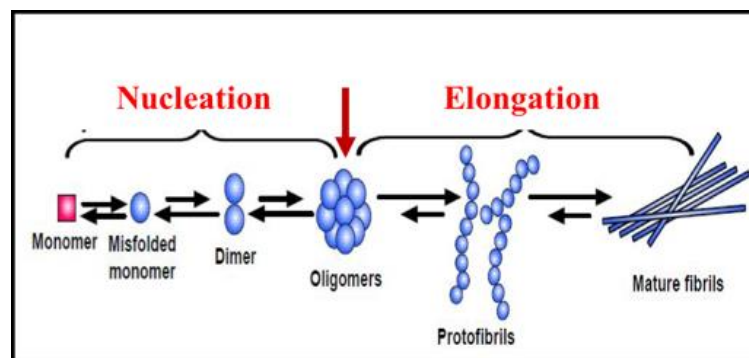
Figure 1.4. Cascade of Aβ aggregation.

Schematic representation of the aggregation kinetic of Aβ peptide. Monomeric Aβ, once misfolded, initiates a nucleation phase, leading to the formation of toxic oligomeric aggregates indicated by the red arrow. Oligomers further aggregate into protofibrils and mature fibrils during the elongation phase. Adapted from Kumar S. and Walter J., 2011 [70].

Aβ aggregation is in actuality far more complex than the linear cascade described in Figure 1.4. The amorphic structure of Aβ, due to a high abundance of intrinsically disordered regions, triggers several alternative pathways and leads to the formation of conformationally different oligomers and aggregates [58,71].

Compelling evidence suggests that AD pathology correlates mainly with oligomeric intermediates of Aβ and tau proteins, as demonstrated *in vitro* and *in vivo* [72–75]. Extensive research has shown that oligomer toxicity is driven by their common conformation, even though the primary structure characterizing these oligomers is of different peptides [76]. The high correlation between the pathogenesis of several neurodegenerative diseases and the release of oligomers, suggests a pivotal role of oligomeric structures in triggering the onset of these disorders [33,77].

Despite decades of research trying to understand what triggers the Aβ cascade, and how to block Aβ-induced toxicity, the design of effective disease-modifying therapies targeting this cascade has been unsuccessful. The instability of oligomeric forms once released during the aggregation kinetic may explain the lack of progress in designing effective approaches against these forms [78]. However, recent findings suggest that not all oligomeric species of Aβ are neurotoxic. It has been proposed that Aβ oligomers under certain conformations at specific doses may even be necessary to regulate synaptic physiology [79–81]. It is therefore crucial to design novel approaches that can specifically target the cascades that lead to the formation of toxic oligomeric species, as explored in the present dissertation.

BEYOND AMYLOID β PEPTIDE NEUROTOXICITY

Because protein misfolding is its main pathological hallmark, AD has been often compared to prion diseases and defined as a "prion-like" disorder, even though, differently from prion diseases, AD is not characterized by infectious features [52,82]. Prions (or

prion-related proteins, PrPs) are small peptides characterized by a high degree of misfolding, thus resulting into uncontrolled aggregation. PrPs misfolding leads to the formation of conformationally different intermediate structures and subsequent deposition of β-sheet rich aggregates [83,84]. Both Aβ and tau proteins share the common mechanism of aggregation that characterize PrPs [85,86].

Even though Aβ formation is an early alteration leading to AD pathology, some studies have suggested that Aβ triggers the disease but does not hasten its progression, and that it is not the sole factor leading to the onset of neurodegeneration [21].

Another critical aspect characterizing both fAD and sAD is mitochondria dysfunction and alteration of glucose metabolism which seem to contribute very early during the progression of the disease [48]. A positive correlation has been shown between the ApoEε4 gene variant and alteration in glucose metabolism in the brains of AD individuals and an increase of oxidative stress leads to cytochrome C release from mitochondria, along with increased alteration in mitochondrial DNA and accumulation of reactive oxygen species (ROS) [87]. A high accumulation of Aβ in mitochondria has been observed in AD individuals, which may result in the alteration of the electron transport chain and therefore dishomeostasis of mitochondrial function and energy metabolism. Indeed, the latter finding suggests a strong link between Aβ toxicity and mitochondrial dysfunction [48,88,89].

Another critical lesion leading to AD pathogenesis is tau pathology. In fact, even though tau hyperphosphorylation and oligomerization is not unique to AD, it is the alteration which best correlates with the synaptic dysfunction and memory loss observed in AD [90,91].

Tau protein is the most abundant microtubule-associated protein and has a physiological role in stabilizing the microtubules of axons [92–94]. In the human brain, tau is present in six different isoforms due to alternative splicing and is highly concentrated in axons [34,95]. As tau protein becomes dysfunctional by aberrant hyperphosphorylation,

tau misfolding and subsequent oligomerization become responsible for the spreading of the toxic species, resulting eventually in neuronal loss [96–98]. Compelling evidence supports the hypothesis that Aβ oligomers have an up-stream role in triggering tau pathology [99,100] and that both Aβ and tau might lead to AD pathology through a converging mechanism [101,102].

Overall, these considerations strongly support the concept that AD is triggered by a complex network of factors that altogether constitute a dishomeostatic circuitry ultimately leading to the symptomatic phase of the disorder. A schematic representation of the possible pathways involved in AD onset and how risk factors might induce amyloid formation, tau propagation, and neurodegeneration is summarized in Figure 1.5.
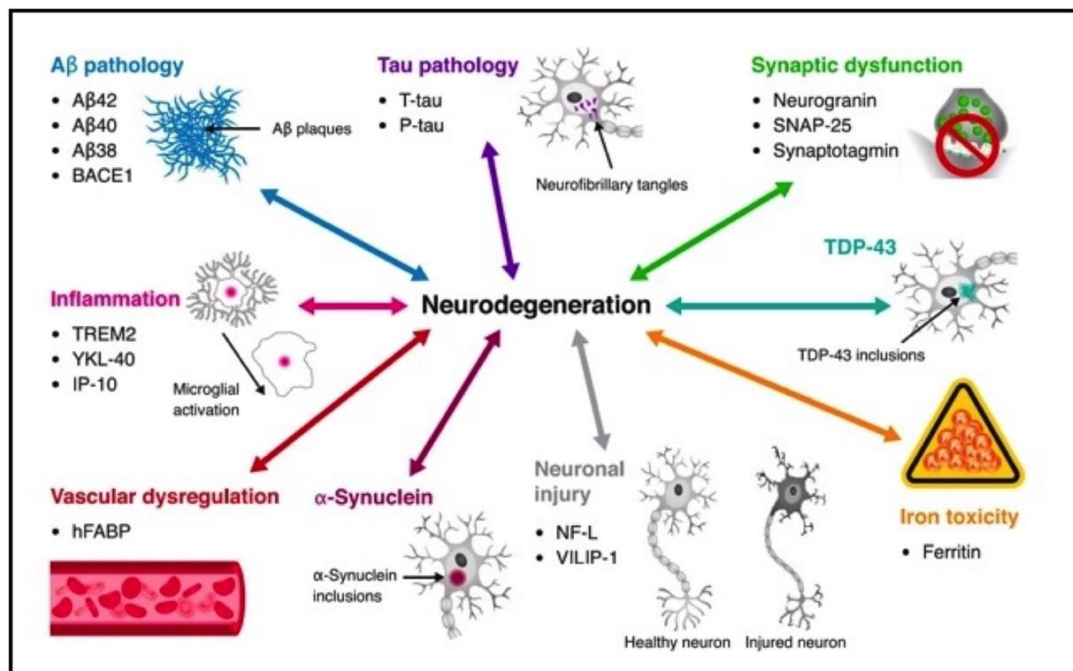
Figure 1.5.The complex biochemical cascade leading to AD

Schematic representation of the complex cascade leading to neurodegeneration in AD reporting that along with Aβ and Tau pathology, there is the contribute to neurodegeneration of inflammation, vascular dysregulation, α-synuclein, neuronal injury, iron toxicity, TDP-43 dysregulation, and synaptic dysfunction. Adapted from Molinuevo et al., 2018 [34].

Currently, there are only two classes of FDA-approved drugs for AD, comprised of only 4 drugs being still manufactured, along with only few additional compounds approved as adjuvants [22]. However, none of these therapeutic approaches is a "disease-modifying" therapy. One class of approved compounds are cholinesterase inhibitors (donepezil, galantamine, and rivastigmine). The mechanism of action of these compounds is to increase acetylcholine (ACh) levels through the inhibition of the cholinesterase enzyme. Inhibition of this enzyme responsible for the degradation of ACh, indirectly increases the availability and duration of this neurotransmitter, thus sustaining central cholinergic function. The use of this class of drugs is recommended mainly during the initial stages of the disease, but can also be prescribed for moderate to severe AD either alone at higher doses, or in combination with other drugs [103]. The mechanism of inhibition is either reversible (donepezil and galantamine) or pseudo-irreversible (rivastigmine).

The other FDA-approved drug for AD is an N-methyl-D-aspartate (NMDA) receptor inhibitor, memantine, which is recommended for those cases with moderate to advanced pathology [22]. Memantine prevents the aberrant activation of the receptor by glutamate via binding to the NMDA receptor at the Mg^{2+} binding site only under pathological conditions, without affecting its physiological function [104,105]. The mechanism of action leading to memantine's beneficial effect for the treatment of AD is not apparent; and could involve decreasing of overall glutamate excitotoxicity reported in AD due to synaptic accumulation of calcium induced by an increased activity of the NMDA receptors at the glutamatergic synapses, along with the synergistic antagonism of 5-HT_3 serotonin receptors [22,106].

The use of other drugs as adjuvants, i.e., COX inhibitors or vitamins (vitamin E or ascorbic acid), has been suggested to protect against the increase in neuro-inflammation that has been observed during AD.

As AD is defined by a very slow progression, an attractive strategy could be secondary prevention. The increased interest in designing specific antibodies or probes able to bind either Aβ or tau proteins seems a very promising strategy toward early targeting of the disease. Examples of these specific antibodies against Aβ are solanezumab, gantenerumab, and crenezumab. Other approaches tested have aimed to target the enzymes involved in APP processing (γ-secretase and BACE1). All clinical trials aiming to reverse AD pathology so far have failed either in phase II or phase III [107]. A possible explanation could be related to the difficulties of trying to deliver drugs during a stage of the disease where they can be most effective [108].

Collectively the above observations further support the notion of AD being a multi-factorial disorder with high level of comorbidity with other disorders, thus making harder to design therapies and possibly explaining the constant failure of previous therapeutic approach tested.

Consequently, there is an urgent need for a clearer understanding of the biochemical cascades leading to AD and how this new knowledge would lead to the design of effective disease-modifying therapies. Both these foundation concepts as they apply to the complex area of cellular chaperons (see below) drive my work as reported in the present dissertation.

THE COMPLEX ROLE OF CHAPERONES IN NEURODEGENERATIVE DISEASES

Compelling evidence suggests a contribution to AD pathogenesis of an age-related failure of the protein quality control machinery, thus supporting the notion that the main risk factor of late onset AD is aging [32,109]. One important component of the protein quality control machinery is the family of chaperones [110].

Chaperones are a class of highly conserved proteins, ubiquitously expressed in both prokaryotes and eukaryotes. These proteins have a critical role in assisting the correct assembly of other newly synthesized proteins or in directing unfunctional proteins to the

31

degradation pathway [111], thus contributing to the maintenance of proper cellular homeostasis [110,112].

Chaperones can be classified according to their molecular weight (MW), as indicated in Table 1 [113]. Chaperones can be divided into super-heavy (MW higher than 200 kDa), heavy (MW between 100-199 kDa), Hsp90s (MW between 81-99 kDa), chaperones (MW between 65-80 kDa), chaperonins (MW between 55-64 kDa), Hsp40 (MW between 35-54 kDa), small Hsps (MW less than 34 kDa) and other (various MW).

Table 1. Classification of chaperones by MW*[113]*.

Name	Alternative name(s) and/or example(s)	Molecular weight (kDa)
Superheavy	Sacsin	≥ 200
Heavy	High MW, Hsp100	100-199
Hsp90	HSP86, HSP89A, HSP90A, HSP90N, others	81-99
Hsp70	Chaperones, DnaK	65-80
Hsp60	Chaperonins (group I and II), Cpn60 and CCT	55-64
Hsp40	DnaJ	35-54
Small Hsp	sHsp, alpha-crystallins, Hsp10	≤ 34
Other	Proteases, isomerases, AAA+ proteins, α-hemoglobin-stabilizing protein	Various

The focus of this dissertation being Hsp60 (Heat shock protein 60 or HspD1), particular attention is given to the class of "chaperonins".

Structurally, chaperonins are characterized by a "basket-like" oligomeric structure formed by 7-9 units. This complex structure allows the mechanisms of protein folding of native peptides, by offering a suitable and insulated environment for proper folding of native proteins. Chaperonins play a pivotal role in assisting the folding of other proteins

even though they do not take part in the final structure of the protein itself [114]. This mechanism of folding is characterized by an initial interaction with the substrate, followed by internalization, refolding and release of the substrate. The chaperone-substrate interaction is usually ATP-dependent [115,116], as will be described more in detail in the following chapter section.

As chaperonins are a large group of chaperones with different properties, this class is further divided into two sub-classes: group I and group II. Group I chaperonins includes bacterial GroEL and eukaryotic Hsp60; group II chaperonins are thermosome expressed in Archaea or CCT and TRiC chaperonins found in the cytosol of eukaryotes [117].

THE STRUCTURE-ACTIVITY RELATIONSHIP OF CHAPERONINS

Chaperonins are crucial for preventing protein aggregation by ensuring proper correct protein folding [111,118,119]. The general mechanism of action is based on their ability to offer a hydrophobic chamber in which a substrate can access to and refold in the absence of a crowded environment, which characterizes the cytosolic compartment. It has also been observed that chaperonins can interact with proteins that are larger than the "folding cavity" and prevent their aggregation, thus suggesting alternative mechanisms of action [116,120,121]. Chaperones' ability to interact with their substrate is facilitated by the presence of intrinsically disordered regions (IDRs) in the chaperone structure [122,123]. These regions are characterized by extended molecular configuration, poor or absent secondary structure and the absence of a defined tertiary structure and therefore are characterized by high flexibility [124–126]. These regions constitute the active site of the chaperone that allows the interaction with their substrate, thus allowing the assembly and the ability to modify the structure of both substrate and other proteins [127,128].

The general structure of class I chaperonins can be summarized using GroEL as a representative model. In detail, the oligomer-forming unit has a secondary structure that is

characterized by three main domains: apical, intermediate and equatorial. The apical domain is essential for the formation of the pore to the folding cavity. The intermediate domain contributes to the overall flexibility of the structure and provides a connecting bridge between the other two domains. The equatorial domain is involved in interactions both within and between rings [129,130]. In their active configuration, class I chaperonins are organized in a double ring complex, which is constituted by the assembly of two homo-heptameric oligomers. This three-dimensional conformation allows the formation of large inner hydrophobic cavity about 45 Å in diameter, the "folding chamber". This cavity becomes even larger when the chaperone is in its active state and bound to ATP and the co-chaperone GroES, which forms the lid of the folding chamber [131]. The mechanism of action of the chaperone is allowed by the positive cooperativity within rings and the negative cooperativity between rings. Both processes are ATP-dependent and require a mechanism of cyclic conformational changes [117].

The mechanism of action of class I chaperonins is also described using as a model the well-studied GroEL-GroES cycle [132]. According to this model, GroEL assembles in a double-ring tetradecameric oligomer and interacts with GroES or its substrates at the apical domain [133,134]. The proper folding of the substrate occurs because of a series of conformational changes of the chaperone complex. As summarized in Figure 1.6, GroEL facilitates the proper folding of the substrate once assembled in an oligomeric complex and is bound to 7 ATP molecules at the equatorial domain and GroES at the apical domain. After the formation of this complex, the substrate can enter the chaperone cavity, which is enlarged by conformational changes of the heteromeric complex. The release of the newly folded substrate occurs upon ATP hydrolysis and ADP release. Overall, this mechanism has been referred to as the model of an "Anfisen cage" [135]. ATP binding is important to trigger the cascade that leads to the complex formation with GroES and to the internalization of the protein that needs to be folded.

ATP binding is also involved in the activation of the second ring of the chaperone which triggers a new process of folding. ATP hydrolysis is important to facilitate the removal of GroES and the release of the newly folded protein [136].
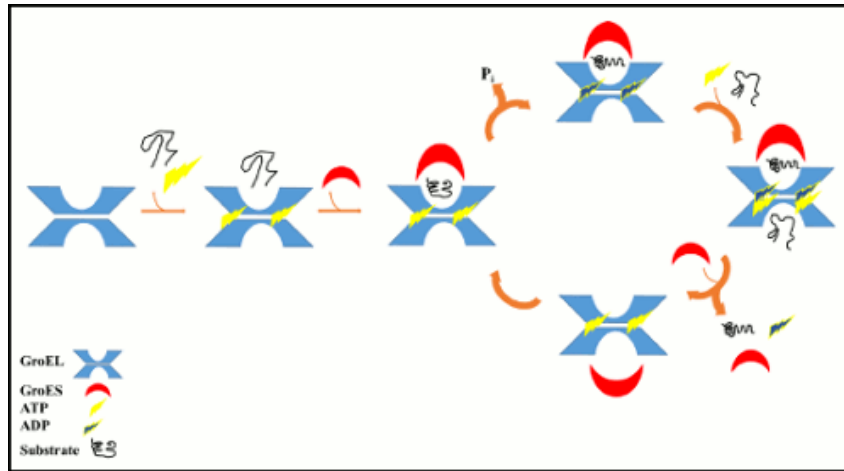
Figure 1.6. GroEL/Hsp60 folding cycle.

Diagram showing the mechanism of refolding of GroEL, the bacterial homologue of Hsp60. The chaperone interacts with a specific substrate in presence of ATP and the co-chaperon GroES. The refolding of the substrate occurs in the folding chamber organized by the chaperone cavity and the binding of the co-chaperone. As the substrate and ADP are released, the chaperone can start a new cycle in the second chamber. Adapted from Skjærven et al., 2015 [117].

Human Hsp60 is a mitochondrial chaperone that is produced by the nuclear Hsp60 gene as a longer inactive form. Human Hsp60, despite the homology with the bacterial form, is structurally different, as it is organized by either 7 or 14 units which form either a single ring (heptameric conformation) or a double ring (tetradecamer) [137,138]. The 26 amino acids long sequence constituting the N-terminus of Hsp60 is referred to as "leader sequence" that is important for mitochondria import. The mechanism of import of the chaperone is highly organized and requires the presence of other chaperones in the mitochondria matrix, along with a finely regulated membrane potential. At the mitochondrial membrane, Hsp60 is cleaved and the process of oligomerization leading to

the active form is ATP-dependent and assisted by other pre-existing Hsp60 oligomers [139].

The shorter and active form of Hsp60 is mainly found into the mitochondria, even though the action of Hsp60 has also been observed in the cytosol as pro-apoptotic mediation through the interaction with the pro-caspase 3 [139].

Other functions of chaperonins are to control and minimize cellular stress due to environmental stress, such as increased temperature, pH change or other stressors. Chaperonins are also regulators of homeostatic functions, such as apoptosis, control of oxidative stress cascade, cooperation with the ubiquitin-proteasome degradation machinery [140].

Group II chaperones are characterized by a higher degree of complexity as compared to class I. In fact, despite the similar organization of oligomer-forming unit in domains, differently from the group I, they form complexes of 8 or 9 monomers, and the oligomeric structure is mainly heteromeric, even though the interactions within and between subunits are not fully understood. Additionally, the mechanism of signaling between rings seems different between the two groups [140]. However, the mechanism of action of this group of chaperones is similar to that of group I, as similar steps characterize it: formation of chaperone complex, ATP binding, interaction with the substrate in the open state, folding of the substrate in closing conformation and release of the folded substrate. Data suggests a higher level of specialization and complexity due to the "functional polarity" of these types of chaperones. Differently from the group I chaperones, it has been suggested a substrate-specificity for group II class of chaperones [117].

CHAPERONES & NEURODEGENERATIVE DISEASES

Chaperones are one of the most conserved guardians of the cellular proteome, and increasing evidence supports their essential role in keeping cellular homeostasis, targeting dysfunctional proteins and facilitating the removal of toxic stressors [136,141]. On a cellular level, proteins are exposed to a crowded environment and any alteration of the balance between protective and damaging factors might induce protein dysfunction. Additionally, aging is the first factor responsible for an impairment of protective factors due to the physiological reduction of "proteostasis network" [141]. It is not surprising that aging is the major risk factor of several pathologies characterized by protein misfolding or cancer. Alterations of chaperone networks have been associated with several diseases: amyotrophic lateral sclerosis, retinal degenerative disease, peripheral neuropathies and AD [113,142,143]. Loss of function of chaperones has been suggested as one of the contributors in AD pathogenesis. These proteins could be a potential target for future therapies. In support of the therapeutic potential of chaperones in neurodegenerative diseases, it has been shown that potentiating the chaperone machinery in an *in vitro* model of amyloid pathology reduces Aβ-driven cytotoxicity and mitochondrial dysfunction [136,144–146]. Different mechanisms linking the role of chaperones and protein dysfunction observed in AD need further clarification, as there are controversies in the field. A role of chaperones in mediating the toxic oligomerization of tau protein or in the translocation of APP and Aβ in the mitochondria *in vitro*, thus contributing to AD pathogenesis has also been proposed [147,148]. Furthermore, it has also been shown a correlation between certain proteinopathies, as polyglutamine disease, with age-related decline of the protein quality control machinery, thus suggesting that a loss of function of chaperone might have a critical role in preserving protein homeostasis during aging [149]. A better understanding of the role of chaperones in promoting or preventing neurodegenerative diseases is critical to clarify these controversies.

AIM OF THE DISSERTATION

AD is the most common form of dementia, affecting almost 6 million Americans worldwide [150]. The high number of risk factors and the complex cascades leading to AD have so far made it challenging to design successful therapies.

The pro-amyloidogenic pathway leading to the neurotoxic accumulation of Aβ, has been hypothesized as one of the earliest causes of the disease [8,52,151]. Additionally, an impairment of the protein quality control machinery either due to aging or the accumulation of protein misfolding in AD could also contribute to worsening of this disease [152].

A crucial component of the protein quality control machinery is the family of chaperones [145], particularly, the focus of this dissertation is on one of the most evolutionary conserved chaperones: Hsp60. This mitochondrial chaperonin is involved both in protecting mitochondria from damage induced by the misfolded protein on a cellular level, and in a cross-talk with the immune system on a systemic level. Additionally, it has been shown that Hsp60 is directly involved in an interaction with APP/Aβ and in downstream protection of mitochondria from Aβ-induced damage [144,147]. Therefore, this dissertation aims to characterize the functional effect of Hsp60 on Aβ, either in its monomeric or oligomeric structure, and to investigate if this interaction results in the formation of less toxic conformations.

The central hypothesis of this project is that Hsp60 effectively inhibits Aβ aggregation and toxicity. This central hypothesis is addressed with three specific aims. In the first aim, I confirmed the direct effect of Hsp60 in inhibiting the aggregation of Aβ using biophysical approaches. Specifically, I addressed this specific aim using circular dichroism, thioflavin T assay, size exclusion chromatography, and atomic force microscopy. In the second specific aim, I investigated the effect of Hsp60 overexpression on APP processing and Aβ release using an *in vitro* approach. I designed a novel cellular model that overexpresses both APP and Hsp60, and I validated the model by western

blotting and immunocytochemistry. Subsequently, I investigated the effect of Hsp60 on APP and Aβ extracellularly, intracellularly and in mitochondria. In the third aim, I confirmed that treatment of pre-formed Aβ oligomers with Hsp60 reduced their neurotoxicity, in terms of reduced neuronal death *in vitro*, reduced binding to synapses and reduced impairment of synaptic plasticity *ex vivo*. To address the third aim I used biophysical approaches and flow cytometry to characterize the effect of Hsp60 on preformed Aβ oligomers. I used a neuroblastoma cell line as an *in vitro* model for testing changes in cytotoxicity and *ex vivo* electrophysiology for testing changes in synaptic plasticity upon treatment with Aβ oligomers, both before and after Hsp60 exposure. As the field is controversial about the role of Hsp60 in AD, this project contributes to elucidating essential mechanisms of action of Hsp60, thus proposing this chaperone as a potential target for future therapies against AD pathology.

CHAPTER 2. CELL FREE INVESTIGATION OF THE INHIBITORY EFFECT OF HSP60 ON Aβ AGGREGATION

Modified in part from:

"Mangione, M. R. et al. Hsp60, amateur chaperone in amyloid-beta fibrillogenesis. Biochim. Biophys. Acta - Gen. Subj. 1860, 2474–2483 (2016)."

I.   INTRODUCTION

The misfolding of Aβ peptide and the downstream formation of neurotoxic oligomers is one of the earliest lesions of AD [74,153]. The presence of intrinsically disordered regions in the protein structure of Aβ contributes to the high propensity to aggregate and to the polymorphic nature of these aggregates [122,125,126,154]. The synaptic accumulation of toxic Aβ oligomers in specific brain regions is one of the leading causes of synaptic dysfunction [91,155]. Therefore, targeting this aggregation process can contribute to the design of successful therapeutic strategies relevant for AD.

In the work presented in this chapter, we aimed to investigate the effect of Hsp60 on Aβ aggregation using a cell-free approach to test changes in the biophysical properties of Aβ. Previous studies suggested a possible interaction between Aβ and Hsp60 [144,147,156], but weather Hsp60 had an effect on Aβ aggregation was still unresolved. To fill this gap of knowledge, we tested the antiaggregating effect of human Hsp60 against $A\beta_{1-40}$ and $A\beta_{1-42}$ peptides, the latter being a more aggressive model of Aβ aggregation. We further tested the effect of the bacterial homolog of Hsp60, GroEL on $A\beta_{1-40}$ aggregation pathway as an alternative chaperone with a high degree of homology to the mitochondrial Hsp60 [139]. Specifically, using spectroscopy, chromatography and microscopy techniques we investigated the ability of Hsp60 to directly interact with

monomeric Aβ and we identified an irreversible anti-aggregative effect of Hsp60 upon its interaction with Aβ monomers.

II.   MATERIALS & METHODS

SAMPLE PREPARATION

Amyloid β peptides: synthetic $A\beta_{1-40}$ (Anaspec) and recombinant $A\beta_{1-42}$ were prepared in monomeric form according to protocols previously published and optimized in the laboratory [157,158]. In detail, Aβ peptides were dissolved in 5 mM NaOH (Sigma-Aldrich) at pH 10 and lyophilized in frozen aliquots overnight to preserve the monomeric status of both peptides. For all experiments, frozen aliquots of Aβ were solubilized in different buffers as summarized in Table 2 and the peptide dispersion was filtered with 0.20 μm (Whatman) and 0.02 μm (Millex-Lg) filters placed in series, to remove large aggregates or impurities. We performed all sample preparations in a 4 °C cold room to avoid uncontrolled aggregation. To calculate the concentration of Aβ peptide we used the Lambert-Beer law [159], which stated a direct proportionality between the intensity of absorbance and protein concentration through a constant defined as the extinction coefficient. We determined the concentration of Aβ using the 276 nm absorbance and the molar extinction coefficient of 1390 $cm^{-1}*M^{-1}$ [160]. For chromatography experiments, all collected fractions of $A\beta_{1-40}$ were subsequently concentrated at 6000 g (Heraeus Multicentrifuge X3R) at 5 °C using a 3 kDa cut-off filter (Millipore). For all experimental procedures, the final concentrations of $A\beta_{1-40}$ was chosen based of previously published protocols to allow a reproducible and controlled aggregation kinetic [161,162]; the concentration of $A\beta_{1-42}$ was optimized for testing the optimal effect of Hsp60.

Hsp60 & GroEL: Human recombinant Hsp60 was purchased in its active form (Hsp60, short form, ATGene). For all experiments, the buffer of the peptide was changed

into the desired buffer using 30 KDa cut-off filters (Amicon Ultra 4, Millipore). For all samples, the final concentration (1 or 2 μM) of Hsp60 was arbitrarily chosen and calculated empirically and samples were prepared either on ice or in a 4 °C cold room. The bacterial homologue GroEL was purchased from Sigma (St. Louis, MO, USA) and prepared at the final concentration of 7 μM in the same buffer used to test Hsp60.

AGGREGATION KINETICS

We prepared both $A\beta_{1-40}$ and $A\beta_{1-42}$ monomers from lyophilizate aliquots that were dissolved in the desired buffer. For all experiments, we confirmed the protein concentration spectroscopically according to the Lambert-Beer law as previously described. To induce protein aggregation, aliquots of Aβ either without or with Hsp60 were incubated at 37 °C and stirred up to 24 h at 200 rpm using a magnetic stirrer and a thermostat. Notably, all kinetics of aggregation of Aβ were conducted up to 72 h, using final concentration of 50 μM for $A\beta_{1-40}$, and either 50 μM or 15 μM for $A\beta_{1-42}$. The latter concentration of $A\beta_{1-42}$was chosen to test the effect of Hsp60 as under these experimental conditions, testing the effect of Hsp60 on $A\beta_{1-42}$ was more reproducible. All aggregation experiments were repeated at least 3 times to confirm the reproducibility of the assay.

THIOFLAVIN T (THT) ASSAY

To measure the formation fibrils of Aβ during the aggregation kinetics, either without or with Hsp60, we added ThT to withdrawals of samples at specific time points (0, 1h, 3h, 5h, 24h). ThT is a benzothiazole derivative that selectively fluoresces in presence of amyloid aggregates due to its exposure to β-sheet rich structures [163–165]. We detected the fluorescence of ThT via spectrofluorometry (JASCO FP-6500) and data were analyzed using xmGrace and GraphPad Prism 8 software. For all experiments, we incubated Aβ

samples with 12 μM ThT and we measured the time course measurements upon excitation at 450 nm and emission at 485 nm using a fixed slit width of 3 nm [166]. For all ThT assay results, data was expressed as a function of ThT fluorescence over time and the assay was repeated at least three times to confirm its reproducibility.

CIRCULAR DICHROISM (CD) SPECTROSCOPY

CD spectroscopy has been used to determine changes in the secondary structure of either Aβ, Aβ + Hsp60 or Hsp60 alone at different time points (0, 1h, 3h, 5h, 24h, 72h). Through the interaction between the polarized light of the instrument and the asymmetrical structure of the protein samples we determined changes of time in both secondary structure and three-dimensionality of all proteins investigated. For each experiment, we used a final volume of 50 μL, and a quartz cuvette of 0.2 mm path. All measurements were acquired at 20 °C and subtracted by the buffer with a n=8 replicates [166].

ATOMIC FORCE MICROSCOPY (AFM)

We used AFM microscopy to characterize the morphology of $A\beta_{1-40}$, $A\beta_{1-40}+$ Hsp60 or Hsp60 alone either before or after 24 h aggregation kinetic. Data was obtained using a Nanowizard III (JPK Instruments, Germany) that was installed either on an Axio Observer D1 (Carl Zeiss, Germany) or on an Eclips Ti (Nikon, Japan) microscopes. Data was generated in collaboration with the "Istituto Italiano di Tecnologie" in Genoa (IT). For all AFM measurements, samples were washed with DDI water AND adsorbed on a disc of MICA for 20 minutes by inflating nitrogen air, either before or after 3 days of aggregation kinetic. NCHR silicon cantilever (Nanoworld) was used to assess the sample morphology upon application of an "intermittent contact mode in air". The parameters chosen for the

acquisition were 21-78 N/m for the spring constant and 250-390 kHrz for the resonance frequency [166].

SIZE-EXCLUSION HIGH PRESSURE LIQUID CHROMATOGRAPHY (SEC-HPLC)

We used SEC-HPLC for the qualitative and quantitative analysis of changes in size and concentration of $A\beta_{1-40}$ aggregates upon interaction with Hsp60. Both Hsp60 and sample buffer were analyzed as controls. All samples were injected using either a 50 μL (qualitative analysis) or 500 μL (quantitative analysis) injection loop connected to a HPLC (Shimatzu, Prominence) supplemented with a mobile phase degasser (DGU-20As, Shimadzu), a quaternary pump (LC-2010 AT, Shimadzu) and a photodiode array detector (SPD-M20A, Shimadzu). For all chromatography separations, we used a direct phase stationary phase to allow separation by size (Superdex 200 10 300 GE Healthcare) and 20 mM Tris HCl (pH 7.7), 3 % glycerol, 30 mM NaCl as mobile phase. Samples were eluted at 0.5-1 mL/min flow rate. The detection of injected samples was done spectroscopically by recording the absorbance at 280 nm [166]. This technique allowed the calculation of the molecular weight of each eluted protein by comparing our data with the chromatogram of a standard mixture of proteins with known molecular weight (Sigma Aldrich). We analyzed the distribution of different aggregates of $A\beta_{1-40}$ that were formed after the aggregation kinetic either in absence or upon Hsp60 treatment. As this technique did not alter Aβ stability [167], we collected the purified fractions using an automated fraction collector (FRC-10A, Shimadzu) and further analyzed them with other biophysical techniques.

III. RESULTS

MODEL VALIDATION OF HSP60- Aβ1-40 PROTEIN-PROTEIN INTERACTION

To test the effect of Hsp60 on monomeric Aβ1-40, we first established the optimal conditions for Hsp60-Aβ1-40 interaction in a cell-free model. As summarized in Table 2, we tested the interaction between 50 μM Aβ1-40 and two different concentrations of Hsp60 (1 and 2 μM). As described in the methods, we performed all aggregation kinetics according to published protocols [168,169] to allow a controlled and reproducible Aβ aggregation from monomeric state to large fibers. To characterize the effect of Hsp60 on aggregation pathway of Aβ, we used Thioflavin T (ThT) assay to assess the formation of fibrils and circular dichroism (CD) spectroscopy to detect changes in secondary structure, as these were very well-established assays for characterizing Aβ1-40 aggregation kinetic [158,162,163,170]. The aggregation properties of Aβ were known to depend on the experimental conditions as pH, ionic strength and agitation [171]. Therefore, we first characterized the aggregation kinetic of Aβ1-40 alone using both ThT assay and CD spectroscopy under our experimental conditions.

Table 2. Experimental conditions tested the optimal effect of Hsp60 on the biophysical properties of Aβ

	Conditions			
Aβ$_{1-40}$ (μM)	50	50	50	50
Hsp60s (μM)	1	-	2	-
Buffer	20 mM Tris HCl, 1.5% glycerol, 15 mM NaCl	20 mM Tris HCl, 1.5% glycerol, 30 mM NaCl	20 mM Tris HCl, 3% glycerol, 30 mM NaCl	20 mM Tris HCl, 3% glycerol, 30 mM NaCl

rpm	200	200	200	200
pH	7.4	7.4	7.4	7.4
T	37 °C	37 °C	37 °C	37 °C
ThT (µM)	12 µM	12 µM	12 µM	12 µM

As summarized in Figure 2.1, we analyzed changes of ThT fluorescence and dichroic spectra of 50 µM $A\beta_{1-40}$ at different time points (0, 1, 3, 5 and 72 h hours) of its aggregation kinetic. Consistent with the extensive literature available [70,170,172], the time course kinetic of $A\beta_{1-40}$ aggregation detected by ThT (Figure 2.1.A) was characterized by an initial low signal of fluorescence referred as "lag phase", representing the phase of nucleation of Aβ seeds. As soon as the concentration of Aβ seeds increased, the lag-phase was followed by the elongation phase, measured by the exponential increase in intensity of emission of ThT [164,173–175]. The latter phase was characterized by the formation of larger aggregates, which preceded the formation of amyloid fibers. In these conditions of temperature, buffer, pH and agitation, we observed Aβ fibers in about 5 to 6 hours. The results obtained with ThT assay were supported by the CD data (Figure 2.1.b). In fact, at time 0 of the aggregation kinetic the CD spectrum of the Aβ was characterized by a minimum of absorbance around 195 nm, which was characteristic of random coil conformation. Notably, it has been shown that this conformation is distinctive of unordered and not aggregated structures [159]. As soon as Aβ was incubated under pro-aggregating conditions, we observed a change in the CD spectrum morphology within 5 hours of incubation. In fact, the CD spectrum of Aβ at 5 hours incubation was characterized by a shift of the minimum around 210 nm, which was typical of β-sheet conformations of aggregated proteins. The data obtained was consistent with the ThT assay previously described. Notably, the aggregation of Aβ was even more pronounced after 72 hours (black

curve, round symbols, Figure 2.1.B). In fact, the CD spectrum recorded at this time point was characterized by a sigmoidal shape with two minima in the range on 215 nm and 220 nm respectively.
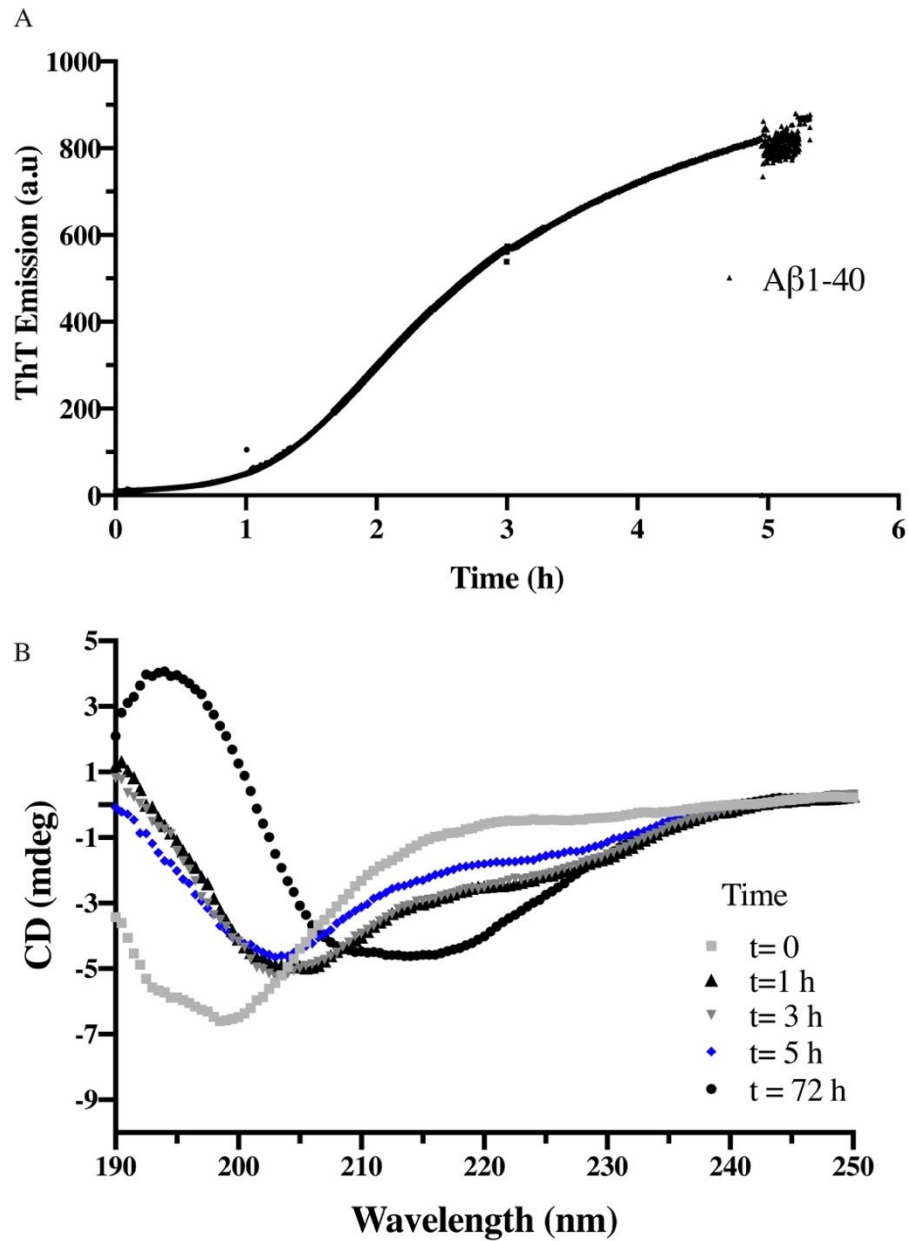
Figure 2.1 Biophysical analysis of Aβ$_{1-40}$ aggregation pathway using Thioflavin T (ThT) and CD assays.

A. Representative ThT assay showing the increasing fluoresce of ThT probe during the time course kinetic of 50 μM Aβ$_{1-40}$, which is indicative of the formation of Aβ aggregates.

The aggregation kinetic of Aβ$_{1-40}$ was conducted in 20 mM Tris HCl buffer (pH 7.7) incubated under pro-aggregating conditions (37 °C, 200 rpm) for at least 5 hours. The assay confirmed the presence of a lag phase, characterized by a fluorescence emission less than 200 a.u. (arbitrary units), which is characteristic of the interaction between ThT and small oligomeric aggregates during the nucleation phase of Aβ aggregation. The exponential increase of ThT fluorescence after 1h of the time course kinetic was indicative of the interaction between ThT and progressively larger aggregates, which characterize the elongation phase of Aβ aggregation. The plateau of ThT fluorescence at 5 h of the aggregation kinetic is characteristic of the intensity of fluorescence of ThT increased exponentially after 1h 30 min due to the increasing aggregation of Aβ. Assay conditions: 12 μM ThT; λexc (ThT)=450 nm; λem (ThT)=484 nm. B. Representative CD spectra of Aβ$_{1-40}$ at different time points of the aggregation kinetic: 0 (t= 0 h, grey line, square symbol), 1 hour (t= 1 h, black line, triangle symbol), 3 hours (t= 3 h, grey line, triangle symbol), 5 hours (t= 5 h, blue line) and 72 hours (t= 72 h, black line, circle symbol). Data confirmed the random coil conformation of Aβ at time zero, which is characteristic of unorganized structures. The transition of the minimum of absorbance of the CD spectrum of Aβ from 195 nm at time zero to 215 nm at 24 h is suggesting of the aggregation of Aβ and the formation of β-sheet conformations, which are characteristic of fibrillary structures. Measurements recorded at 20 ºC and expressed as the average of 30 measurements. Data expressed in mdeg over wavelength.

As the CD spectrum of Hsp60 is characterized by an α-helix conformation that could overlap the dichroic spectrum of Aβ, in parallel experiments, we characterized the CD spectrum of 2 µM Hsp60 over time. As shown in Figure 2.2, Hsp60 was characterized by an alpha-helix secondary structure, with a maximum of absorbance ranging around 196 nm and two minima of absorbance around 209 and 220 nm respectively.
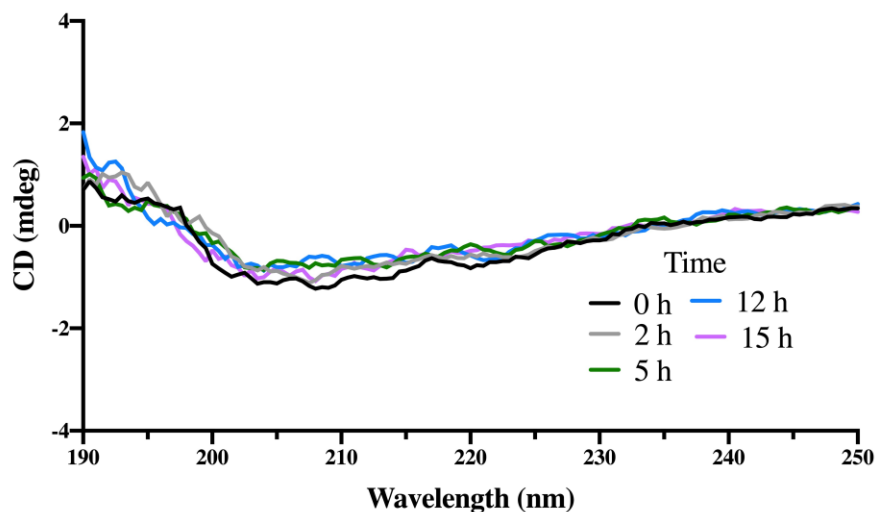
Figure 2.2. Analysis of the secondary structure of 2 μM Hsp60 using circular dichroism (CD) spectroscopy.

Representative time course kinetic of Hsp60 at different time points of a time course kinetic at 37 °C analyzed by CD spectroscopy: 0 (0 h; black line); 2 hours (2 h; grey line); 5 hours (5 h; green line); 12 hours (12 h; light blue line) and 15 hours (15 h; magenta line). Data showing that the dichroic spectra of Hsp60 is characterized by two minima between 205 nm and 210 nm, which are characteristic of a α-helix secondary structure, that is stable over time. Experimental conditions: buffer 20 mM Tris (pH= 7.7), 3% glycerol, 30 mM NaCl, pH = 7.7, T = 20 ºC. Data presented as the average of 30 measurements and expressed in mdeg over wavelength.

Once the biophysical properties of both Aβ_{1-40} and Hsp60 in these specific experimental conditions were defined, we tested the effect of two different concentrations of Hsp60 (1 μM and 2 μM) on the aggregation kinetic of Aβ_{1-40} using ThT assay and CD analysis of the secondary structure, as previously described for the two proteins alone. Notably, as the CD spectra of Hsp60 partially overlapped with Aβ spectra, to test the effect of Hsp60 on the dichroic properties of Aβ, we subtracted mathematically the contribution of Hsp60 to all CD spectra of Aβ_{1-40} that was treated with Hsp60. We considered this manipulation of our results acceptable based on other studies showing that Hsp60 loses the folding stability at higher temperatures and concentrations [176].

As summarized in Figure 2.3, 1 μM Hsp60 slowed Aβ_{1-40} aggregation by increasing the lag phase as shown by ThT assay (Figure 2.3.A), thus suggesting a change in the

nucleation phase of Aβ$_{1-40}$ seeds when Hsp60 was present in the 50:1 molarity ratio (Aβ$_{1-40}$:Hsp60). In addition, CD spectroscopy analysis confirmed that the presence of Hsp60 reduced Aβ aggregation when we compared it to Aβ$_{1-40}$ alone (Figure 2.3.B). CD data suggested that when incubated with Hsp60, Aβ$_{1-40}$ assembled into an organized β-sheet conformation not after three hours of the aggregation kinetic, but after 5 hours, thus suggesting a slower process of aggregation in presence of Hsp60.
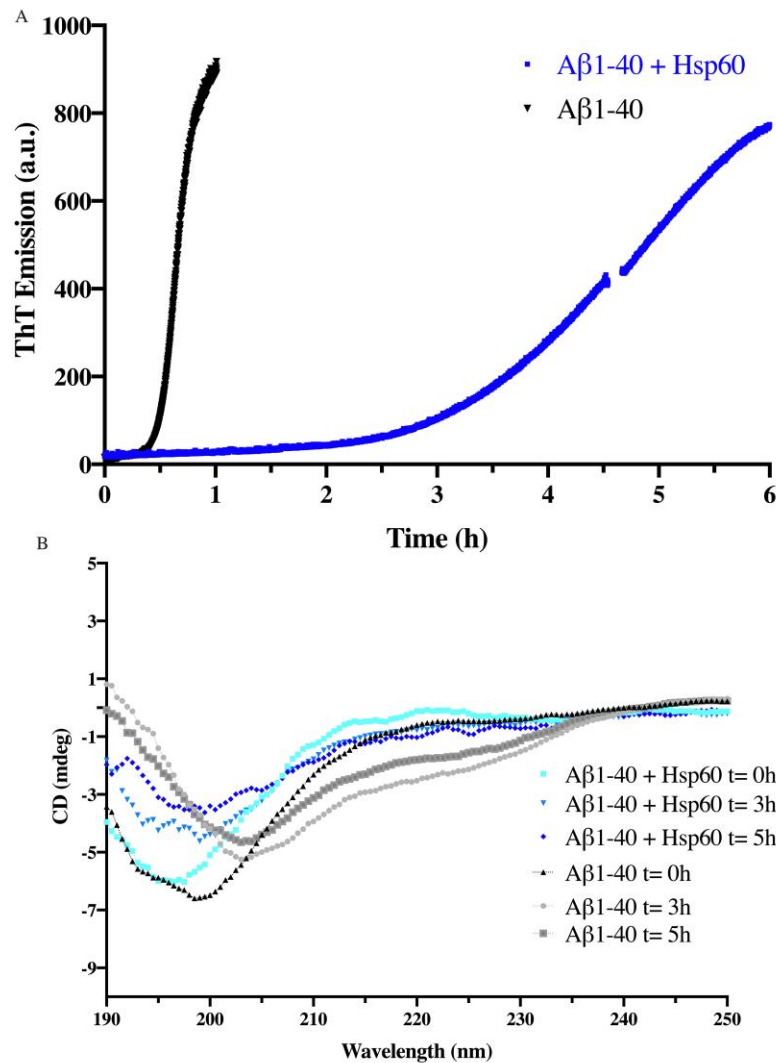
Figure 2.3. Biophysical analysis of Aβ$_{1-40}$ upon treatment with 1 μM Hsp60.

A. Representative time course kinetic of 50 μM Aβ$_{1-40}$ incubated with 1 μM Hsp60 for 6 hours at 37 °C and stirred at 200 rpm in presence of ThT 12 μM, showing the slower

increase of ThT emission over time, which is indicative of a longer lag-phase of Aβ aggregation when Aβ is exposed to Hsp60 (blue line), as compared to Aβ alone (black line). Assay conditions: λexc ThT=450 nm; λem ThT=484 nm. B. Representative CD spectra of Aβ$_{1-40}$ under pro-aggregating conditions (200 rpm, 37 ℃) either with or without 1 μM Hsp60, at time zero (t= 0 h; Aβ, black curve; Aβ + Hsp60, light blue curve), 3 hours (t=3 h; Aβ, light grey curve; Aβ + Hsp60, indigo blue curve) or 5 hours (t= 5 h; Aβ, dark grey curve; Aβ + Hsp60, blue curve) aggregation kinetic, suggesting that Hsp60 affected the secondary structure of Aβ over time by reducing the formation of beta-sheet conformations after 5 h of the aggregation kinetic as compared to Aβ alone. Measurements recorded at 20 ℃ and expressed as the average of 30 measurements, expressed in mdeg over wavelength.

We further tested the effect of Hsp60 on Aβ$_{1-40}$ aggregation pathway using a different molarity ratio between the two proteins. We tested the effect of 2 μM Hsp60 on 50 μM Aβ$_{1-40}$ (25:1 molarity ratio Aβ$_{1-40}$: Hsp60) using both ThT assay and CD spectroscopy. As shown in Figure 2.4, we observed that in these conditions Hsp60 had a stronger anti-aggregating effect on Aβ$_{1-40}$. In fact, differently from Aβ$_{1-40}$ alone, ThT fluorescence in presence of Aβ$_{1-40}$ incubated with Hsp60 did not increase up to 6 hours, thus suggesting that in presence of Hsp60, Aβ$_{1-40}$ did not form seeds able to trigger the elongation phase. Overall, this data suggested that Aβ$_{1-40}$ exposed to Hsp60 lost the ability to aggregate. We further confirmed the antiaggregating effect of Hsp60 by the CD analysis that is summarized in Figure 2.4B.

We tested the fibrillogenic properties of Aβ$_{1-40}$ both with or without Hsp60 up to 72 h and we observed that when exposed Hsp60, Aβ$_{1-40}$ retained an unorganized conformation, that was closer to a random coil structure, without assuming a β-sheet conformation as observed in the untreated sample.

Overall, data suggested that Hsp60 successfully inhibited the aggregation kinetic of Aβ$_{1-40}$.
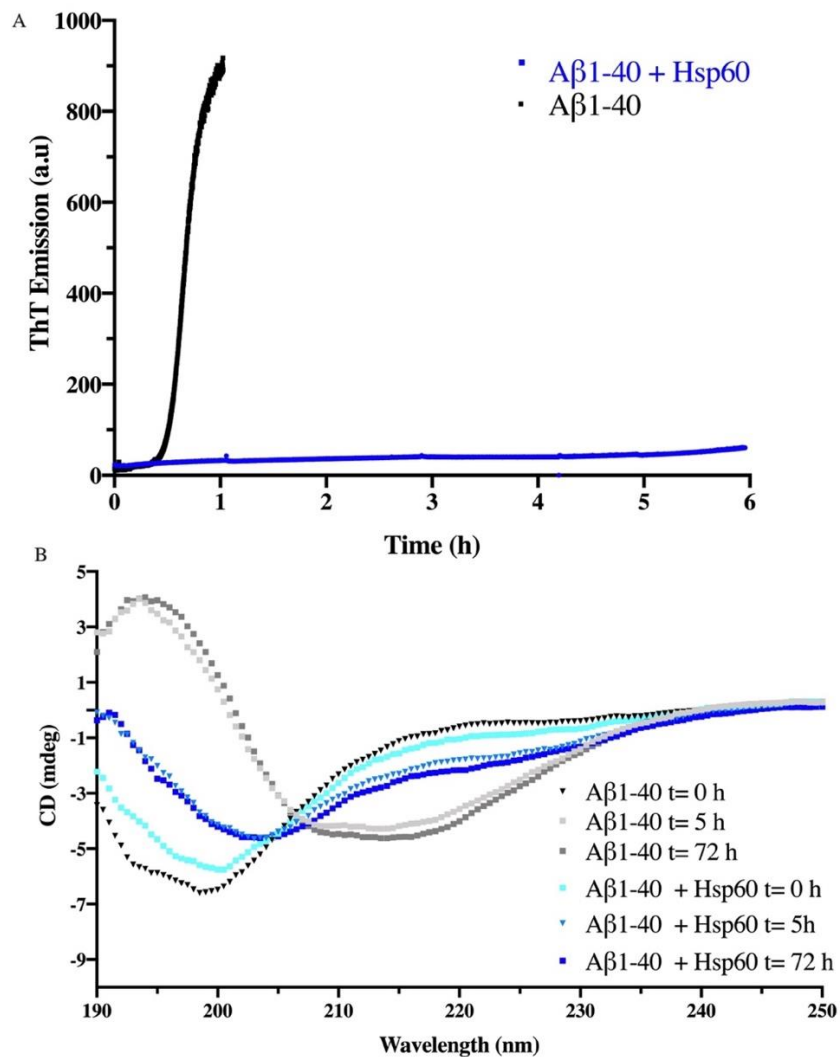
Figure 2.4. Biophysical analysis of Aβ$_{1-40}$ upon treatment with 2 μM Hsp60.

A. Representative time course kinetic of 50 μM Aβ$_{1-40}$ incubated with 2 μM Hsp60 for 6 hours at 37 °C and stirred at 200 rpm in presence of ThT 12 μM, showing a reduced ThT emission over time when Aβ is exposed to Hsp60 (blue line), as compared to Aβ alone (black line), which is indicative of an inhibition of Aβ aggregation. Experimental conditions: λexc ThT=450 nm; λem ThT=484 nm. B. Representative CD spectra of Aβ$_{1-40}$ under pro-aggregating conditions either with or without 2 μM Hsp60, at time zero (t= 0 h; Aβ, black curve; Aβ + Hsp60, light blue curve), 5 hours (t= 5 h; Aβ, light grey curve; Aβ + Hsp60, indigo blue curve) or 72 hours (t= 72 h; Aβ, dark grey curve; Aβ + Hsp60, blue curve) aggregation kinetic, suggesting that Hsp60 affected the secondary structure of Aβ by preventing the formation of beta-sheet conformations. Measurements recorded at 20 °C and expressed as the average of 30 measurements, expressed in mdeg over wavelength.

THE EFFECT OF HSP60 ON Aβ₁₋₄₀ AGGREGATION: AFM MORPHOLOGY

To further validate the inhibitory effect of Hsp60 on Aβ$_{1-40}$ aggregation, samples of Aβ$_{1-40}$, either exposed or not to Hsp60 (25:1 molarity ratio Aβ$_{1-40}$: Hsp60) were analyzed using AFM microscopy for morphologic characterization at time zero and after 24 hours of aggregation kinetic. Data summarized in Figure 2.5 were obtained in collaboration with the Italian Institute of Technology in Genova by Dr. Canale. In detail, consistent with data from several other laboratories [177,178], monomers of Aβ$_{1-40}$ were almost below detection limits as this protein is around 4.5 kDa (Figure 2.5, panel a). Conversely, when we incubated Aβ$_{1-40}$ under pro-aggregating conditions for 24 hours, we observed long fibers that were in the range of microns (Figure 2.5, panel b). Consistent with CD and ThT assays previously shown, the presence of Hsp60 completely inhibited the formation of Aβ$_{1-40}$ fibers, as there was no morphological difference between samples analyzed at time zero and after 24 hours of aggregation (Figure 2.5, panels c and d), and the particles observed in the range of 3 nm were consistent with Hsp60 size as reported by studies one by others [179]. AFM results further confirmed that Hsp60 inhibits the aggregation kinetic of Aβ$_{1-40}$.
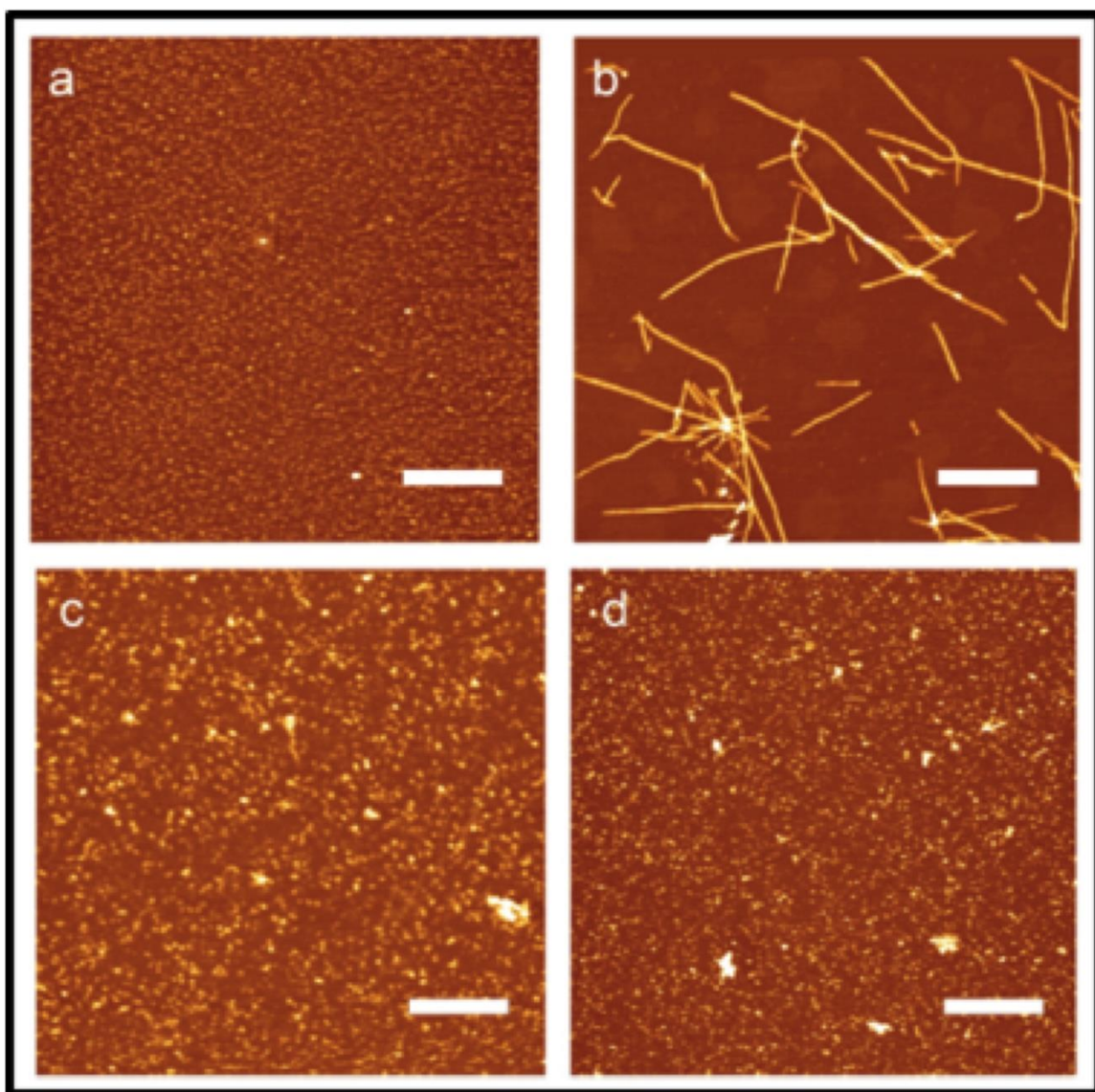
Figure 2.5. Atomic force microscopy (AFM) analysis of Aβ$_{1-40}$ morphology changes upon incubation with Hsp60.

Representative AFM acquisitions of 50 μM Aβ$_{1-40}$ showing no aggregation at time 0 (a) and elongated fibrils after 24 h aggregation kinetic at 37 °C and 200 rpm (b). Conversely, when Aβ$_{1-40}$ was incubated with 2 μM Hsp60, either at time 0 (c) or after 24 h (d) we observed only 2-10 nm spherical species compatible with Hsp60 size, suggesting that Hsp60 inhibited Aβ$_{1-40}$ aggregation. Scale bar: 1 μm, Z-range: (a,b,c) 7nm;(d) 9.6 nm. Adapted from Mangione et al., 2016 [166].

CHARACTERIZATION OF THE EFFECT OF HSP60 ON Aβ$_{1-40}$ AGGREGATION PATHWAY USING SEC-HPLC CHROMATOGRAPHY

As our previous results strongly suggested a direct effect of Hsp60 on Aβ$_{1-40}$ aggregation kinetic, we further tested the effect of Hsp60 on the aggregation propensity of Aβ$_{1-40}$ using SEC-HPLC. In detail, we performed a both qualitative and quantitative analysis of Hsp60-Aβ$_{1-40}$ protein-protein interaction. We analyzed changes in the retention time (R.T.), expressed by the time of elution, of Aβ$_{1-40}$ upon treatment with Hsp60, as a qualitative parameter; the area under curve of each specific peak of the chromatogram was used as a quantitative parameter to determine the changes in concentration of monomeric Aβ after its aggregation. As the pores of the stationary phase did not allow the passage of large aggregates through the column, under these experimental conditions we could not quantify the aggregates with the size of fibers, as they eluted in the void volume. We estimated the amount of aggregates formed by comparing the area under the curve of the monomeric fractions at two time points of the aggregation kinetic (0 and 24 hours) and the quantification of the formation of fibers was calculated the complementary of the monomeric fraction. Results are shows in Figure 2.6.
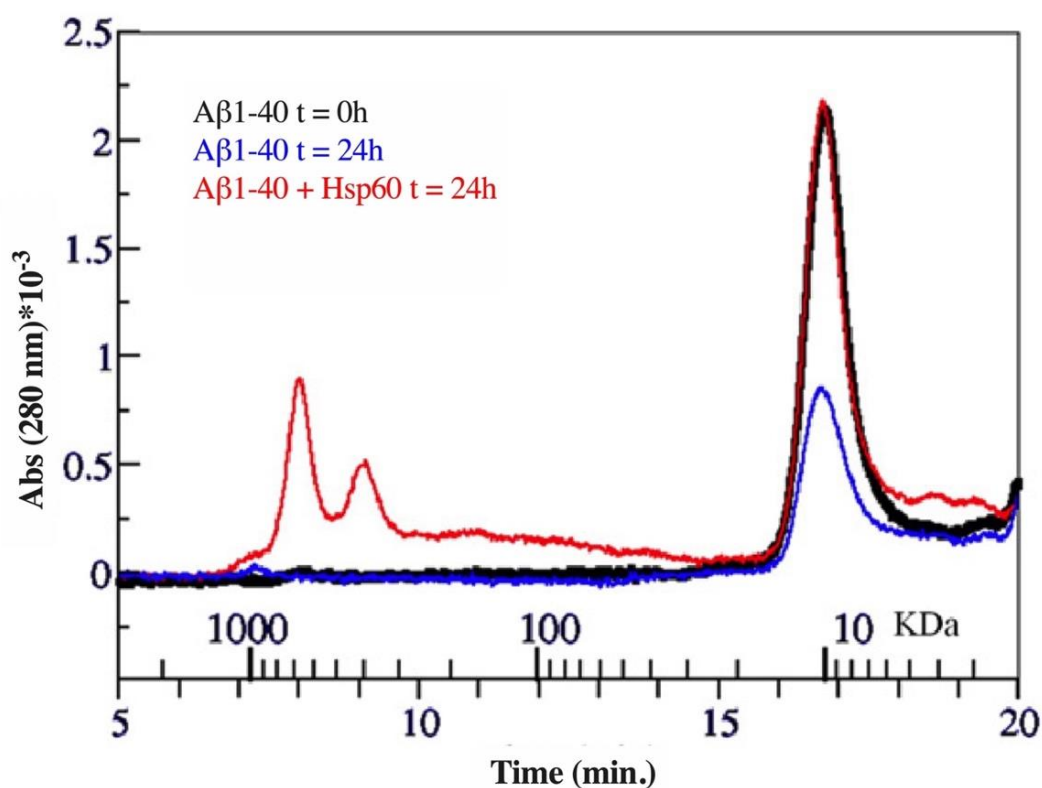
Figure 2.6. Analysis of the effect of Hsp60 on Aβ$_{1-40}$ using size exclusion chromatography (SEC-HPLC).

Representative chromatograms comparing 50 μM Aβ$_{1-40}$ at time zero (black curve), after 24 h aggregation kinetic without (blue curve) or with 2 μM Hsp60 (red curve). Data showed a reduced area under the peak of monomeric Aβ$_{1-40}$ around 17 min after 24 h aggregation that was rescued when Aβ$_{1-40}$ is incubated with Hsp60, thus suggesting the antiaggregating effect of Hsp60. The presence of the two peaks around 8 minutes of elution in the Aβ$_{1-40}$ + Hsp60 chromatogram are characteristic of Hsp60 heptamers and tetradecamers. Molecular weights shown in Figure was calculated using globular protein standards. Adapted from Mangione et al. [166].

In detail, we isolated and analyzed by SEC-HPLC Aβ$_{1-40}$ fractions either incubated or not with Hsp60. As controls, we injected a sample of monomeric Aβ$_{1-40}$ and Hsp60 to estimate the R.T. of both proteins alone. The injection of freshly prepared Aβ$_{1-40}$ monomers (black curve, Figure 2.6), produced a chromatogram characterized by a peak with a retention time around 17 minutes. Conversely, the injection of the same sample of Aβ$_{1-40}$ incubated for 24 h under pro-aggregating conditions, produced a peak with the same R.T.

but reduced area, suggesting the formation of larger aggregates that could not be detected under these experimental conditions (blue curve, Figure 2.6). As we compared this data to a chromatogram of $A\beta_{1-40}$ incubated 24 h with Hsp60 under pro-aggregating conditions (red peak, Figure 2.6), we observed that the peak corresponding to the monomeric fraction of $A\beta$ was very similar in both quality (R.T.) and quantity (area under the peak) to the untreated control, thus further confirming the anti-aggregating effect of Hsp60 on $A\beta_{1-40}$.

We also confirmed that the two peaks around 8 and 9 min. where characteristic of the two forms of Hsp60, heptameric and tetradecameric, upon injection of Hsp60 under the same conditions as shown in Figure 2.7.
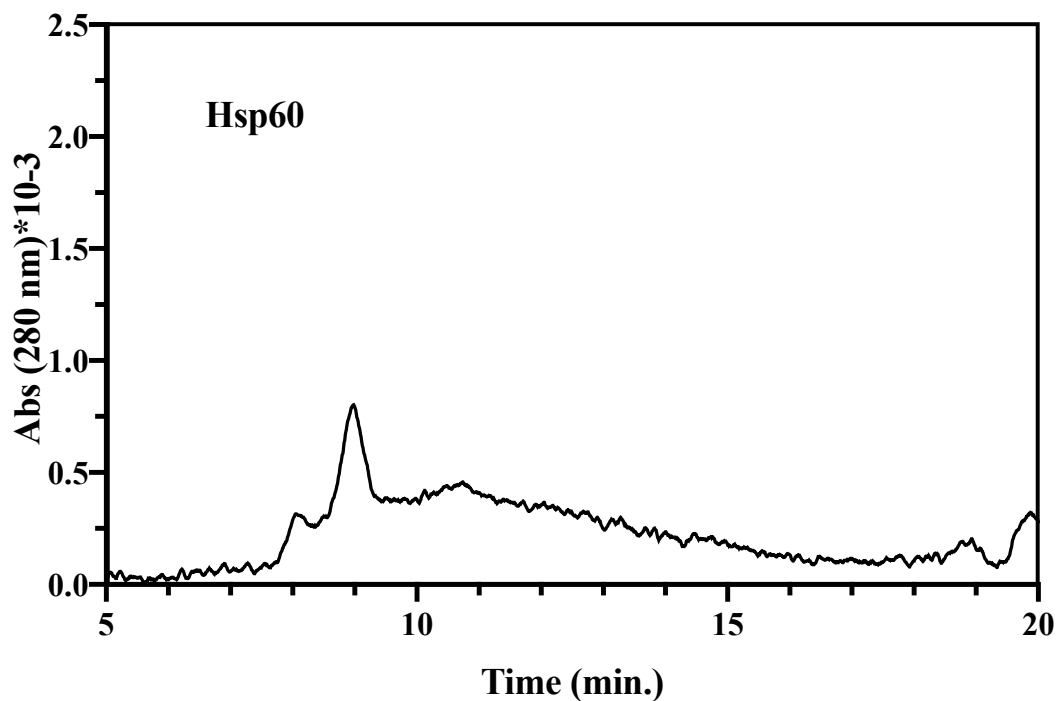
Figure 2.7. Chromatographic analysis of Hsp60.

Representative chromatograms of 2 μM Hsp60 using size exclusion chromatography (SEC-HPLC), showing two peaks around minutes 8 and 9, that are characteristic of the heptameric and tetradecameric aggregates of Hsp60.

We further tested the misfolding ability of $A\beta_{1-40}$ upon exposure to Hsp60 and investigated if this interaction affected the misfolding nature of $A\beta$. Therefore, after SEC-HPLC purification we tested the aggregation of $A\beta_{1-40}$ either not treated or treated with Hsp60 using the ThT assay as we showed previously. This test for simplicity has been referred as "aggregation assay". In detail, we collected both $A\beta$ fractions (not treated or treated with Hsp60) from SEC-HPLC with a R.T. around 17 minutes, which represented the fractions of purified monomeric $A\beta$. We incubated both purified fractions under pro-aggregating conditions (24 hours, 37 °C and 200 rpm) and we tested changes in ThT emission and CD spectra. As shown in Figure 2.8, $A\beta$, once exposed to Hsp60, was no longer able to aggregate even after the removal of Hsp60. Conversely, chromatographic fractions purified from a sample of $A\beta_{1-40}$ gave statistically higher ThT fluorescence, due to fiber formation.
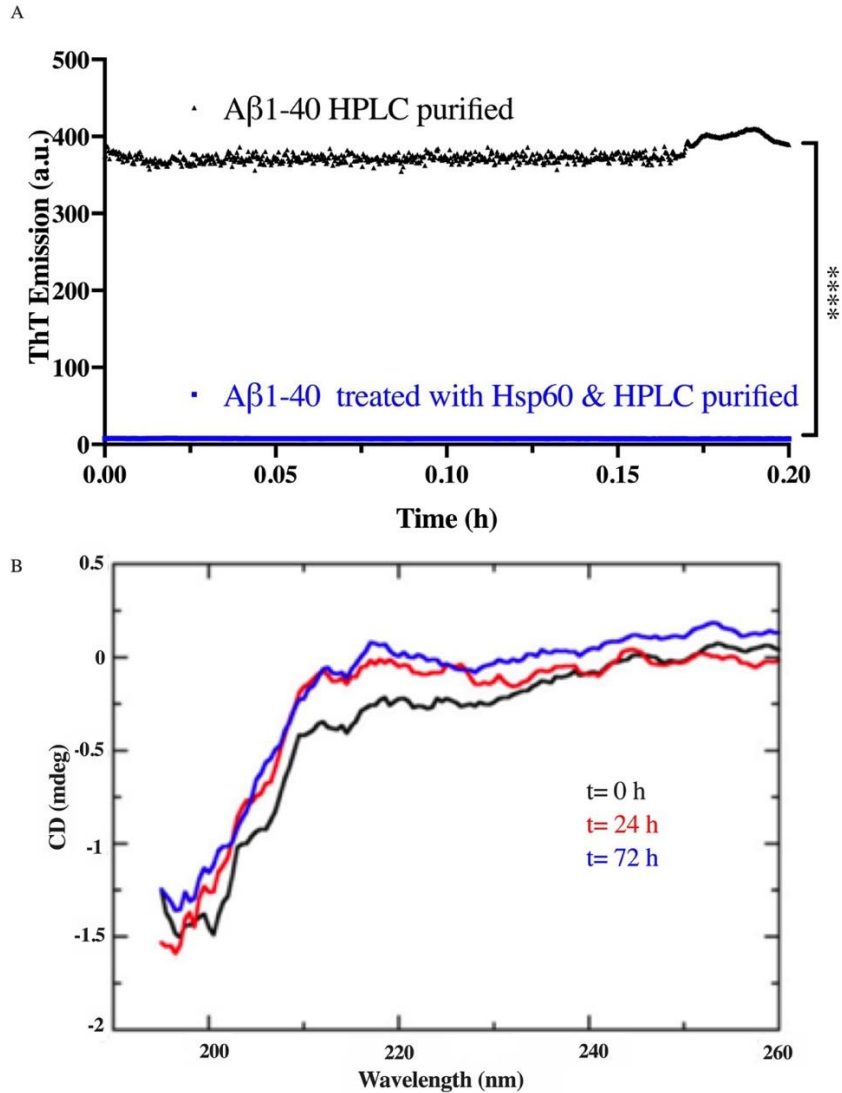
Figure 2.8. Testing the pro-aggregating property of $A\beta_{1-40}$ upon interaction with Hsp60.

A. ThT assay of SEC-HPLC-purified fractions of $A\beta_{1-40}$ pre-incubated with Hsp60 (blue curve) or not (black curve) prior SEC-HPLC purification showed in figure 2.6. Data suggested that purified $A\beta$ monomers have lost the ability to aggregate despite the removal of Hsp60, as compared to $A\beta$ alone. Experimental conditions: ThT 12 μM; λexc ThT=450 nm; λem ThT=484 nm. B. Representative CD spectra of $A\beta_{1-40}$ pre-incubated with Hsp60 and purified with HPLC at time 0 (t = 0 h, black spectrum), 24 hours (t = 24 h, red spectrum) and 72 hours (t = 72 h, blue spectrum), confirming that $A\beta$, upon interaction with Hsp60, retained a random coil structure characteristic of non-aggregated species, as confirmed by the stability of the CD spectrum over time and the minima of absorbance at 195 nm. Adapted from Mangione et al. [166].

EFFECT OF HSP60 ON Aβ1-42 AGGREGATION PATHWAY IN A CELL FREE MODEL

We further validated the anti-aggregating effect of Hsp60, using Aβ$_{1-42}$ as an alternative model of amyloid aggregation. Differently from Aβ$_{1-40}$, the aggregation kinetic of this peptide was much faster and, due to the immediate formation of large aggregates, when prepared at the same experimental conditions used for testing the effect of Hsp60 on Aβ$_{1-40}$ aggregation (50 μM, 37 °C and 200 rpm) as confirmed by the high ThT fluorescence a time zero of the aggregation kinetic (grey spectrum, figure 2.9). As the goal of our investigation was to test the effect of Hsp60 on Aβ$_{1-42}$ aggregation kinetic, we optimized a concentration that allowed a more controlled aggregation kinetic and detection by the ThT assay. As summarized in Figure 2.9, preliminary investigations suggested an anti-aggregating effect of Hsp60 also under this more aggressive model of aggregation. However, further investigation is needed to validate the effect antiaggregating of Hsp60 on Aβ$_{1-42}$ peptide.
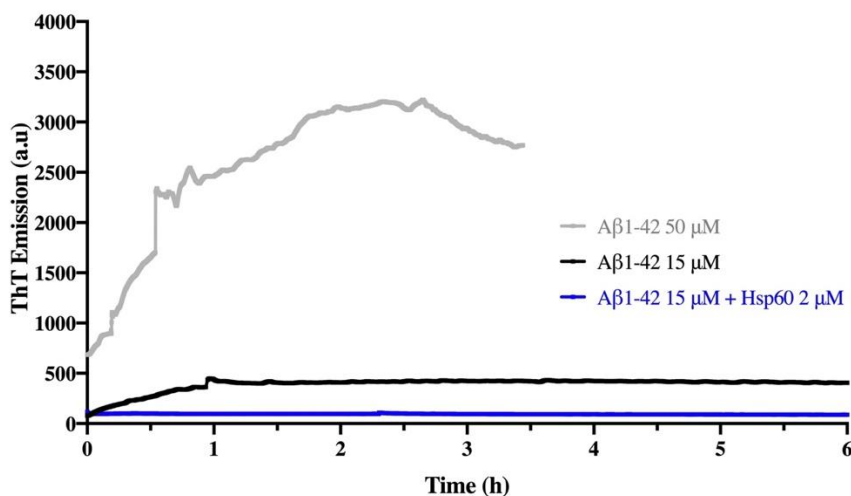
Figure 2.9. Testing the effect of Hsp60 in the aggregation kinetic of Aβ1-42.

Representative ThT assays of a time course kinetics of 50 μM (grey curve),15 μM Aβ$_{1-42}$ alone (black curve) and 15 μM Aβ$_{1-42}$ incubated with 2 μM Hsp60. Data suggests that at the concentration of 50 μM, Aβ$_{1-42}$ is highly unstable and forms large aggregates prior incubating the peptide under pro-aggregating conditions (50 μM, 37 °C and 200 rpm), as confirmed by the ThT fluorescence at 700 a.u. at time zero of the time course measurement.

Conversely, the ThT assay suggests that 15 μM A$\beta_{1\text{-}42}$ is characterized by an exponential nucleation phase and a plateau of ThT fluorescence after 1 h of aggregation, that is not observed when A$\beta_{1\text{-}42}$ is incubated with Hsp60, thus suggesting the antiaggregating effect of Hsp60. Experimental conditions: ThT 12 μM, λexc ThT=450 nm; λem ThT= 484 nm.

EFFECT OF THE CHAPERONIN GROEL ON THE BIOPHYSICAL PROPERTIES OF A$\beta_{1\text{-}40}$

We further tested if the results we obtained with human Hsp60 were reproduced by the bacterial homolog, GroEL. As compelling evidence suggests that Hsp60 activity differs from the less evolved bacterial precursor GroEL [133,134,176,180], we tested the interaction between GroEL and A$\beta_{1\text{-}40}$ using concentrations obtained by the isothermal titration calorimetry analysis done by our collaborators: A$\beta_{1\text{-}40}$ 25 μM and GroEL 7 μM [176]. As previously shown with Hsp60, we tested the effect of GroEL on A$\beta_{1\text{-}40}$ aggregation using both ThT assay and CD spectroscopy (Figure 2. 10). ThT assay showed the effect of GroEL in increasing the lag phase of Aβ aggregation, even though the kinetic was not completely blocked. This data was consistent with CD data summarized in panel B of Figure 2.10.
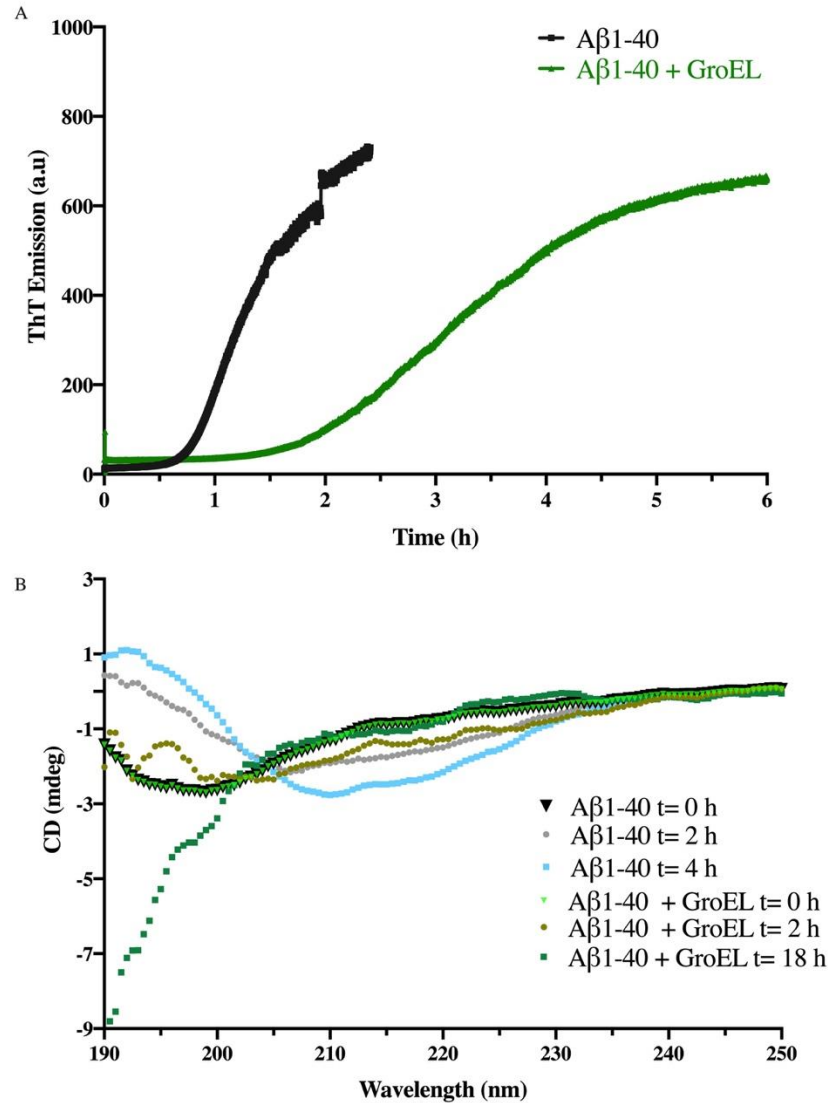
Figure 2.10. Testing the effect of GroEL on the biophysical properties of Aβ1-40.

A. Representative ThT assays of time course kinetics of 25 μM Aβ_{1-40} in 20 mM Tris HCl buffer (pH 7.7) incubated under pro-aggregating conditions (37 °C, 200 rpm) with 7 μM GroEL or alone, suggesting a slower increase of ThT emission over time which is indicative of a moderate effect of GroEL on Aβ aggregation (green curve) as compared to Aβ alone (black curve). Experimental conditions: ThT 12 μM λexc ThT=450 nm; λem ThT=484 nm. B. Representative CD spectra of 25 μM Aβ_{1-40} under pro-aggregating conditions either with or without 7 μM GroEL, at time zero (t= 0 h; Aβ, black curve; Aβ + GroEL, light green curve), after 2 hours (t= 2 h; Aβ, light grey curve; Aβ + GroEL, army green curve) or at the end of the aggregation kinetic (Aβ1-40, t = 4 h, dark grey curve; Aβ + GroEL, t=18 h, emerald green curve), suggesting that GroEL moderately affected the secondary structure of Aβ, as not treated Aβ forms β-sheet conformations after 4 h due to the shift of the spectrum minimum from 195 to 210 nm, that was not observed when Aβ

was incubated with GroEL for 18 h. Measures recorded at 20 ºC and expressed as the average of 30 measurements, expressed in mdeg over wavelength.

Overall, our data suggested that GroEL, under these experimental conditions, delays the process of Aβ nucleation, but differently from the eukaryotic equivalent Hsp60, and does not completely inhibit Aβ aggregation pathway.

IV.   CONCLUSIONS

Hsp60 chaperonin is known to assist the refolding of other proteins [136,181,182], thus giving the rationale to test the direct interaction between Hsp60 and Aβ peptide, which is characterized by a high misfolding and aggregation propensity.

In the work presented in this chapter, we characterized the interaction between these two proteins using Thioflavin T assay, circular dichroism spectroscopy, atomic force microscopy and size exclusion chromatography. Using a cell-free system we investigated protein-protein interactions without the complexity of a cellular environment. We confirmed that the mitochondrial form of human Hsp60 successfully inhibited the aggregation of either $A\beta_{1-40}$ and $A\beta_{1-42}$ peptides, in absence of ATP. Therefore, a possible mechanism of Hsp60 could involve non-covalent interactions between the hydrophobic regions that characterize the inner part of the "donut-structure" of Hsp60 in its active form. The interaction between Aβ and these non-covalent regions could force the aggregation pathway of Aβ toward an "off-pathway" cascade leading to the formation of amorphous aggregates that no longer aggregate. This phenomenon has been already observed for Aβ upon exposure to fatty acids [70]. Interestingly, we could not reproduce the same antiaggregating effect with the bacterial homolog GroEL, thus further suggesting that the possible mechanism of direct inhibition observed with the human homolog Hsp60 could

be linked to a more evolved ability to function when the co-chaperone and ATP are not available, thus making this chaperone more evolved than the bacterial homologue GroEL.

CHAPTER 3. *IN VITRO* ANALYSIS OF THE EFFECT OF HSP60 OVER-EXPRESSION ON APP/Aβ LEVELS

I.   INTRODUCTION

The biophysical investigation of Hsp60-Aβ protein-protein interaction presented in the previous chapter suggested a direct and irreversible inhibitory effect of Hsp60 on Aβ aggregation. As Aβ is known to be a cleavage product of the pro-amyloidogenic processing of APP, in the study presented in this chapter we investigated the effect of Hsp60 on Aβ processing and release from APP *in vitro*.

Previous studies have shown that Hsp60 binds to APP and Aβ *in vitro* [147]. However, the role of Hsp60 in the co-localization of APP/Aβ in the mitochondria remained unknown.

In this work, we aimed to characterize the effect of Hsp60 on APP and Aβ levels using an *in vitro* cell model that stably overexpresses the Swedish variant of APP (7PA2 cells) and that is known to release human Aβ oligomers in the culture medium. Specifically, we designed and characterized a novel cellular model that co-expresses both human APP and Hsp60 and characterized whether overexpressing Hsp60 modulated levels of both APP and Aβ oligomers. We further tested the effect of Hsp60 overexpression on the down-stream toxicity of the naturally secreted Aβ oligomers in the media, as it has been shown that these oligomers are toxic both *in vitro* and *in vivo* [183–185]. Our results suggested that the overexpression of Hsp60 while did not affect APP levels, it significantly reduced the release in the media of toxic Aβ oligomeric species, independently from their concentration, thus proposing Hsp60 as an attractive target for future therapies aiming to reduce Aβ neurotoxicity.

II.   MATERIALS & METHODS

CELL CULTURE

Chinese Hamster Ovary cells (CHO) and 7PA2 cell line (CHO overexpressing human APP751 carrying the V717F or Swedish mutation) were generously donated by Dr. Dennis Selkoe at Harvard Medical School, Boston, MA. For all experiments, cells were used within 10 passages and cultured with DMEM (Corning), 10% FBS (heat inactivated 15 minutes, 56 °C, Sigma Aldrich), 1% penicillin/streptomycin (P/S, Gibco), without (CHO cells) or with G418 antibiotic (0.4 mg/mL, Gibco; 7PA2 and 7PA2/H60 cells), as the plasmid overexpresses both the cDNA for APP and for the resistance for G418/neomycin antibody. 7PA2/H60 cell line was kept in culture for less than 10 passages is the same media used for 7PA2 cells, supplemented with hygromycin B (Corning) 0.6 mg/ml to select only cell that were co-expressing both APP and Hsp60 cDNA, as the plasmid encoding for Hsp60 also carried the resistance for the hygromycin B antibiotic. A detailed description of the transfection of 7PA2 cells is described in the following paragraph.

SH-SY5Y neuroblastoma cell line (ATCC, Manassas, VA) was grown in DMEM/F12 (Corning), 10% FBS (heat inactivated 15 minutes, 56 °C, Sigma Aldrich), 1% P/S (Gibco) and cells were seeded on a 24- or 96-wells plates, the day before each treatment in regular media end treatments were given in serum free/antibiotic free DMEM/F12 media for 24 hours.

For all cell culture studies, experiments were performed at least in triplicates using either cells at different passages or cells from different frozen stocks to allow the statistical analysis of the results obtained.

PLASMID TRANSFECTION

The cell transfection of plasmids, either empty pCMV6 or pCMV6-Hsp60 (both OriGene), was performed with Lipofectamine 2000 (Life technologies, Protocol Pub. No. MAN0007824 Rev.1.0) using the protocol recommended by the manufacturer [186]. In detail, cells were seeded a day prior in order to be 70% confluent at moment of transfection. The day of transfection, lipofectamine was diluted and incubated for 10 minutes at room temperature, to allow the formation of the lipophilic complex of Lipofectamine. Subsequently, pCMV6 plasmids (empty or encoding for human Hsp60 protein) were added to the lipid complex of Lipofectamine and incubated for 10 minutes at room temperature. We used 10% FBS in DMEM media to block the transfection after 5 hours, to allow cells to recover and facilitate replication and internalization of the plasmid. Either 24- or 48-hours post-transfection, cells were seeded on a multi-well plate at desired confluency for further experiments. To obtain the optimal transfection conditions, we tested either different volumes of lipofectamine 2000 (7, 9, 12 µL) or different plasmid concentrations (1,3,5,7 µg) as summarized in Supplementary Table 1 (appendix A) and we tested the expression of the recombinant Hsp60 protein overexpressed by the plasmid using immunocytochemistry. We used DDK antibody to detect recombinant Hsp60, as this antibody recognizes a sequence that is encoded by the pCMV6-Hsp60 plasmid. DAPI (4',6-diamidino-2-phenylindole) was used to counterstain nuclei of the fixed cells. A representative immunocytochemistry of the different transfection conditions tested on both CHO and 7PA2 cells (Supplementary Figure A.1, Appendix A). To quantify the efficacy of the cell transfection, we used western blotting to quantify protein levels (n=3) and immunocytochemistry to quantify the number of positive cells (n=5). For both experiments, we used two-way ANOVA with Tukey's multiple comparisons test to

determine statistical significance between conditions, considering any p value less than 0.05 as statistically significant.

IMMUNOCYTOCHEMISTRY (ICC)

To validate the protein expression, we performed ICC on fixed cells (CHO, 7PA2 and 7PA2/H60) and quantified levels of recombinant Hsp60, total Hsp60 and APP/Aβ proteins. In detail, we first seeded the cells on autoclaved cover-glasses (Fisher Scientific) for 24 hours and washed twice with cold PSB (10 mM in DDI water, pH 7.4, Thermofisher) to remove the culture media prior fixation with cold Methanol/Acetone (50:50 v/v, Sigma Aldrich). Cells were then incubated for 1 hour on ice to allow proper fixation of the cells on the coverslips. Cells were then washed twice for 5 minutes with cold PBS and blocked for 1 hour with 3% BSA (Calbiochem) and 0.05% Tween 20 (Acros) in PBS. All primary antibodies were incubated for 18 hours at 5 ºC and secondary antibodies were incubated for 1 hour at room temperature in the dark, after washing two times for 10 minutes with PBS. All acquisitions were performed with a Nikon A1+ confocal microscope, on fixed cells mounted on Super/frost slides (Fisherbrand, Fisher scientific). Notably, nuclei were stained with DAPI, Aβ/APP proteins were stained with 6E10 antibody (1:250 mouse, Covance), total Hsp60 was stained with anti-Hsp60 antibody (rabbit, Abcam or Origene), recombinant Hsp60 was stained with anti-DDK antibodies (1:1000, mouse Origene or rabbit, Santacruz). Alexa-594 (1:400, red, mouse or rabbit, Abcam), Alexa-488 (1:400, green, mouse or rabbit, Abcam) or Alexa-647 (1:250, far red, mouse or rabbit, Abcam) were used as secondary antibodies. Prior incubation, all antibodies were properly diluted in 1.5% normal goat serum (NGS) diluted in PBS. All confocal acquisitions were analyzed using ImageJ software and statistical analysis of the quantification was done using GraphPad prism 7, using 5 representative fields per condition. Data quantification was expressed as the percentage of positive cells that were also positive to DAPI

counterstaining. The statistical significance of the ICC quantification was determined using ordinary two-way ANOVA, followed by the Tukey's multiple comparison test. Any p-value less than 0.5 was considered as statistically significant.

WESTERN BLOTTING (WB)

We analyzed protein levels in all samples under denaturing conditions, using a sample buffer made with Tris base, glycerol, SDS, H_2O, bromophenol blue and 2-mercaptoethanol (Sigma Aldrich). Electrophoretic runs were performed at constant voltage (80 V for 10 minutes followed by 120 V until the end of the run). Proteins were transferred on a 0.2 μm nitrocellulose membrane (GE Healthcare) at 0.4 A current kept constant for either 1 hour 30 minutes in ice or 18 hours at 0.02 A for 18 h if total proteins loaded into the gel was equal to or higher than 70 μg. After proteins were transferred on the membranes, we performed the antigen retrieval by microwaving the membranes in PBS for 1 minute, followed by 4 minutes wash in PBS. Prior to the blocking step, the presence of transferred proteins on the membrane was assessed by Ponceau Red staining. Membranes were then blocked with Odyssey blocking solution at room temperature for 1 hour. 6E10 (mouse, 1:1000, Covance) or 4G8 (mouse, 1:1000, Santa Cruz) were used to detect APP or Aβ proteins as 6E10 antibody binds to the a. a. sequence 1-16 of Aβ and 4G8 antibody binds to the a. a. sequence 17-14 of Aβ. The total amount of Hsp60 expressed in all CHO, 7PA2 and 7PA2/H60 cells was detected with anti-Hsp60 antibody (1:5000, Abcam). DDK antibody (1:1000, OriGene) was used to detect the recombinant Hsp60 protein overexpressed in 7PA2/H60 cells. β-actin (mouse, 1:2000, Sigma Aldrich), was used as loading control for cytosolic proteins, as β-actin is a component of the cytoskeleton; SOD2 (Genetex, rabbit, 1:1000) was used to confirm the quality of isolated mitochondria as SOD2 protein is specifically expressed in the mitochondria. WB acquisitions were performed with Odyssey LI-COR using manufacturer's protocol. All protein bands were analyzed using

ImageJ software to quantify the band density on n=3-5 blots obtained using biological replicates. The quantification of all western blotting results was expressed as the relative expression by normalizing the band densities to the loading control. The statistical analysis was obtained using 2-tailed unpaired Student's T to compare the different protein expression between different cells. Any p-value smaller than 0.05 was considered as statistically significant. All analyses were obtained using GraphPad Prism 7 or 8.

SUB-CELLULAR FRACTIONATION

Mitochondria were isolated from total cell lysates using a mitochondria isolation kit (Q-proteome, Qiagen) and the quality of the preparation was validated by western blotting using SOD2 antibody (1:1000, rabbit, Genetex). Extracellular fluids were isolated using a revised protocol optimized by others [187] for obtaining a culture media enriched in Aβ species, referred as "conditioned media" (CM) throughout this chapter. Briefly, we first seeded CHO, 7PA2 and 7PA2/H60 cell lines in 10mm X 15 mm Petri dishes (Corning) at about 90% of confluency (1.6 mln cells/mL). Cells were allowed to attach for 3 hours in regular media supplemented with 10% FBS and antibiotics. Subsequently, cells were incubated in serum-free- antibiotics-free- DMEM media for 20 hours in the incubator. Once collected, the media was either concentrated up to 20 times for analysis of Aβ levels via WB and ELISA, or either used not concentrated to assess its cytotoxicity on SH-SY5Y cells as described in the following paragraph of this chapter. To concentrate the culture media, 3 kDa cut-off (Vivaspin, Sartorius) filters were first washed one time with 0.1% BSA (Sigma Aldrich) diluted in DMEM media (Corning) by centrifuging the filters at 6000 rcf for 30 minutes at 5 °C, followed by one wash with DMEM media (20 minutes, 6000 rcf., 5 °C), to reduce the binding of amyloids to the filters. Subsequently, the media collected from CHO, 7PA2 and 7PA2/H60 cells was concentrated in the same filters at

6500 rcf at 5 °C, up to 20 times for about 95 minutes. Once collected, the media was either used or stored a -80 °C supplemented with 50 mM EDTA (Sigma Aldrich).

LACTATE DEHYDROGENASE (LDH) CYTOTOXICITY ASSAY

Cell death of SH-SY5Y neuroblastoma cells was measured 24 hours after treatments with either CM or vehicle using the "Cytotoxicity Assay kit" (Roche), following the manufacturer protocol. Briefly, cytotoxicity was detected indirectly by measuring the absorbance of a dye sensitive to the LDH released in the culture media by damaged cells. We detected the colorimetric reaction spectroscopically using a multi-plate reader (μQuant, Biotek). The cytotoxicity percentage was calculated using the following formula: Cytotoxicity % = [(experimental value – low control)/ (high control – low control)] *100 [188]. Low control was referred to the absorbance value obtained by the spontaneous release of LDH from cells treated with vehicle and was calculated using media from cells treated with serum-free culture media (DMEM/F12 medium, Sigma Aldrich). High control was calculated using media from cells treated with 10% Triton-X 100 serum free culture media and was used as a control from maximum LDH release when cells were exposed to a substance 100% cytotoxic. To obtain a reproducible assay, prior to testing all treatment conditions, we optimized the assay by quantifying both the spontaneous and maximum LDH release of increasing seeding density of SH-SY5Y cells and selected the optimum seeding density for our experiments (Supplementary Figure A4, Appendix A) All samples used for cell treatments were diluted 1:10 or 1:5 in serum-free culture media. Cells were treated either with DMEM media, CHO CM, 7PA2 CM or 7PA2/H60 CM. For all experiments, n=3 biological and n=3 technical replicates were used to assess statistical difference among treatment conditions. Statistical analysis was determined using 2-tailed unpaired Student's T-test and any p-value less than 0.05 was considered statistically significant. All analyses were performed using GraphPad Prism 7.

BI-CINCHONIC ACID (BCA) ASSAY

We determined the protein concentration of all biological samples using a colorimetric assay referred as the BCA assay (Thermo Fisher) according to the manufacturer protocol [189]. In detail, diluted samples (1:40 dilution in DDI water) were incubated for 30 minutes at 37 °C with a mixture of reagents A and reagent B (200 μL final volume, 1:50 v/v) provided by the BCA kit. The colorimetric reaction between samples and reagent mixture was detected based on changes of the absorbance of the bi-cinchonic acid at 562 nm upon interaction with different concentrations of proteins. Absorbance readings were determined using a spectrophotometer (μQuant, Biotek). The concentration of all samples was obtained using the equation obtained from the absorbance intensities of bovine serum albumin (BSA) determined using fixed concentration, from 0 to 1000 μg/mL as a standard.

ELISA

We quantified Aβ levels in cell culture media isolated from CHO, 7PA2 and 7PA2/H60 cell lines and using Human Aβ42 solid phase sandwich ELISA kit (life technologies). To increase the detection, we prepared the culture media concentrated up to 20 times following the previously mentioned protocol [187], and we calculated the protein concentration using the BCA assay. In detail, we diluted 10 μg of samples in a final volume of 50 μl of standard diluent buffer provided by the ELISA kit, supplemented with protease inhibitor cocktail (Thermo Scientific). Each sample was incubated for 3 hours at room temperature in the multi-well pre-coated with primary antibody. Subsequently, we washed the wells four times with wash buffer and incubated for 1 hour at room temperature the samples with secondary antibody (Anti-rabbit IgG-HRP) and chromogen (30 minutes) to allow the detection of Aβ levels in the samples. The detection was obtained spectroscopically using a multiplate reader (μQuant, Biotek) and intensities of emission

acquired at 450 nm. The quantification of Aβ levels in all samples was extrapolated from the polynomial equation obtained by a standard curve of human Aβ over a range between 0 and 1µg/mL and upon subtraction of the background absorbance. To analyze the statistical significance of Aβ levels between 7PA2 and 7PA2/H60 media, we used 2-tail unpaired Student's T test to analyze n=3 biological experiments with n=2 technical replicates. Any p value less than 0.05 was considered as statistically significant.

STATISTICAL ANALYSIS

All statistical analyses were done using GraphPad Prism 7. Two-tailed unpaired Student's T-test was used to compare two group of results and any p-value less than 0.05 was considered as statistically significant. Two-way ANOVA was used to analyze the significance between multiple data sets and for the comparison of multiple variables either within the same group of data or between different group of data. For all two-way ANOVA tests, Tukey's test for multiple comparisons was used for post-hoc analysis and a p value less than 0.05 was considered as statistically significant.

III.   RESULTS

DESIGN OF 7PA2/H60 CELL LINE AND BIOMOLECULAR CHARACTERIZATION

To test the effect of Hsp60 on APP and Aβ proteins, we designed the "7PA2/H60" cell line that co-expresses both the Swedish mutated form of human APP and human Hsp60. As summarized in Figure 3.1, we first transfected 7PA2 cells with either a pCMV-empty plasmid or pCMV6- encoding for human Hsp60 protein. We obtained the selection of the cell clone co-expressing both APP and Hsp60 proteins using specific antibiotics,

based on the antibiotic resistance delivered by the plasmids. To preserve the expression of both recombinant proteins, we used doses of antibiotics that were known to be toxic for the naïve CHO cells, the latter cells being used as untransfected control (data not shown). The plasmid carrying APP overexpression in 7PA2 cell line expressed the resistance for neomycin (or G418 antibody), while the plasmid encoding for Hsp60 expressed also hygromycin B resistance. We obtained the co-expression of APP and Hsp60 in the 7PA2/H60 cell line using G418/hygromycin B 0.6 mg/0.6mg in DMEM, 10 % FBS, 1% P/S. As summarized in Figure 3.1, upon plasmid transfection, we validated the 7PA2/H60 cell line using both western blotting and immunocytochemistry.

As previously mentioned, Hsp60 is mostly active in the mitochondria [133,190] while Aβ is mainly released extracellularly from the pro-amyloidogenic cleavage of APP which is a transmembrane protein [8]. Therefore, we analyzed changes of APP and Aβ levels upon Hsp60 overexpression in the mitochondria, intracellularly and extracellularly.
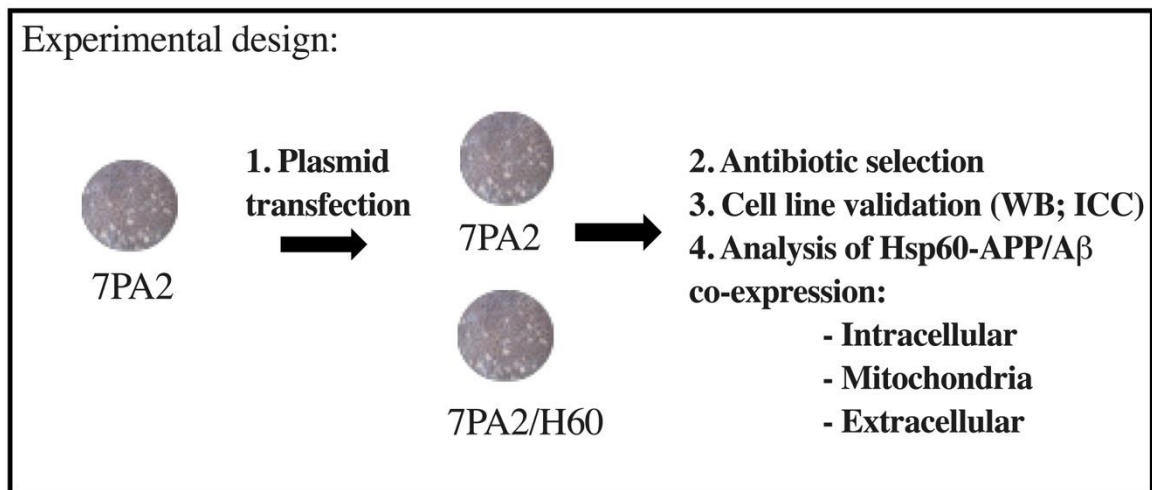
Figure 3.1. Experimental design of 7PA2/H60 cell line design and characterization.

1. 7PA2 cell line was first transfected with pCMV6 plasmids either empty, as a control, or encoding for Hsp60 protein to obtain the 7PA2/H60 cell line. 2. Antibiotic selection of 7PA2/H60 positive cells was obtained using hygromycin B antibiotic, based on the antibiotic resistance carried by the pCMV6 plasmid and expressed only by transfected cells. 3. 7PA2/H60 cell line validation was obtained using WB and ICC to compare protein levels (APP, Aβ and Hsp60) to 7PA2 and naïve CHO cells as controls. 4. Sub-cellular

fractionation and analysis of Hsp60-APP/Aβ co-expression using either WB or ELISA in subcellular fractions: intracellular, mitochondria and extracellular.

To validate the positive expression of both APP and Hsp60 proteins, we tested protein levels using western blotting, to confirm the positive expression of both recombinant APP and Hsp60, compared to naïve CHO cells and 7PA2 cells transfected with an empty pCMV6- plasmid (Figure 3.2). Western blotting results confirmed the overexpression of recombinant Hsp60 in 7PA2/H60 cell line, as confirmed by the 60 kDa band detected by DDK antibody, as this antibody selectively detects the tag expressed in the recombinant protein (DDK). Further, the co-localization between DDK and Hsp60 antibodies further validated the overexpression of Hsp60 protein in 7PA2/H60 cells (Figure 3.2. A) as compared to 7PA2 cells that were either not transfected or transfected with an empty pCMV6- plasmid.

We also confirmed APP overexpression in both 7PA2 and 7PA2/H60 cells using the anti-amyloid 6E10 antibody, which detects a band around 120 kDa, which is relative to APP protein and multiple bands a lower molecular weight, which are relative to different aggregation forms of Aβ. Notably, Hsp60 protein was detectable in all cell lines, as this chaperone is ubiquitously expressed. A quantification of the protein levels is summarized in Figure 3.2.B. In detail, we observed a significant expression of APP in both 7PA2 and 7PA2/H60 cells (*$p<0.0001$) and a significant expression of recombinant Hsp60, detected by DDK antibody, only in 7PA2/H60 cells (*$p=0.0212$).

As our goal was to test APP and Hsp60 levels in different cellular fractions, we further tested the long-term stability of APP and Hsp60 co-expression in 7PA2/H60 cells, to avoid possible false negative results due to a loss of one of the plasmids. As summarized in Figures 3.2 C and D, we validated the 7PA2/H60 cell lines after 1 week and 1 month of transfection and our results confirmed the long-term co-expression of both APP and Hsp60 proteins.
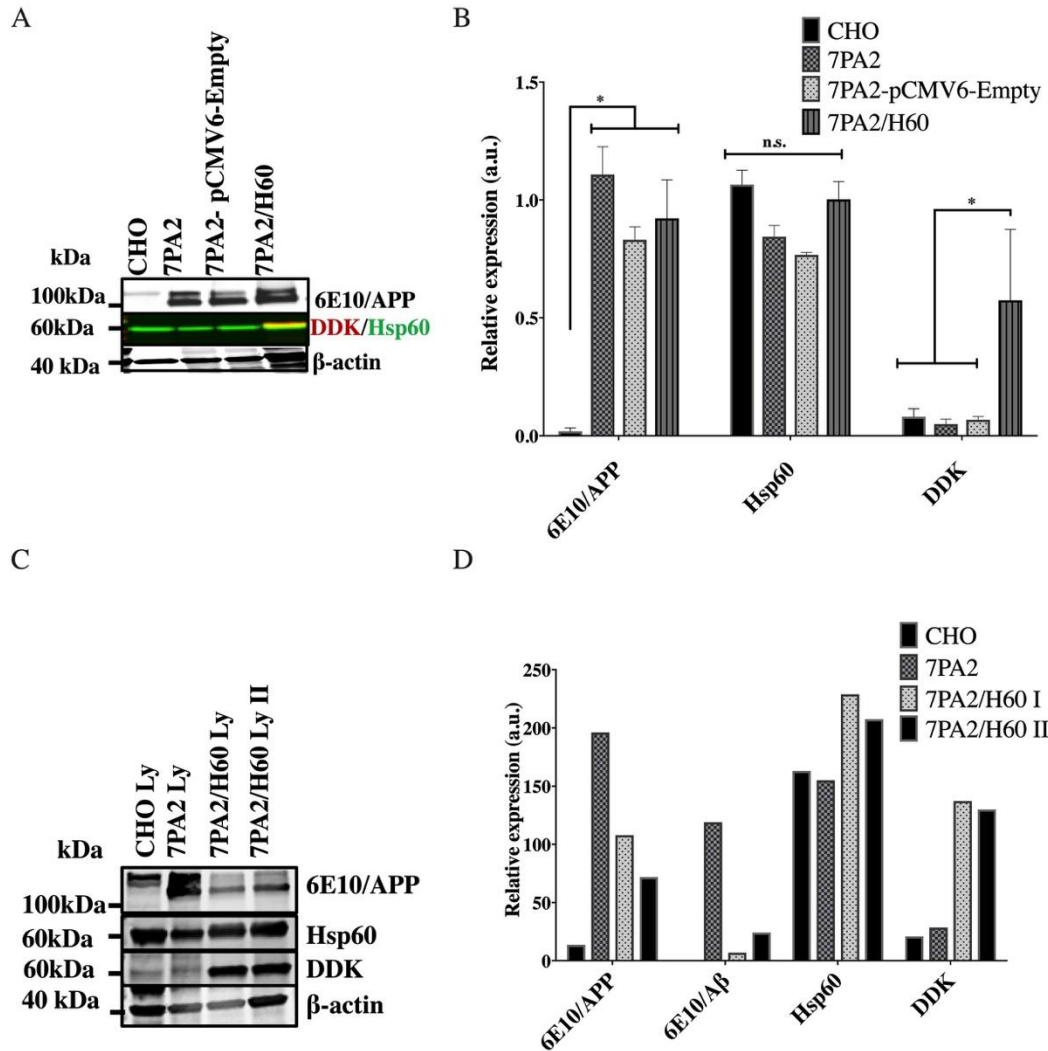
Figure 3.2. Validation of 7PA2/H60 cell line using WB.

A. Representative WB of CHO, 7PA2 and 7PA2/H60 cell lysates 1 week after transfection, confirming that 7PA2 (II and III lane) and 7PA2/H60 (IV lane) cells were positive to 6E10 antibody which detects APP protein, that only 7PA2/H60 is positive to DDK antibody, which detected recombinant Hsp60, and that all cell lines were positive to total Hsp60 antibody as Hsp60 chaperone is ubiquitously expressed. β-actin was used as a loading control, to normalize the quantifications shown in B and D. B. Normalized expression of protein levels detected by WB shown in A, showing the statistical analysis done using 2-way ANOVA followed by Tukey's multiple comparisons test (n=3; 6E10, $*p<0.0001$; DDK, $*p=0.0212$ (CHO vs. 7PA2/H60), $p=0.0133$ (7PA2 vs. 7PA2/H60), $p=0.0175$ (7PA2/H60 vs 7PA2-pCMV6-Empty). Results presented as the average of the relative expression of proteins normalized to β-actin ± SD. C. Representative WB of total lysates of CHO, 7PA2 and 7PA2/H60 cells after 1 week (7PA2/H60 Ly I) and after 1 month of plasmid transfection (7PA2/H60 Ly II) using 6E10 to detect APP and Aβ, DDK and Hsp60 antibodies to validate the co-expression of both total and recombinant Hsp60 proteins in 7PA2/H60 cell line. D. Quantification of protein levels in total cell lysates showing the

76

increased expression of APP and Aβ in 7PA2 and 7PA2/H60 lines detected by 6E10 antibody and the increased expression of recombinant Hsp60 in 7PA2/H60 detected by DDK antibody. Data presented as relative expression normalized using β-actin as loading control.

In parallel experiments, we further characterized 7PA2/H60 cell line using ICC as shown in Figures 3.3 and 3.4. Specifically, we used 6E10 antibody to validate the expression of APP and Aβ proteins in both 7PA2 and 7PA2/H60 cell lines, compared to CHO cells; we used DDK antibody to confirm the expression of recombinant Hsp60 only in 7PA2/H60 cell line.
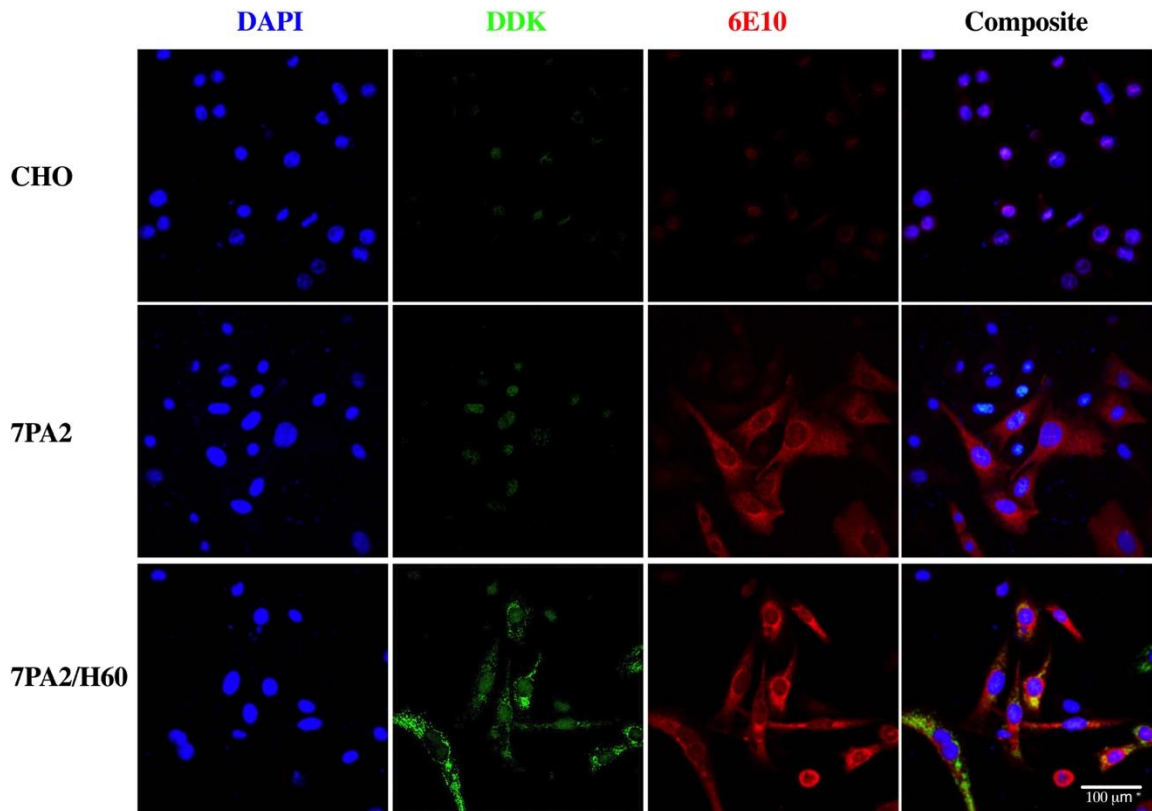
Figure 3.3. Validation of recombinant Hsp60 and APP co-expression in 7PA2/H60 cell line using ICC.

Representative confocal acquisitions confirming the co-expression of both APP/Aβ and recombinant Hsp60 only in 7PA2/H60 cell lines, as compared to CHO that does not express APP/Aβ nor recombinant Hsp60, and as compared to 7PA2 cells that only express APP/Aβ. In blue, DAPI staining for nuclei; in green, DDKrb conjugated to Alexa-Fluor 488 used to stain recombinant Hsp60; in red, 6E10ms conjugated to Alexa-Fluor 647 used to stain

APP/Aβ proteins. The composite panels represented the merge of all three channels. Scale bar: 100 μm.
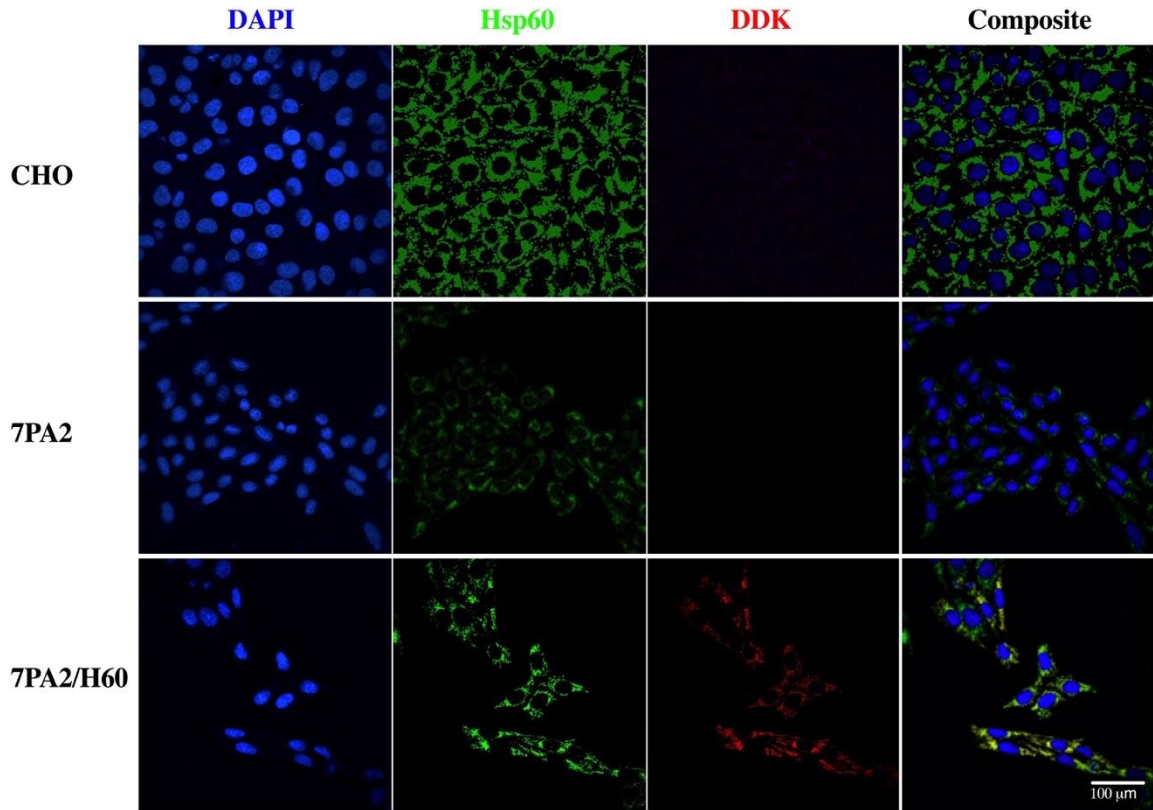
Figure 3.4. Validation of recombinant Hsp60 in 7PA2/H60 cell line using ICC.

Representative confocal acquisitions confirming the co-expression of recombinant Hsp60 and total Hsp60 only in 7PA2/H60 cell lines, as compared to both CHO and 7PA2 cells that are only positive for total Hsp60 antibody. In blue, DAPI staining for nuclei; in green, Hsp60rb conjugated to Alexa-Fluor 488 staining for total Hsp60; in red, DDKms conjugated to Alexa-Fluor 647 staining for recombinant Hsp60 protein. The composite panels represented the merge of all three channels. Scale bar: 100 μm.

A quantification of the immunocytochemistry data obtained is shown in Figure 3.5.
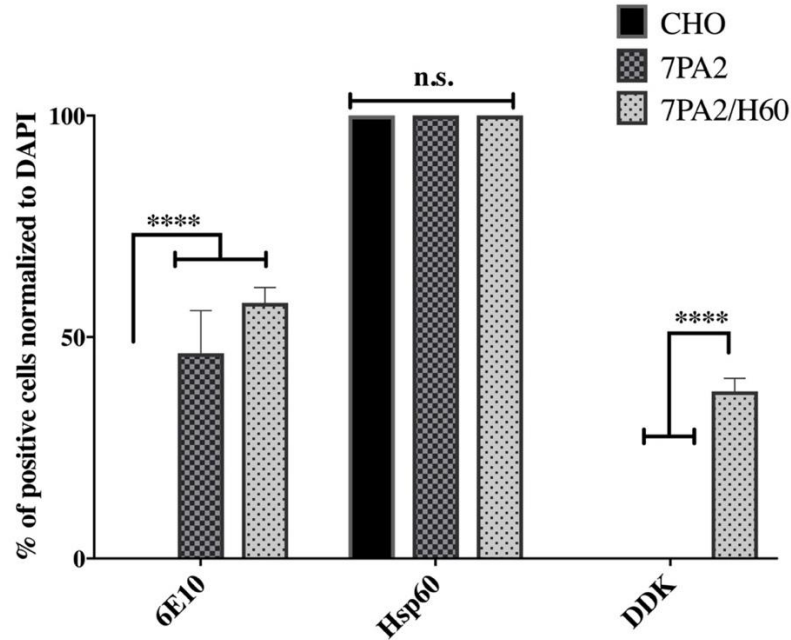
Figure 3.5. Quantification of Hsp60 and APP/Aβ staining to validate 7PA2/H60 cell line.

Quantification of the number of positive cells expressing APP/Aβ detected by 6E10 antibody, total Hsp60 detected by anti-Hsp60 and recombinant Hsp60, that is detected by DDK antibody using ICC. Data confirming the significant expression of APP/Aβ only in 7PA2 and 7PA2/H60 as compared to CHO cells and the significant expression of recombinant Hsp60 only in 7PA2/H60 as compared to CHO and 7PA2 cells. Hsp60 was detected in all three cell lines as this protein is ubiquitously expressed. Data is expressed as the average ± SD of the percentage of positive cells normalized to DAPI, that was used to counterstain the nuclei in all cells. Statistical significance was calculated using multiple 2-tailed unpaired Student's T-test and any p-value less than 0.05 was considered as statistically significant (n=5; ****p<0.0001).

Overall, data suggested a successful co-expression of Hsp60 and APP proteins in 7PA2 cells and therefore the newly designed 7PA2/H60 cell line can be a suitable model for testing the co-expression of both Hsp60 and APP proteins *in vitro*.

INVESTIGATING APP/HSP60 CO-EXPRESSION OF IN SUB CELLULAR COMPARTMENTS

We investigated whether Hsp60 had any effect on APP or Aβ levels using 7PA2/H60 cell line as a model. To analyze the co-expression of both proteins in different sub-cellular fractions, we first validated and optimized the protocols to collect both mitochondria, intracellular and extracellular fluids, as described in the method section, in Supplementary Table 1 and in Supplementary Figure 1 (Appendix A).

Once all protocols were validated, we investigated the effect of Hsp60 overexpression on APP/Aβ levels using 6E10 and Hsp60 antibodies using western blotting. Even though 6E10 antibody has been extensively used to quantify Aβ aggregates [18,191,192], we previously confirmed the molecular weight of 6E10 bands in different cell lysates from CHO, 7PA2 and 7PA2/H60 (n=4) and we confirmed that the bands we selected were not APP fragments using c-APP antibody, an antibody specific for APP (Supplementary Figure 2, appendix A).

As shown in Figure 3.6.A, the representative western blotting shows that in CHO, 7PA2 and 7PA2/H60 cell lysates, 6E10 detected multiple bands that are relative to APP and Aβ in different aggregation stages, while Hsp60 antibody detected a 60 kDa band relative to total Hsp60 levels. We also used β-actin antibody as loading control for all samples for the quantification of the antibody levels shown in panels B and C of Figure 3.6. We analyzed the normalized intensities of 6E10 positive bands for APP levels and CHO, 7PA2 and 7PA2/H60 cell lysates (3.6.B), and the 6E10 positive molecular weight bands from 4 to 20 kDa, that are relative to small Aβ aggregates (3.6.C). Overall, data suggest that overexpressing Hsp60 does not affect APP levels and Aβ levels, despite being not significant (p= 0.5081) trended to be reduced in 7PA2/H60 line compared to 7PA2 cells.
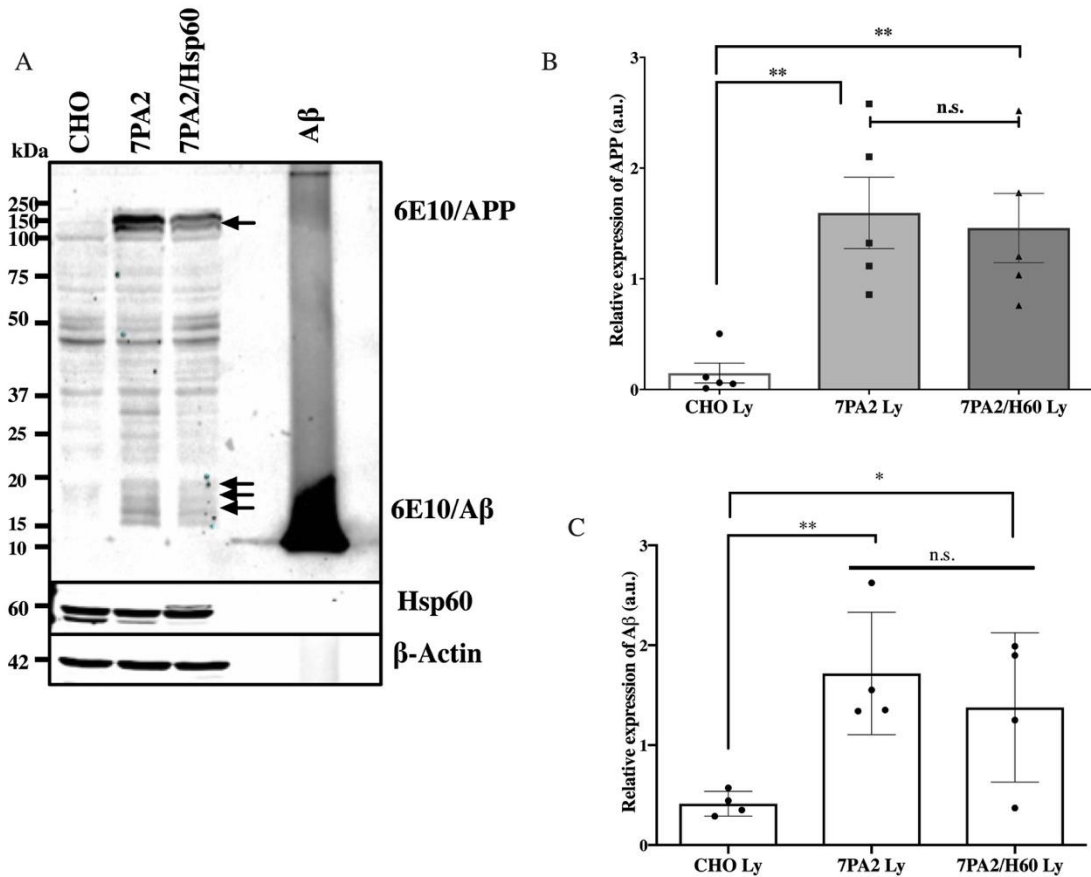
Figure 3.6. Analysis of Hsp60- APP/Aβ co-expression intracellularly using WB.

A. Representative WB of total cell lysates of CHO, 7PA2 and 7PA2/H60 cell lysates, using 6E10 antibody to detect both APP and Aβ proteins, anti-Hsp60 to detect total levels of Hsp60 and anti-β-actin antibody to detect actin as loading control, suggesting that APP/Aβ levels were not affected by Hsp60 overexpression. Black arrows indicating APP (~120 kDa band) and Aβ forms (~8-20 kDa bands) B. Quantification of APP levels using 6E10 antibody indicating a significant expression of APP in both 7PA2 and 7PA2/H60 cells, as compared to CHO and not significant changes in APP levels upon Hsp60 over-expression when compared 7PA2 to 7PA2/H60 cells using 2-tailed unpaired Student's T test (n=5; **p= 0.0025 (CHO vs. 7PA2), **p=0.0038 (CHO vs. 7PA2/H60). C. Quantification of less than 20 kDa molecular weight bands (indicated by the black arrows in A) detected by 6E10 antibody, indicating a trend of reduced Aβ levels upon Hsp60 overexpression, that was not significant as reported by the Student's T-test (**p=0.0059; *p=0.0439). The quantification of WB bands presented in panel B, C was done using ImageJ software on n= 4 blots and statistical significance calculated using GraphPad Prism. Data presented as the average ± SD of the relative expression of protein levels normalized to β-actin.

81

As Hsp60 is a chaperone known to be mostly active in the mitochondria, and previous studies suggested that APP accumulates in the mitochondria [147], we tested changes of the levels of both proteins in the mitochondria as shown in Figure 3.7.
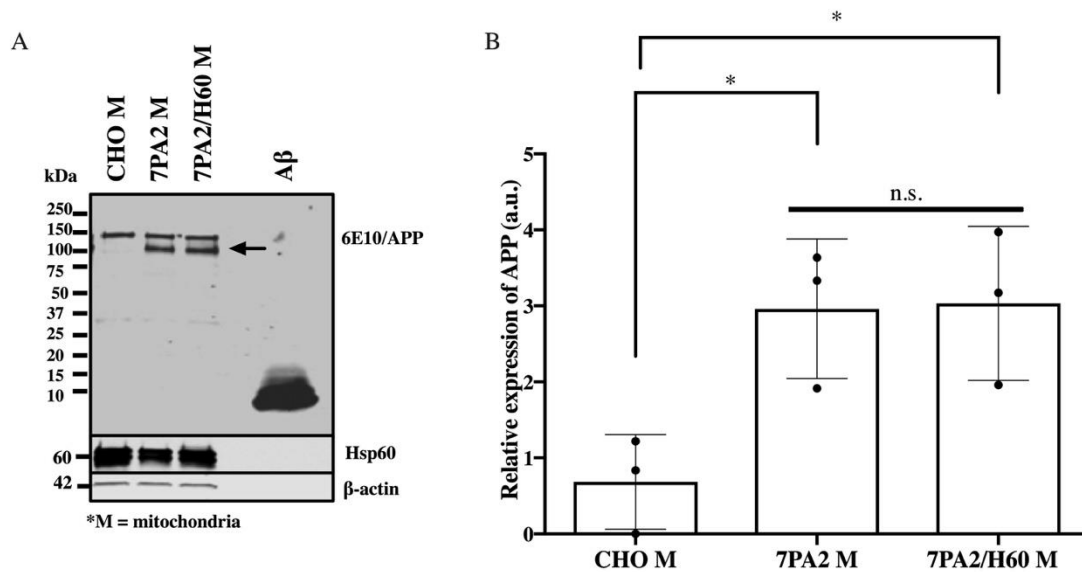
Figure 3.7. WB analysis of Hsp60- APP/Aβ co-expression in mitochondria fractions.

A. Representative WB of mitochondria fractions (M) of CHO, 7PA2 and 7PA2/H60 cells, using the anti-amyloid antibody 6E10 to detect APP levels (indicated by the black arrow), anti-Hsp60 to detect total Hsp60 and anti-β-actin as loading control, suggesting that APP levels were not affected by Hsp60 overexpression. B. Quantification of APP levels in mitochondria fractions detected by the anti-amyloid 6E10 antibody indicating a significant expression of APP in both 7PA2 and 7PA2/H60 cells, as compared to CHO and not significant changes in APP levels upon Hsp60 over-expression when compared 7PA2 to 7PA2/H60 cells. Quantification of WB bands was done using ImageJ software on n= 3 blots and statistical significance was verified using 2-tailed unpaired Student's T-test. Data presented as average ± SD of the relative expression of protein levels normalized to β-actin.

Our analysis reported that APP levels were not affected by Hsp60 overexpression, thus suggesting that Hsp60 does not affect APP localization in mitochondria. Conversely, we were not able to detect Aβ in mitochondria neither in 7PA2 or 7PA2/H60 in our experimental conditions.

As it has been widely established that 7PA2 cells secreted Aβ into the culture media that aggregate into toxic oligomers once released [184,187], we tested whether Hsp60 had an effect on the levels of Aβ released in the media. As shown in Figure 3.8, we first attempted to optimize a protocol for improving the detection of both APP and Aβ in the media, as 7PA2 cells secrete Aβ in the range of picomolar, which is below detection limits of common western blotting techniques. However, western blotting results revealed that secreted Aβ in the media was below detection limits even upon concentration of the media 20 times. Therefore, we analyzed the concentration of Aβ secreted in the media of both 7PA2 and 7PA2/H60 cells using a much more sensitive Aβ42 ELISA (Figure 3.8.B).
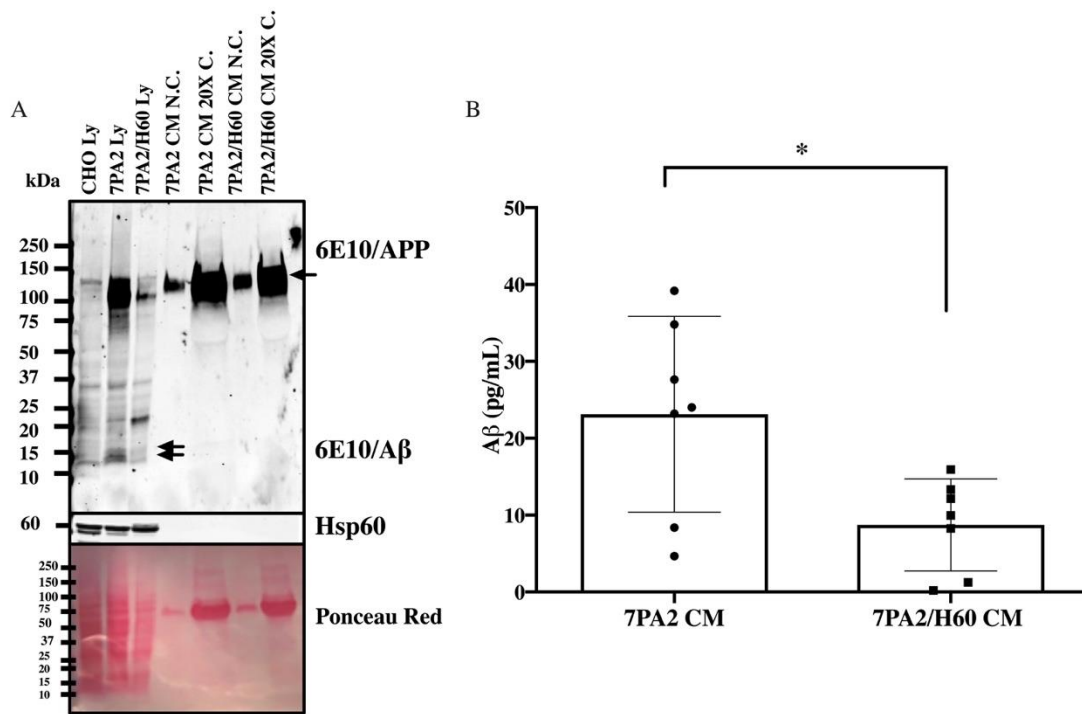
Figure 3.8. Hsp60 overexpression significantly reduces the release of Aβ in extracellular fluids.

A. Representative WB and red Ponceau membrane staining of CHO, 7PA2 and 7PA2/H60 cell lysates (Ly) and secreted conditioned media (CM) either not concentrate (N.C.) or concentrated 20 times (CM 20X C.), using anti-amyloid 6E10 antibody to detect APP and Aβ proteins as indicated by the black arrows, anti-Hsp60 antibody to detect total Hsp60. Data suggesting that both 7PA2 and 7PA2/H60 cells release in the media 6E10 positive

bands compatible with APP protein (~ 120 kDa band). Media was analyzed both not concentrated or concentrated to increase the detection of Aβ that however was below WB detection under these experimental conditions. Anti-Hsp60 WB suggests that Hsp60 is only present intracellularly (Ly) and not in the media (CM). Ponceau red was used to control secreted proteins in the culture media. B. Aβ$_{1-42}$ ELISA of conditioned media (CM) concentrated from CHO, 7PA2 and 7PA2/H60 cell lines suggests that Hsp60 overexpression significantly reduces the amount of Aβ secreted in the media. 2-tailed unpaired Student's T test was used to test statistical significance between the two conditions. Aβ levels are expressed as the average concentrations expressed in pg/mL ± SD (n=7; *p=0.0191).

Interestingly, Hsp60 overexpression significantly reduced Aβ secreted levels in 7PA2/H60 media compared to 7PA2, as confirmed by the statistical analysis of ELISA results.

Overall, data suggested that overexpression of Hsp60 might not have a direct effect on APP protein levels, but it might affect either the downstream cascade of APP processing or the clearance of APP-derived fragments, thus resulting in a reduction in Aβ levels in the extracellular fluids.

THE EFFECT OF HSP60 UP-REGULATION ON THE DOWNSTREAM TOXICITY OF AMYLOID BETA OLIGOMERS

Our next goal was to test whether Hsp60 changed Aβo-driven neurotoxicity *in vitro*. Mainly, we investigated the effect of Hsp60 over-expression on naturally secreted oligomers, released *in vitro* by 7PA2/H60 cell line and we compared our results to cells treated with 7PA2 extracellular media, as this cell media is known to be cytotoxic due to the release toxic oligomers in the media [184]. We quantified changes in cytotoxicity using LDH assay, as described in material and methods.
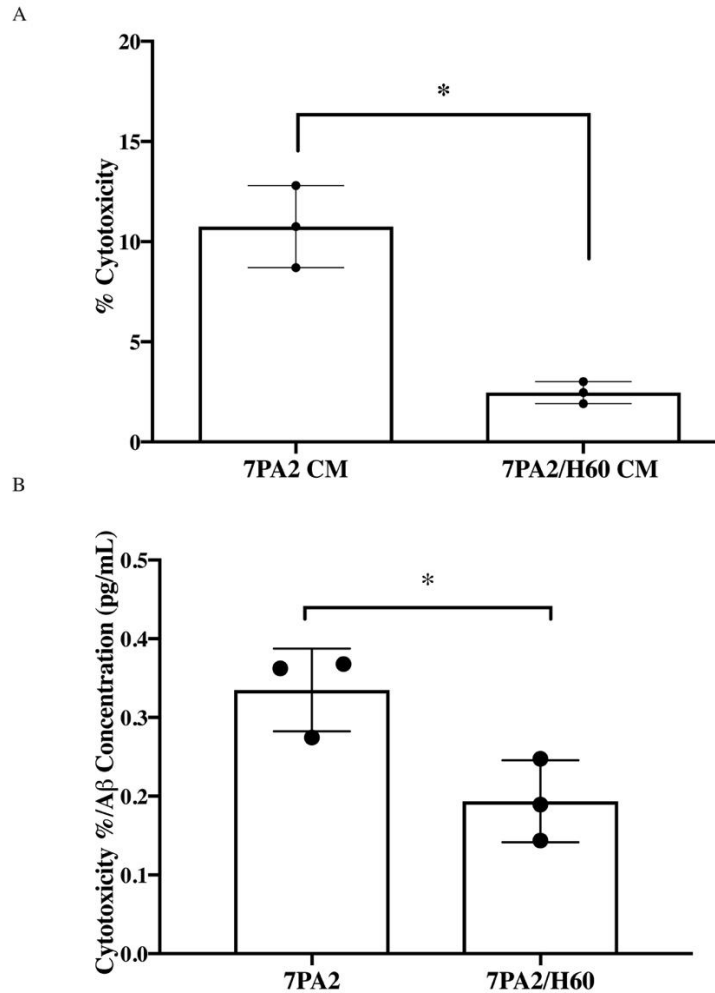
Figure 3.9. Hsp60 overexpression significantly reduces the cytotoxicity of naturally secreted Aβ in the culture media (CM).

A. LDH assay of SH-SY5Y cells treated 24 hours with conditioned media extracted from 7PA2 and 7PA2/H60 cell lines (7PA2-CM or 7PA2/H60-CM), suggesting that Hsp60 overexpression significantly reduces both Aβo-derived secreted cytotoxicity. Statistical significance calculated using 2-tailed unpaired Student's T-test (n=3; *p=0.0025). Data is expressed as the average of cytotoxicity % ± SEM. B. Statistical analysis of the ratio between cytotoxicity % data shown in A and the Aβ levels secreted in the media obtained by ELISA shown in Fig.3.8. Data confirms that Hsp60 overexpression reduces the cytotoxicity independently from the concentration of Aβ. Data is expressed as the average ± SEM and statistical significance obtained using 2-tailed unpaired Student's T-test (n=3; *p=0.0294).

As expected, 7PA2 cell line media was toxic for neuroblastoma cells, because of the release of cytotoxic Aβo in the media (Figure 3.9.B). However, as we compared the

cytotoxicity of 7PA2 media to 7PA2/H60 media, data suggested that 7PA2/H60 media was significantly less toxic than 7PA2 media. This result suggested that Hsp60 overexpression either reduced the total levels of Aβ released in the media or reduced specifically toxic Aβo species in the media as we reported in the previous chapter that Hsp60 directly inhibits Aβ aggregation. We further analyzed the cytotoxicity results normalized by the concentration of Aβ released in the media obtained by ELISA. Interestingly, comparing the ratio between cytotoxicity and Aβ concentration between 7PA2 and 7PA2/H60 media suggested that 7PA2/H60 was significantly different from 7PA2 media.

IV.   CONCLUSIONS

Our data suggest a direct effect of Hsp60 on Aβ release without affecting the intracellular levels of both APP and Aβ. The analysis of the changes in cytotoxicity of naturally secreted Aβ, upon Hsp60 overexpression *in vitro,* suggested that Hsp60 significantly reduced the cytotoxicity of naturally secreted Aβ oligomers. Further, our analysis also suggested that the reduced cytotoxicity observed with 7PA2/H60 might be due to a specific effect of Hsp60 on toxic Aβ oligomers.

The protective action of Hsp60 into the mitochondria and the crucial role of Hsp60 in preserving mitochondria homeostasis from misfolded proteins was already proposed [89,193]. Further, *in vitro* studies from others already suggested that Hsp60 could interact with both APP and Aβ, but the effect of this interaction was still poorly investigated [147]. Our results strongly suggest that up-regulation Hsp60 affects the pro-amyloidogenic processing of APP; possibly by preventing the formation of cytotoxic Aβ oligomeric species.

CHAPTER 4. THE PROTECTIVE EFFECT OF HSP60 AGAINST Aβ OLIGOMER SYNAPTIC TOXICITY

I.   INTRODUCTION

In our previous studies we showed the interaction between Hsp60 and monomeric Aβ in a cell-free model and that Hsp60 irreversibly inhibited its aggregation [166]. We further discussed how Hsp60 overexpression reduced naturally secreted Aβ in the extracellular media and reduced cytotoxicity of the culture media. However, whether Hsp60 can also interact with preformed Aβ oligomers (Aβo) and negate their neurotoxicity via altering their structural polymorphism was not clarified.

Among all triggering factors contributing to the onset of AD, the synaptotoxicity of Aβo is believed to be one of the earliest events leading to the clinical manifestation of the disease [14,72,194]. Therefore, to find effective strategies to prevent Aβo synaptotoxicity could contribute to the design of disease-modifying therapies relevant for AD.

The goal of the study presented in the following chapter is to investigate the interaction between Hsp60 and pre-formed Aβo, and to test whether this interaction caused changes in the Aβo aggregation pathway and a downstream change of Aβo-derived synaptic toxicity. We used both *in vitro* and *ex vivo* approaches to characterize the effect of Hsp60 on preformed Aβo. Our results supported a direct impact of Hsp60 on Aβo toxic

structure thus alleviating Aβo-induced synaptic toxicity and the impairment of long-term potentiation, which are two of the main alterations that characterize early AD pathogenesis.

II. MATERIALS AND METHODS

PREPARATION OF THE PROTEIN SAMPLES

Amyloid β oligomers (Aβo): Aβo for *in vitro* experiments were prepared as previously published [153]. Briefly, 1 mg of lyophilized peptide was solubilized in 1.5 ml acetonitrile/water 1:1 (v/v), to remove impurities. The suspension was left at room temperature for 10-15 minutes and aliquoted into three 1 ml tubes (Eppendorf) containing 0.03 mg of Aβ and further lyophilized and stored at -20 °C until use. The day of the experiment, aliquots were suspended in Hexafluoro-2-propanol, HFIP (200 μL for each aliquot used) and left at room temperature for 10-20 minutes. The solution was then transferred to a new tube with a stirrer and diluted with DDI water (700 μL for each aliquot) in order to obtain a nominal concentration of 95 μM. The peptide solution was gently mixed and covered with a cap with holes to allow the evaporation of HFIP and the process of protein aggregation. The peptide was left oligomerize at room temperature and under agitation for 2 days. Oligomers are either used immediately or stored at -80 °C until use.

Hsp60: for cell culture experiments, aliquots of active human Hsp60 (ATGen) were diluted to 2 μM or 1 μM in buffer PBS 1X and further diluted in DMEM/F12 to 10-fold for cytotoxicity experiments. All sample preparation procedures were conducted in asepsis conditions. All samples' final concentrations were calculated mathematically, and final samples were prepared on ice. The final concentrations of Hsp60 was kept consistent with our published biophysical investigations [195].

IMMUNOPRECIPITATION (IP)

Pre-formed Aβo was incubated with Hsp60 as described previously and immunoprecipitated using magnetic beads (dynabeads, Life technologies) coated with the anti-amyloid β antibody 4G8 (1:250 in PBS 1X, mouse, Covance) according to manufacturer. In detail, 50 μL dynabeads were incubated with antibody overnight with 4G8 antibody at 4 °C under constant agitation to allow the binding of the antibody to the magnetic beads. Subsequently, the beads were washed three times with 0.05 % Tween 20 in PBS and incubated with either vehicle, 5 μM Aβo, 5 μMAβo + 0.2 μM Hsp60 or 0.2 μM Hsp60 (final volume: 100 μL) overnight at 4 °C to allow the pulldown of the proteins that are able to interact with 4G8 antibody. Samples were then analyzed by western blotting using anti-Hsp60 antibody (1:5000, rabbit, Abcam) to detect Hsp60 protein and anti-amyloid β 6E10 antibody (1:1000, mouse, Covance) to detect Aβo. As controls, IP with no proteins, input and unbound fractions were also tested to exclude any aspecific binding of the antibodies. The immunoprecipitation was performed in triplicate using different stocks of both Aβo and Hsp60.

PK ASSAY

Proteinase K (PK) assay of 50 μM Aβo, 50 μM Aβo + 2 μM Hsp60 or 2 μM Hsp60 was done using a protocol previously published by others [60] that allow to test the different sensitivity of protein to the enzymatic digestion of PK. Briefly, all samples were incubated at 37 °C for 1 h prior incubating all samples with 0.05 μg/μL PK (Millipore) at 37 °C, for 2 h. Digestion activity of PK was blocked at the desired incubation time (0, 30', 1 h, 2 h) by boiling the samples prior analysis by WB (n=3).

BIS-ANS ASSAY

According to what previously published [196], 4,4'-dianilino-1,1'-binaphyl-5,5'disulfonic acid, dipotassium salt (bis-ANS) was freshly dissolved in 10 mM glycine-NaOH buffer (pH 7.4) at a final concentration of 10 μM and kept in the dark until use. 247.4 μL of bis-ANS solution was then added to 2.6 μL sample of 50 μM Aβo, 50 μM Aβo + 2 μM Hsp60, 2 μM Hsp60 alone or vehicle. All time course kinetics (n=3 independent experiments with n=3-5 technical replicates) were performed in the dark at room temperature and the fluorescence of the bis-ANS probe was measured spectroscopically at specific time points (0, 2, 4, 6, 8, 24 h) upon excitation at λexc 380nm at λem 520 nm using a spectrofluorometer (SpectraMax M2 multiplate reader, Molecular Devices.). Both negative (buffer only) and positive controls (bis-ANS alone) were also analyzed under the same conditions. Statistical difference between experimental conditions was estimated using 2-way ANOVA, followed by Tukey's test for multiple comparisons using GraphPad Prism 8. Any p-value less than 0.05 was considered as statistically significant.

WESTERN BLOTTING (WB)

WB was performed using a 4-20% pre-casted gels to allow a better resolution of the multiple Aβo aggregates in denaturing conditions using a sample buffer made with Tris base, glycerol, SDS, H_2O, bromophenol blue and 2-mercaptoethanol (Sigma Aldrich). Electrophoretic runs were performed at constant voltage (80 V for 10 minutes followed by 120 V until the end of the run) using a vertical electrophoretic chamber (Bio-Rad). Proteins were transferred on a 0.2 μm nitrocellulose membrane (GE Healthcare) at 0.4 A current kept constant for 1 hour in ice. Membranes were blocked for 1 h using Odyssey blocking buffer (Licor) and probed with primary antibodies either for 1h at room temperature or over-night. Washes of the membranes were done using TBS-T buffer and secondary

antibodies (Licor) were probed for 1 h at room temperature and acquired with Odyssey LI-COR image analyzer. Quantification of the bands was done with ImageJ software. Antibodies: 6E10 (mouse, 1:1000, Covance) and 4G8 (mouse, 1:1000, Covance) was used to detect Aβ; anti-Hsp60 (1:5000, Abcam) was used to detect the total amount of Hsp60 expressed; b-tubulin (rabbit, 1:1000, Cell Signalling), synaptophysin (rabbit, 1:1000, Cell Signalling) and PSD95 (rabbit, 1:1000, Cell Signalling) were used to test the quality of synaptosomes.

CELL CULTURE

SH-SY5Y neuroblastoma cells (ATCC, Manassas, VA) were cultured in DMEM/F12 media (Corning), 10% heat-inactivated fetal bovine serum (FBS, Sigma Aldrich) and 1% penicillin/streptomycin (Gibco). A humidified incubator (Thermo Fisher) was used to keep cells at 37 °C and 5% CO_2 for less than ten passages in either T-75 flasks (Corning) or in 48 well plates during treatment incubations. Phase-contrast micrographs of the cells used for cytotoxicity experiments were done using a light microscope (Axiovert 200, Carl Zeiss) connected to a digital camera (Axiocam MRc5, Carl Zeiss). For all cell culture studies, experiments were performed at least in triplicates using either cells at different passages or cells from different frozen stocks to allow the statistical analysis of the results obtained using both biological and technical replicates.

LACTATE DEHYDROGENASE (LDH) CYTOTOXICITY ASSAY

Cell death of SH-SY5Y neuroblastoma cells was measured 24 hours after treatments with pre-formed Aβo either pre-treated or not treated with Hsp60 using the "Cytotoxicity Assay kit" (Roche), following the manufacturer protocol. Cytotoxicity was detected indirectly by measuring the absorbance of a dye that was sensitive to LDH

released in the culture media by damaged cells. We detected the colorimetric reaction spectroscopically (μQuant, Biotek) and cytotoxicity calculated as a percentage using the following formula: Cytotoxicity % = [(experimental value – low control)/ (high control – low control)] *100 [197]. Low control was used to quantify the spontaneous LDH release using and calculated using media from cells treated with serum-free culture media (DMEM/F12 medium, Sigma Aldrich); high control was calculated using media from cells treated with 10% Triton-X 100 serum free culture media to ensure 100% cell death. All samples used for cell treatments were diluted 1:10 or 1:5 in serum-free culture media. Cells were treated either with oligomers, Hsp60, oligomers exposed to Hsp60 upon optimization of the optimal seeding density. For all experiments, n=3 biological replicates were used to assess statistical difference among treatment conditions. Statistical analysis was performed using ordinary one-way ANOVA along with Tukey's multiple comparisons test, using GraphPad Prism 7. Any p value less than 0.05 was considered as statistically significant.

ANIMALS

3 months old (m.o.) male C57B/l6 (Jackson laboratory) were used to test *ex vivo* electrophysiological changes (n=4,5 animals per treatment conditions). In detail, all animals were housed at the UTMB vivarium according the United States Department of Agriculture (USDA) standards and kept with food and water ad libitum in a 12:12 light dark cycle until the day of sacrifice. All animals were exposed to a lethal dose to isoflurane prior to perform intracardial perfusion of O_2/CO_2 (95:5) aerated NMDG holding buffer (93 mM NMDG, 2.5 mM KCl, 1.2 mM NaH_2PO_4, 30 mM $NaHCO_3$, 20 mM HEPES, 25 mM glucose, 5 mM Na-ascorbate, 2mM thiourea, 3 mM Na-pyruvate, 10 mM $MagSO_4·7H_2O$, 0.5 mM $CaCl_2·2H_2O$, 12 mM N-acetyl L-Cysteine)[198]. All protocols adopted were approved by Institutional Animal Care and Use Committee (IACUC).

SYNAPTOSOMES ISOLATION AND FLOW CYTOMETRY EX VIVO BINDING ANALYSIS

Hippocampal brain extracts were isolated from 3 m.o. wild type C57b/6 male mice and homogenized in Syn-Per (Thermofisher) solution supplemented with phosphatase and protease inhibitor cocktails (Thermofisher). Synaptosomes were isolated according to the manufacturer protocol and the pellet containing the synaptosomes was suspended in HEPES-buffered Krebs-like (HBK) buffer for binding experiments or in RIPA buffer for quality analysis using western blotting. Prior binding experiments, synaptosomes were counted using flow cytometry (Guava Easy Cyte 8 -Millipore) and correct size between 1 μm and 5.6 μm for the analysis was chosen using standard size beads as reference (EMD Millipore). Binding experiments were performed on aliquots of 2 million synaptosomes using pre-formed Aβo cross-seeded with fluor-tagged Aβ-ALEXA-647 peptide (AnaSpec, Inc.) either not treated or treated with Hsp60 (1:25) for 1 Hr. at 37°C. After 1 Hr. incubation at room temperature with either vehicle, Aβo or Aβo + Hsp60, synaptosomes were washed three times with HEPES-buffered Krebs like (HBK) buffer by centrifugation. Each sample was run in both biological (n=3) and technical (n=3) replicate. Analysis of flow cytometry plots was done using Incyte software (EMD Millipore) and binding analysis was done using GraphPad Prism 8.

ELECTRON MICROSCOPY (EM)

Ultrastructure analysis of synaptosomes was performed on 5 μL drop adsorbed on a 200-mesh coated resin grid (FCF 200 – CU Formavar/Carbon, Electron Microscopy Sciences) and stained with 2% aqueous uranyl acetate for negative staining. Both before and after staining, adsorbed samples were washed three times with DDI water 0.2 μm filtered. Resins were blotted with filter paper and dried with warm light. Acquisitions were performed using a J EM- 1400 80 KV (Jeol).

EX VIVO **ELECTROPHYSIOLOGY**

    Ex vivo field recording was performed on 350 nm thick hippocampal brain slices, dissected from wild type C57b/l6 male mice (n=30). Anesthesia and all procedures were performed according to IACUC-approved protocols. Slices were equilibrated in artificial CFS (92 mM NaCl, 2.5 mM KCl, 1.2 NaH_2PO_4, 30 mM $NaHCO_3$, 20 mM HEPES, 25 mM Glucose, 5 mM sodium ascorbate, 2 mM thiourea, 3 mM sodium pyruvate, 2 mM $MgSO_4·7H_20$, 2 mM $CaCl_2·2H_20$, 12 N-Acetyl L-Cysteine, Sigma Aldrich) prior to each experiment and then treated with pre-formed Aβo, either exposed or not to Hsp60, for 1 hour in HEPES based holding buffer (92 mM NaCl, 2.5 mM KCl, 1.2 NaH_2PO_4, 30 mM $NaHCO_3$, 20 mM HEPES, 25 mM Glucose, 5 mM sodium ascorbate, 2 mM thiourea, 3 mM sodium pyruvate, 2 mM $MgSO_4·7H_20$, 2 $CaCl_2·2H_20$, 12 N-Acetyl L-Cysteine) at room temperature. All brain slices were washed and transferred to the recording chamber equilibrated with aCSF buffer. Field recordings were performed using a 22 kΩ resistance electrode placed in the Schaffer collateral/commissural pathway of the CA1 region of the hippocampus after stimulation of the CA3 region of the hippocampus using a 22 kΩ resistance electrode. LTP was obtained from recordings of excitatory postsynaptic potentials (fEPSPs) with a 3-100 Hz trains for 1 second, with 20 second inter-train intervals. For each condition n=6-8 slices either from same of other animals were used for statistical analysis (refer to Supplementary Figure B2, Appendix B, for the experimental design of the electrophysiology protocol). Analysis of the slopes were performed using Clampfit software (molecular devices). LTP data was obtained from the analysis of the post-HFS fEPSP slope over time, expressed as a percentage of the baseline recorded prior HFS. The statistical analysis of LTP upon treatment conditions was obtained from the analysis of the last 10 minutes post-HFS recordings using two-way ANOVA test followed by Bonferroni's multiple comparisons test. For synaptic strength and physiology analyses, paired pulse ratio (PPR), input-output (I/O) analysis were also performed. PPR was

performed by delivering a paired stimulus of 30 μA for 10 minutes both before and after HFS. The resulting response was analyzed as the ratio between the fEPSP slope post-HFS and the fEPSP slope pre-HFS. I/O was performed both pre- and post-HFS by delivering increasing stimulus from 10 μA to 100 μA for 10 minutes. The resulting traces were used to analyze the fEPSP slope and the fiber volley (FV) that were used to calculate the synaptic strength, that was expressed as I/O fEPSP slope over FV amplitude. Differences in both PP50 and synaptic strength between treatment conditions were analyzed statistically using non-parametric one-way ANOVA, followed by Dunn's test for multiple comparison (n=6-8 per treatment condition). Any p value less than 0.05 was considered as statistically significant.

STATISTICAL ANALYSIS

All statistical analyses were done using GraphPad Prism 7. Two-tailed Student T-test was used to compare paired or unpaired results; two-way ANOVA followed by Tukey's multiple comparisons test was used to analyze statistical significance for the electrophysiology data. One-way ANOVA followed by Tukey's multiple comparisons test was used to analyze changes of *in vitro* cytotoxicity upon different treatment conditions of neuroblastoma cells. For all tests a p values less than 0.05 were considered as statistically significant.

III.   RESULTS

HSP60 MODIFIES THE BIOPHYSICAL PROPERTIES OF PRE-FORMED Aβo

We wanted to test if Hsp60-Aβo interaction changed the biophysical properties of pre-formed Aβo. As reported in the experimental design in Figure 4.1, we first used IP to test if the two proteins directly interact. Aβo was prepared using a standardized protocol

[153,199] and subsequently incubated either alone or with Hsp60 (henceforth referred to as "Aβo + Hsp60") for 1 h at 37°C and immunoprecipitated with the anti-amyloid 4G8 antibody, along with Hsp60 and vehicle as controls as described in the method section.

Aβo
Aβo+Hsp60
Hsp60
Buffer

1. IP: 4G8 (1:250) — 18 h / 5°C → IP: Dynabeads — 3 h / R.T. → WB (Hsp60 or 6E10)

2. PK Assay: 0.05 μg/μL PK — 1 h / 37 °C → Kinetic (0-2 h) — t= 5' / 98 °C → WB (Hsp60 or 6E10)

3. bis-ANS Assay: 10 μM Bis-ANS → Kinetic (0-24 h)
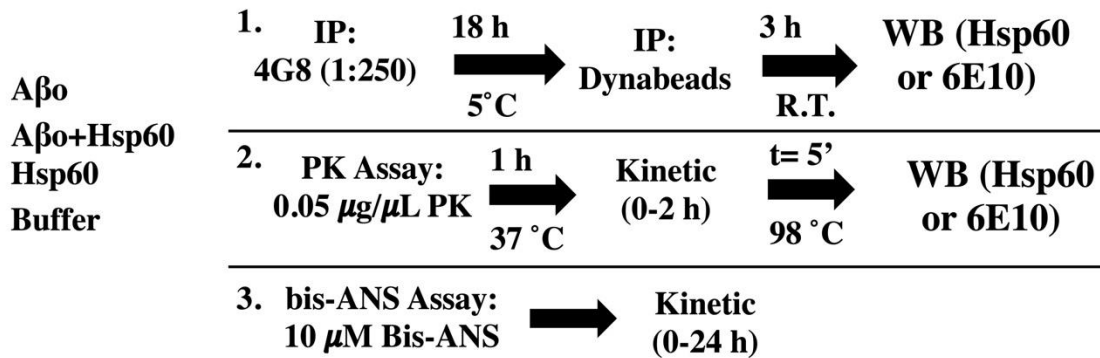
Figure 4.1. Experimental design.

Diagram reporting the approach used to test whether Hsp60 pre-treatment affected the conformation Aβo as compared to untreated Aβo, Hsp60 or control buffer. Immunoprecipitation (1) was used to test the direct binding between the two proteins by pulling down the sample with the anti-Aβ 4G8 antibody and confirming the presence of both Aβo and Hsp60 proteins by WB using the anti- Aβ antibody 6E10 and anti-Hsp60 antibody to detect Hsp60. PK assay (2) was used to test changes in PK sensitivity of Aβo upon pre-treatment with Hsp60 as an indirect measure of conformation changes. Both not treated or Hsp60 pre-treated Aβo were incubated up to 2 h at 37 °C and changes in PK sensitivity was measured upon heat-inactivation of PK using WB probed with both 6E10 and Hsp60 antibodies. Bis-ANS Assay (3) was used to further validate the effect of pre-treating Aβo with Hsp60 by testing changes in bis-ANS fluorescence upon 24-hour incubation kinetic with either vehicle, Aβo, Aβo + Hsp60 or Hsp60.

As shown in Figure 4.2, when comparing Aβo to Aβo + Hsp60, the WB probed with Hsp60 antibody detected a 60 kDa band, in both input and immunoprecipitated fractions which corresponded to Hsp60 bound to Aβo in the Aβo + Hsp60 sample. Conversely, the immunoprecipitation of Hsp60 alone with 4G8-coated beads reported a positive band in the unbound fraction, which was indicative of the low affinity of Hsp60 to the 4G8 antibody. Further, in both Aβo and Aβo + Hsp60 but not in Hsp60 sample, WB probed with 6E10 antibody detected positive bands that are indicative of the presence of

Aβ that have been immunoprecipitated by the coated beads. Therefore, IP data suggested a direct interaction between Aβ and Hsp60 proteins. We further tested the effect of Hsp60 on Aβo conformation upon their interaction, as we have already shown that Hsp60 was capable of interfering with Aβ aggregation pathway[166]. To achieve this goal, we used PK assay to analyze either the digestion pattern and the presence of PK resistant aggregates of Aβo and Aβo + Hsp60 according to published protocols [60]. As summarized in Figure 4.2B, we treated Aβo alone, Aβo + Hsp60 and Hsp60 with 0.05 μg/μL PK up to 2 h and analyzed the time course kinetic qualitatively using western blotting. Interestingly, when comparing the Aβ-positive bands between the Aβo sample and the Aβo + Hsp60 sample using the anti-amyloid antibody 6E10, it was possible to detect different patterns, thus suggesting a different interaction with PK when Aβo were pre-incubated with Hsp60. This data was further supported by the analysis of the 4-8 kDa, 16 kDa and 28-30 kDa bands in both Aβo alone and Aβo + Hsp60 incubated with PK at different time point. As reported in figure 4.2 C-E, the band analysis was obtained as a percentage of the total amount of Aβ detected by 6E10 antibody, prior treatment with PK. The overall analysis of the normalized optical density detected suggests a possible effect of Hsp60 on the biophysical properties of pre-formed Aβo, thus resulting in a different interaction with PK upon treatment with Hsp60.
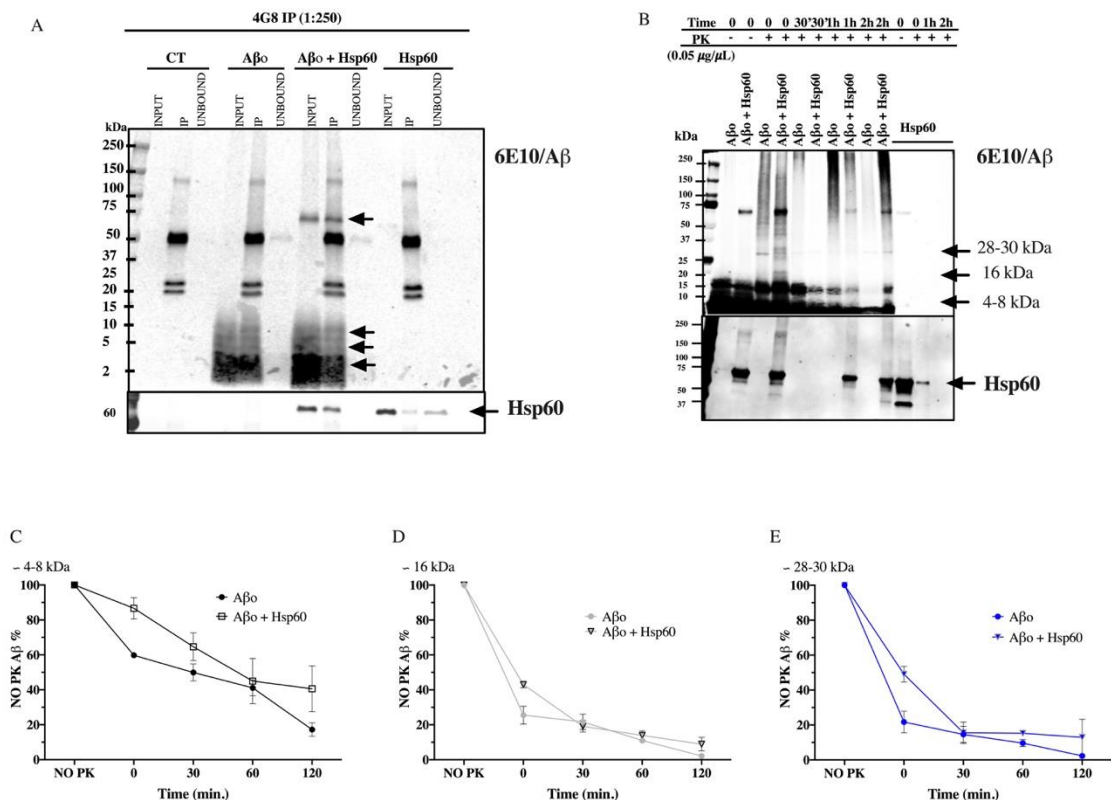
Figure 4.2. Hsp60 binding to pre-formed Aβo and downstream effect on the biophysical properties of Aβ using PK assay.

A. Representative immunoprecipitation analysis of Aβo alone and Aβo + Hsp60, suggesting a direct binding between the two proteins, as confirmed by the anti-amyloid 6E10 antibody detection of 4-16 kDa bands in both inputs and IP lanes of Aβo and Aβo + Hsp60 samples and a 64 kDa band only in input and IP lanes of Aβo + Hsp60 sample (top blot, significative bands indicated by black arrows) and by the anti-Hsp60 antibody detection of 60 kDa bands in both inputs of Aβo + Hsp60 and Hsp60 and in the IP fraction of Aβo + Hsp60 sample. (bottom blot, bands highlighted by the black arrow). As controls, vehicle and Hsp60 proteins were also analyzed. B. Representative western blotting of Aβo, with or without Hsp60, incubated with proteinase K (PK) up to 2 h. anti-amyloid 6E10 western blotting (top blot) showing a different pattern of PK-resistant fragments when Aβo are compared to Aβo + Hsp60, suggesting an effect of Hsp60 on Aβo conformation and aggregation. Bottom blot showing a representative blot probed with Hsp60, suggesting that Hsp60 becomes PK-resistant upon interaction with Aβo. C-E. Graphs showing the relative percentage of representative 6E10 positive bands (4-8 kDa, C; 16 kDa, D; 28-30 kDa, D) during increasing exposure to PK in both pre-formed Aβo not treated or pre-treated with Hsp60, suggesting different sensitivity to PK of Aβo pretreated with Hsp60.

We further confirmed the effect of Hsp60 on Aβo using the bis-ANS assay, which allowed to detect changes of hydrophobic protein cavities spectroscopically upon interaction with bis-ANS probe [196]. In detail, we incubated both Aβo and Aβo + Hsp60 with bis-ANS along with all controls (Hsp60, vehicle, bis-ANS alone) and detected changes in fluorescence up to 24 h. As summarized in Figure 4.3C, there was a statistically significant change in bis-ANS signal in the Aβo + Hsp60 sample after 6, 8 and 24 h, suggesting that upon interaction with Hsp60, Aβo change their hydrophobic content, thus predicting a possible shift in Aβo conformation. Overall, these data indicate that Hsp60 directly binds to Aβo and modulates the biophysical properties of Aβo, as suggested by both PK and bis-ANS assays.
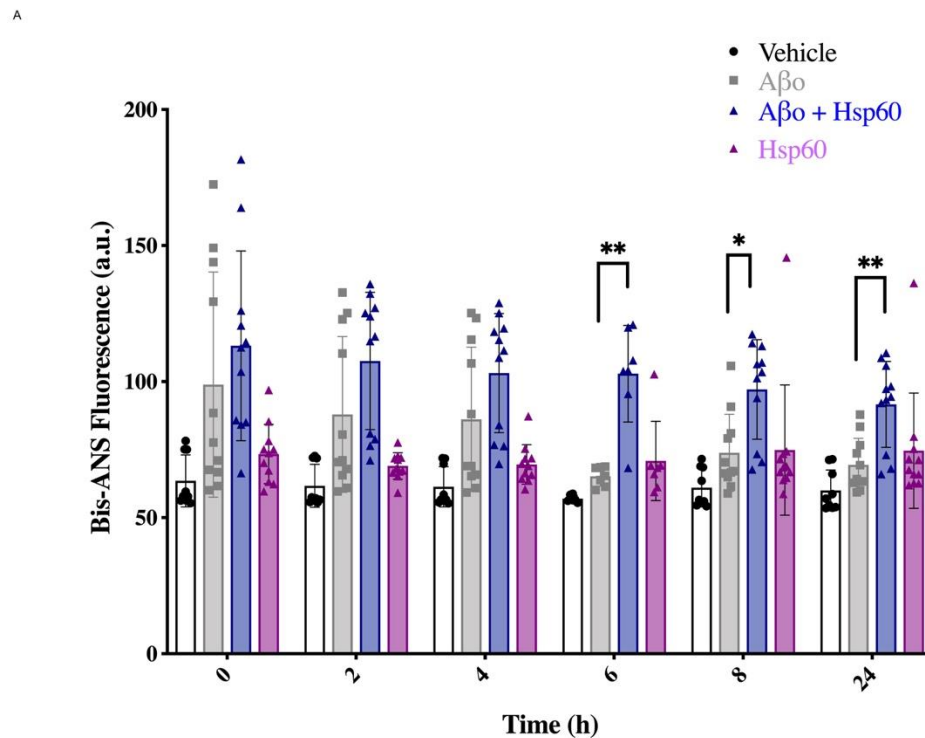
Figure 4.3. Effect of Hsp60 pre-treatment on the biophysical properties of pre-formed Aβo using bis-ANS Assay.

Bis-ANS assay of Aβo and Aβo + Hsp60 showing that after 6 h of incubation, the fluorescence of bis-ANS is significantly different when incubated with Aβo + Hsp60,

compared to Aβo alone (**p=0.0048, q=7.792, DF=6.480). bis-ANS fluorescence between Aβo and Aβo + Hsp60 samples is significantly different also after 12 h (**p=0.0168, q=4.722, DF=18.81) and 24 h (**p=0.0052, q=5.604, DF=16.61), suggesting a stable change in conformation

HSP60 REDUCES AβO CYTOTOXICITY *IN VITRO*

To determine whether the effect of Hsp60 on Aβo conformation resulted in a downstream effect on Aβo-induced cytotoxicity, we tested *in vitro* the toxic effect of Aβo + Hsp60 in neuroblastoma cells (SH-SY5Y) using LDH assay and microscopy. We first established the optimal conditions to obtain quantifiable cytotoxicity in a model of neuronal cells, SH-SY5Y, as shown in Supplementary Figure B1. Subsequently, we incubated a stock sample of Aβo with Hsp60 (1 h at 37 °C using a 25:1 molar ratio [166]) and the quality of the oligomers (either treated or not with Hsp60) verified using western blotting (Supplementary Figure B2b, c). As depicted in the schematic shown in 4.4 A, we treated SH-SY5Y cells with Aβo, Aβo + Hsp60 or control for 24 h and quantified cytotoxicity by LDH assay and confirmed it by light microscopy. Treatment of SH-SY5Y cells with pre-formed Aβo resulted in significantly increased cytotoxicity as compared to control cells (Figure 4.3). On the other hand, cells receiving Aβo + Hsp60 showed reduced cytotoxicity as compared to cells treated with Aβo alone (Figure 4.4.B). These results were confirmed by light microscopy observation of cell morphology as shown in Figure 4.4.C. Overall, these results suggest that *in vitro* treatment with Hsp60 effectively reduces the toxicity of pre-formed Aβo.
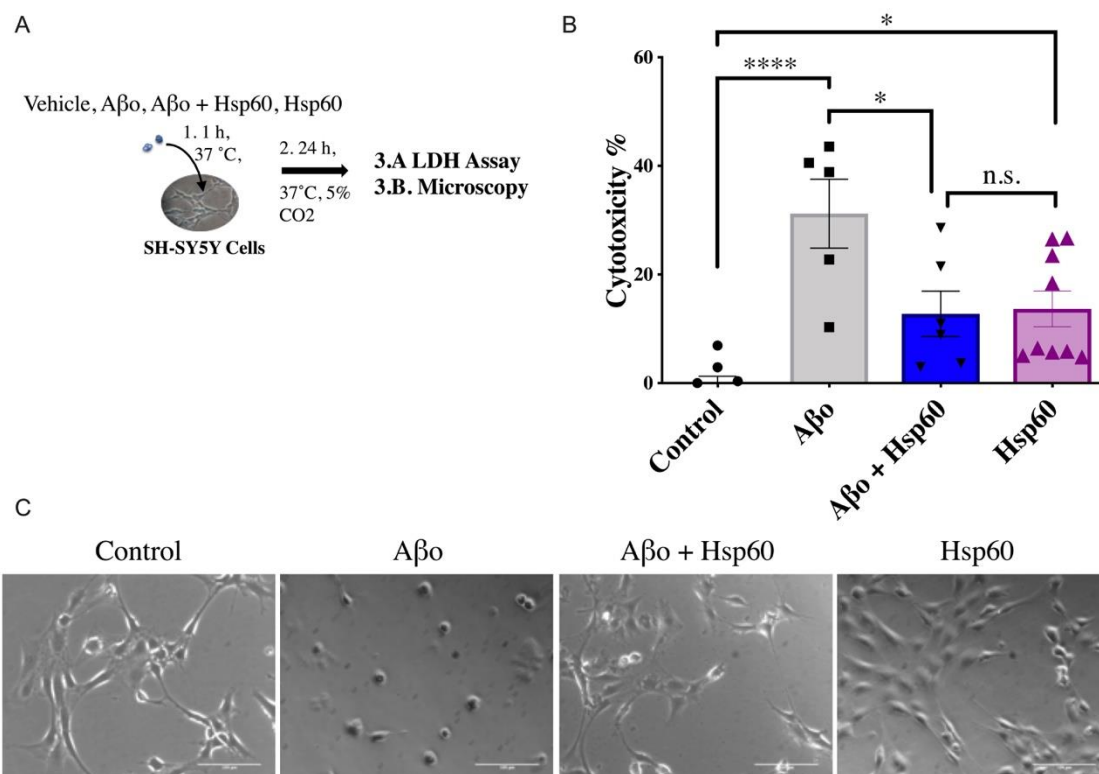
Figure 4.4. Pre-treatment of Aβo with Hsp60 reduces cytotoxicity.

A. Experimental design of SH-SY5Y treatment showing that all samples (control, Aβo, Aβo+Hsp60) are incubated for 1 h at 37 °C, prior dilution at their final concentration in serum-free cell media. After 24 h, LDH assay and microscopy acquisitions were performed. B. LDH assay results of SH-SY5Y cells treated with control, 5 µM Aβo (Aβo) or 5 µM Aβo pre-treated with 200 nM Hsp60 (Aβo + Hsp60). Cytotoxicity % in cells treated with Aβo was significantly higher than cells treated with Aβo + Hsp60 or control vehicle, suggesting that pre-treatment with Hsp60 reduces the downstream cytotoxicity of pre-formed Aβo (Control vs. Aβo, ****$p<0.0001$; Aβo vs. Aβo + Hsp60, *$p=0.0165$; *$p=0.0158$; Aβo vs. Hsp60, *$p= 0.013$, Aβo + Hsp60 vs. Hsp60, n. s.; Control vs. Aβo + Hso60, n. s.; Control vs. Hsp60, *$p=0.0247$). Data plotted as mean ± SEM. C. Representative micrographs of SH-SY5Y cells treated with vehicle (control), with 5 µM Aβo (Aβo), with 5 µM Aβo pre-treated with 200 nM Hsp60 (Aβo + Hsp60), or with 200 nM Hsp60 (Hsp60) confirming the reduced cytotoxicity when Aβo are pre-treated with Hsp60 as compared to Aβo. Data in agreement with the LDH assay results shown in (B). Scale bars 100 µm.

101

We further tested the effect of Hsp60 on Aβo-induced impairment of synaptic plasticity using *ex vivo* field electrophysiology.

We first analyzed changes in PPR and pre-synaptic strength upon each treatment, as shown in Figure 4.5A. Our results showed no alteration of the PPR in any of the treatment conditions, thus suggesting that the pre-synaptic release probability was not affected by any of the treatments tested as compared to control. Further, as reported in Figure 4.5B, we analyzed the pre-synaptic strength prior to applying the HFS protocol to test changes in synaptic plasticity for each treatment condition. As described in the methods, to analyze the synaptic strength, we tested the I/O response to increasing current stimuli and expressed the synaptic strength as the percentage of the baseline slope of the fEPSP as a function of the FV amplitude. The statistical comparison between all treatment conditions to control did not report any significant change in pre-synaptic strength among different treatments. Thus, these data suggest that neither Hsp60, Aβo or Aβo+Hsp60 treatments affected synaptic physiology.
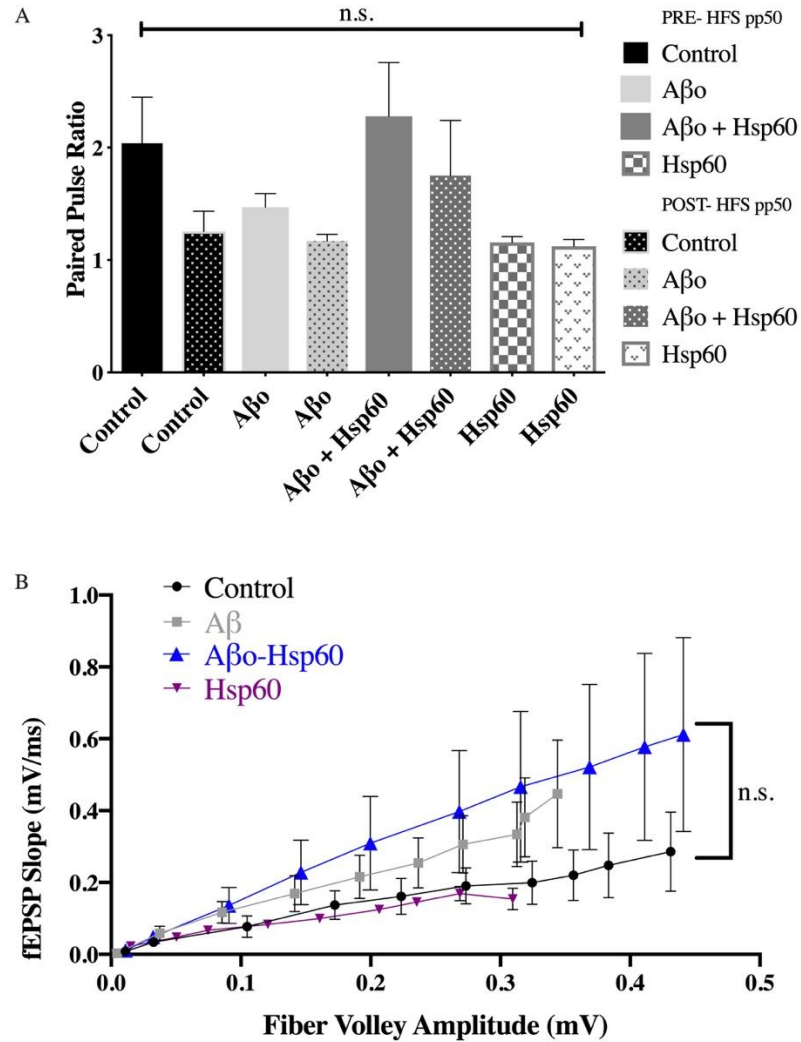
Figure 4.5. Synaptic physiology is not affected by ex vivo treatments.

A. Comparison of paired-pulse ratio analysis between treatment showing that none of the treatments (control vehicle or CT, Aβo, Aβo + Hsp60, Hsp60) affected the synaptic physiology of the Shaffer collateral pathway (approximate p-value p=0.4289, α=0.05). B. Representative plot of the pre-synaptic strength analysis comparing all treatment conditions investigated prior testing changes in LTP (control vehicle, Aβo, Aβo + Hsp60, Hsp60), expressed as field excitatory post-synaptic potential slope as a function of the fiber volley amplitude, showing that there is no change upon high-frequency stimulation of the synaptic strength.

Once established the synaptic strength, we determined changes in hippocampal

LTP upon treatment of mouse hippocampal brain slices with Aβo, Aβo + Hsp60, Hsp60 or

control vehicle. As expected, we observed that the percentage of the post-synaptic field potential (fEPSP) slope upon high-frequency stimulation (HFS= 3X 100 Hz, 20s) was significantly reduced in slices pre-treated with Aβo as compared to control (Figure 4.6A). We also tested the effect of Hsp60 on synaptic plasticity, and due to its oligomeric nature, we observed synaptic toxicity as compared to control slices. However, despite the adverse effect of Hsp60 on synaptic plasticity, we found that the Aβo + Hsp60 treatment impaired significantly less the synaptic plasticity as compared to Aβo alone. This result suggested that the interaction between Hsp60 and Aβo leads to the formation of oligomers that impaired less the synaptic plasticity. The statistical analysis of the last 10 minutes of LTP averages (n=6-10 slices from 4-5 animals per condition), further confirmed this finding (Figure 4.6B). Representative electrophysiology traces of brain slices of all treatment conditions are represented in Figures 4.6C-F.
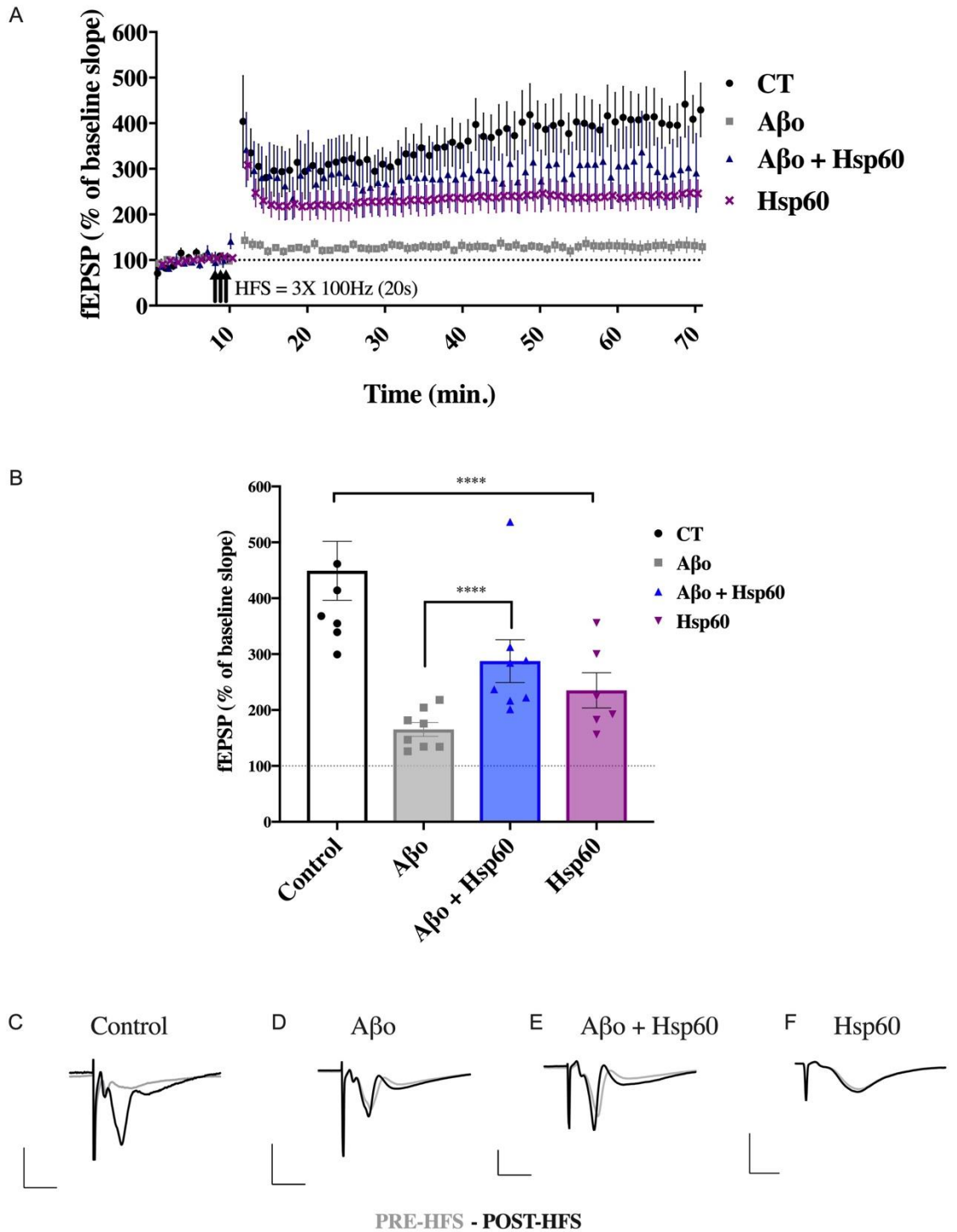
Figure 4.6. Hsp60 protects against the impairment of synaptic plasticity caused by Aβo.

A. Full traces comparison of LTP changes expressed as the percentage of the baseline slope (field excitatory post-synaptic potentials , fEPSP) over time (min.) upon high frequency stimulation of the CA3 region of the hippocampus (HFS, 3 X 100 Hz, 20s), showing the rescue of LTP when Aβo were pre-treated with Hsp60 (blue curve) as compared to

untreated Aβo (grey curve). Treatment of brain slices with vehicle was used as control (black curve) and treatment with Hsp60 was used as substance control (magenta curve). Data presented as the average ± SEM (n=6-8). B. Analysis of the fEPSP slopes for the last 10 minutes post-HFS for each treatment condition (control, Aβo, Aβo + Hsp60, Hsp60), showing that pre-treatment of Aβo with Hsp60 (blue bar) significantly reduced LTP impairment caused by Aβo alone (light grey bar), as compared to control (black bar; ****$p<0.0001$; Aβo vs. Hsp60, *$p=0.0171$; df treatment=3, $F_{(3, 27)} = 7.177$, $p=0.0011$). C-F. Representative electrophysiology traces of brain slices treated either with vehicle (2. Control), 200 nM Aβo (3. Aβo), 200 nM Aβo pre-treated with 8 nM Hsp60 (4. Aβo + Hsp60) or with 8 nM Hsp60 (5. Hsp60) showing that only Aβo causes an impairment of synaptic plasticity, compared to all other conditions. All traces represent recordings performed *ex vivo* at the CA2 region of the hippocampus both prior HFS (PRE-HFS in grey) and after HFS stimulation of the CA3 region of the hippocampus (POST-HFS in black). Scale bars: x= 10 ms; y= 1mV.

HSP60 INHIBITS THE BINDING TO SYNAPSES OF Aβo

In order to explore a possible mechanism underlying the decreased Aβo-induced impairment of LTP observed in the Aβo + Hsp60 treatment, we used flow cytometry to test whether the pre-treatment of Aβo with Hsp60 affected the ability of Aβo to bind to synaptosomes. We first characterized the quality of the synaptosomes isolated from the hippocampus of WT mice using both western blotting and electron microscopy (Figure 4.6). We confirmed that in the isolated synaptosomes both pre- and post- synaptic structure were present using synaptophysin as a pre-synaptic marker and post synaptic density 95 (PSD95) as a post-synaptic marker. As reported in Figure 4.6 B, we confirmed that the synaptosomes we isolated were significantly enriched in these two markers.
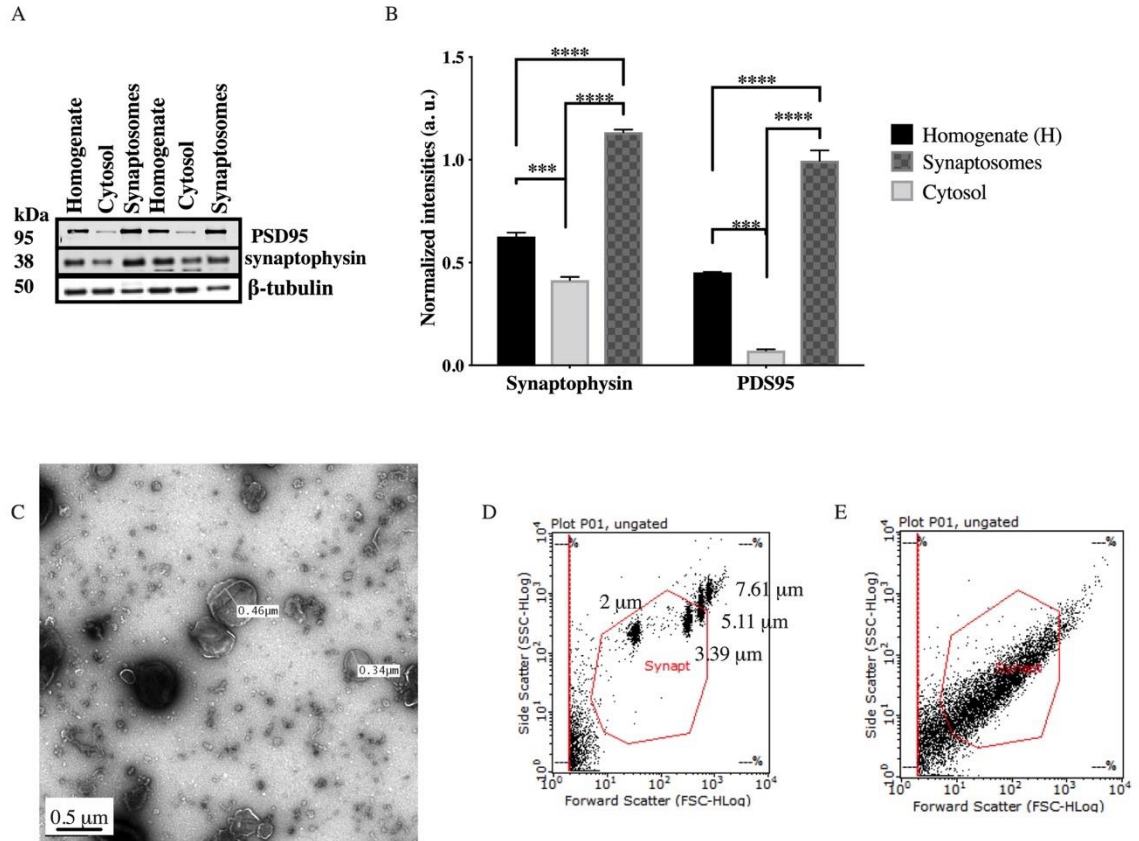
Figure 4.5. Quality control of isolated synaptosomes from dissected hippocampi using western blotting and electron microscopy.

A. Representative western blotting of synaptosomes preparation using SynPer protocol, showing that synaptosomes fraction has enriched synaptophysin and PD95 proteins, respectively pre- and post- synaptic marker, compared to hippocampal homogenate and cytosolic fractions. B. Quantification of n=3 blots normalized by β-tubulin antibody used as a loading control using image J to analyze the band intensities detected by anti-synaptophysin and anti-PSD95 antibodies. Statistical significance of the abundance of pre- and post- synaptic markers between fractions was analyzed by ordinary two-way ANOVA ($F_{(1, 12)} = 129.0$, $p<0.0001$ between conditions; $F_{(2, 12)}= 622.5$, $p<0.0001$, within conditions) and Sidak's multiple comparison tests. P-values less than 0.05 were considered as statistically significant C. Representative electron micrograph showing the morphology and the size of synaptosomes in the preparation. Scale bar 0.5 μm. D. Representative flow cytometry plots showing the gating applied using standard size beads to define the correct synaptosomes size between 1 to 5.6 µm. E. Representative flow cytometry data showing the gating applied to determine the correct size to synaptosomes to be used for the binding studies shown in figure 4.7.

We also confirmed by electron microscopy both size and ultra-structure of the synaptosomal vesicles, as reported in Figure 4.6C. Subsequently, we exposed

synaptosomes to increasing concentrations of Aβo labeled with fluorescent 647-Alexa dye and evaluated the extent of binding using flow cytometry after gating for proper synaptosomes size (Figures 4.6 D-E). Consistent with previously reported data [198], the binding to synaptosomes of increasing doses of Aβo (0-15μM) followed a second order kinetic reaching a plateau between 7.5 μM and 15 μM. This binding was significantly reduced when synaptosomes were challenged with Aβo + Hsp60 (Figures 4.7A-B). Quantitative Scatchard plot analysis of binding data (Figures 4.7 C) confirmed a significantly reduced B_{max} in synaptosomes treated with Aβo+Hsp60 as compared to Aβo alone with no changes in the calculated dissociation constant (Kd).

Overall, our data suggest that exposing pre-formed Aβo to Hsp60 decreases their ability to bind to synaptosomes.
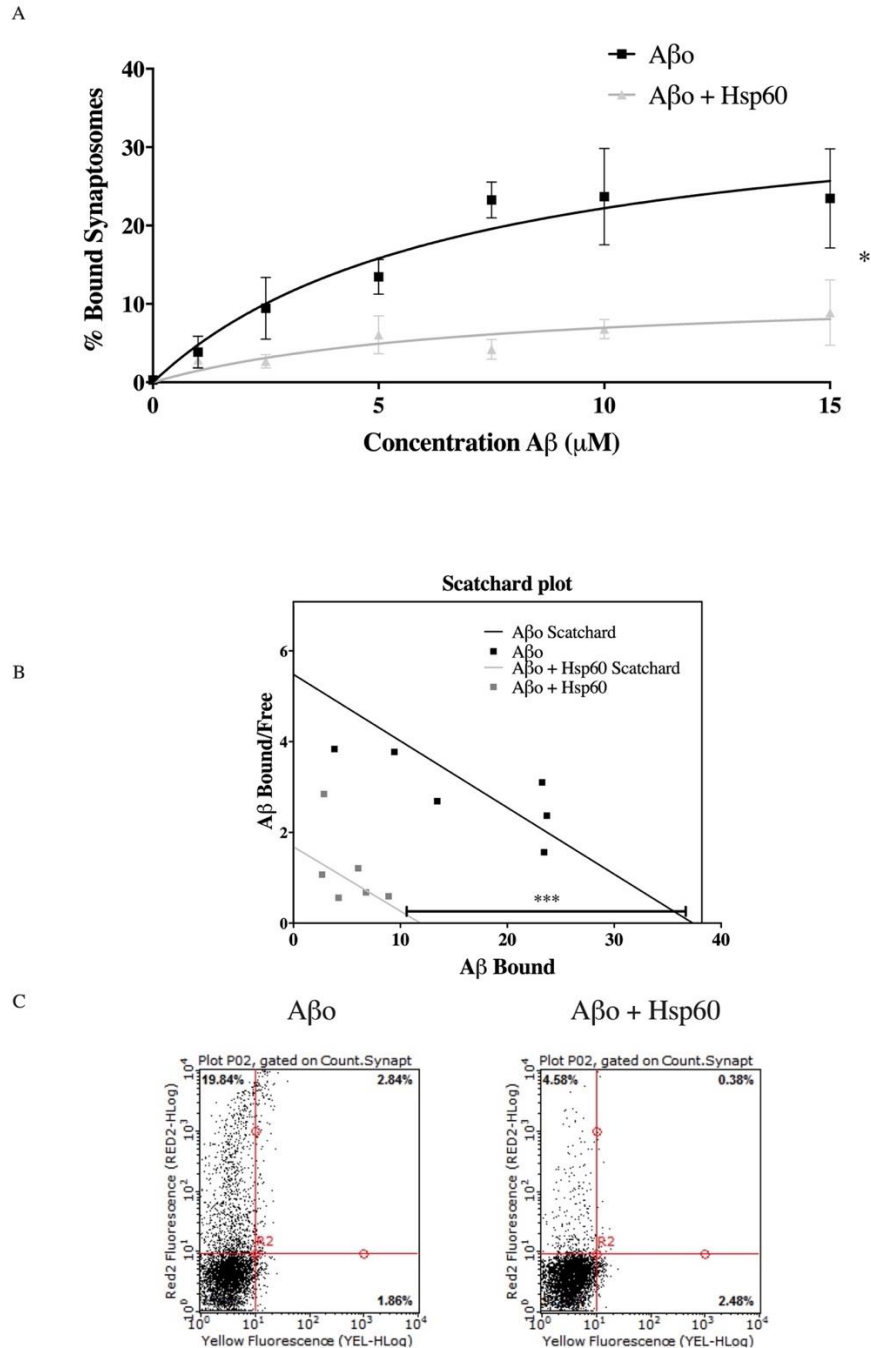
Figure 4.6. Pre-treatment of Hsp60 changes Aβo binding to synaptosomes ex vivo.

A. Binding analysis of isolated synaptosomes treated *ex vivo* with pre-formed Aβo flour labeled with Alexa-Fluor-647 either not treated or pre-treated 1h with Hsp60 showing that the binding curves of the % of Aβo bound to synaptosomes at increasing concentrations of Aβo are significantly different between the two treatments. Data represented as the mean ± SEM (n=3; *p=0.0217; DF=18). B. Scatchard plot analysis of the binding curves shown in A showing that synaptosomes pre-treatments with Aβo decrease the Bmax

(***p=0.0001, DF=12, n=3) values without affecting the Kd (n.s., p=0.9976, DF= 12). C. Representative flow cytometry data of synaptosomes treated with 15 µM Aβo, compared to Aβo + Hsp60 under the same conditions.

Table 3. Kinetic parameters obtained by the Scatchard analysis.

	Bmax	Kd
Samples	Value ± SEM	Value ± SEM
Aβo	37.347 ± 7.116	6.813 ± 2.885
Aβo + Hsp60	11.87 ± 3.801	7.057 ± 4.951

IV. CONCLUSIONS

Aβo is known to affect cytotoxicity, synaptic plasticity and neurotransmitter release. Collectively, these effects are earliest dysfunctional events leading to dementia in AD[101,194,200]. Here, we characterized the effect of Hsp60 on toxic Aβo conformations, and the downstream effects of the direct interaction between Hsp60 and Aβo. We first established if Hsp60 directly interacted with Aβo and if this interaction resulted in a modulation of Aβo conformations, as increasing evidence shows that specific toxic conformations drive synaptic toxicity of Aβo[201,202]. Immunoprecipitation experiments confirmed the direct binding between Aβo and Hsp60 and both PK and bis-ANS assays strongly suggested that Hsp60 significantly affected Aβo conformations.

Aβo are highly polymorphic species, with different epitope exposure, antibody-binding properties and peculiar toxicity features[203]. Therefore, we tested if Hsp60-Aβo interaction resulted in the release of less cytotoxic Aβo conformations by determining their toxicity in SH-SY5Y neuroblastoma cells and we found that Aβo pre-treated with Hsp60

were less toxic compared to Aβo alone. These results suggest a physical interaction between the chaperone Hsp60 and Aβo resulting in the conversion of these latter to a lesser toxic oligomeric species.

Some of the most relevant toxic effects of Aβo at the synapses include synaptic degeneration[204–206] and inhibition of synaptic plasticity, thus resulting in the impairment of long-term potentiation (LTP)[183,184,194,207]. Our results suggest that pre-treating Aβo with Hsp60 significantly reduces the Aβo-driven impairment of LTP in hippocampal slices as compared to Aβo alone. As Aβo interacts directly with synapses, thus leading to synaptic degeneration[184,208], in an attempt to establish a possible mechanism underlying the reduced synaptic toxicity of Aβo after exposure to Hsp60, we tested if the impact of Hsp60 on pre-formed Aβo lead to the formation of conformations less prone to bind to synapses. We found that pre-treating Aβo with Hsp60 significantly reduced binding of Aβo to synaptosomes *ex vivo*, as confirmed by flow-cytometry analysis of isolated synaptosomes and further quantification of flow-cytometry data by Scatchard analysis. Collectively these data suggest that a possible mechanism through which Hsp60 renders Aβo less synaptotoxic is via decreasing their ability to bind to synapses.

The interaction between Hsp60 and toxic Aβo, leading to a conformational change of the amyloid protein toward less toxic forms as reported here, while novel, is consistent with previous reports describing an overall role of chaperones such as Hsp70/Hsp90 in misfolded tau pathology [209–211] and supports the growing idea of a key function of chaperones in neurodegenerative disorders. Overall, this work contributes to characterize the mechanism of protection of the mitochondrial chaperonin Hsp60 against Aβo, one of the main neurotoxic species in the AD brain and proposes Hsp60 as a potential target for the development of novel therapies.

CHAPTER 5. GENERAL DISCUSSIONS AND CONCLUSIONS

AD is the leading cause of dementia worldwide and therapies are still lacking [24]. One of the earliest lesions leading to AD pathogenesis is the release of Aβ and its aggregation into toxic oligomers, followed by a generalized protein misfolding, and the impairment of protein quality control machinery [21].

My project aimed to characterize a possible approach to target Aβ toxicity. Based on our current knowledge on Aβ misfolding and aggregation, there are several strategies that can be used to inhibit this process such as: inhibition of Aβ aggregation; increase of clearance of toxic aggregates; re-routing of toxic Aβ aggregates from their "on-pathway" toward less toxic "off-pathways" [70,212]. Increasing evidence suggests that chaperones are protective machines that can counterbalance the toxic effect of misfolded proteins such as Aβ [213–215].

The well-characterized native properties of the chaperonin Hsp60 in assisting the refolding of misfolded proteins gave the rationale to propose a direct interaction between Hsp60 and Aβ proteins. Only a few studies have investigated the effect of Hsp60 against Aβ, and what mechanism controls this protective effect of Hsp60 was still poorly understood.

In the present study, I proposed to investigate the functional interaction between Hsp60 and Aβ peptide at different stages of its formation, aggregation and downstream toxicity. I characterized the changes in Aβ aggregation in the presence of Hsp60 using Thioflavin T assay, circular dichroism spectroscopy, atomic force microscopy, and size exclusion chromatography. The cell-free system confirmed that Hsp60 successfully and irreversibly inhibits the aggregation of both $A\beta_{1-40}$ and $A\beta_{1-42}$ peptides. This phenomenon could be due to the ability of Hsp60 to stabilize either monomers or small oligomeric seeds of Aβ in an amorphic structure that no longer misfolds. It is possible that Hsp60 re-addresses the aggregation of Aβ toward an "off-pathway" cascade, by offering a mainly

112

hydrophobic surface. This effect of Hsp60, can be classified as a "holdase activity" [216], as Hsp60 prevents Aβ to further aggregate. This last evidence suggests that the eukaryotic Hsp60 can also operate when the whole machinery (ATP and Hsp10 co-chaperone) is not available, thus making this chaperone more evolved than the bacterial homolog GroEL, as already described by others [133,180].

The finding that the effect of Hsp60 on Aβ aggregation is irreversible has a significant translational meaning, as this mechanism of action of Hsp60 could contribute to preventing further spreading of AD pathology.

We further investigated the effect of Hsp60 on Aβ production, compartmentalization, and release by creating a novel cellular model that overexpresses both human APP and human Hsp60 (referred as 7PA2/H60 cell line). This model demonstrated that overexpressing Hsp60 significantly reduced the release of Aβ in the media without affecting levels of APP, as confirmed by ELISA. This finding allows speculating that Hsp60 might hold Aβ monomers and promote their degradation by other components of the proteostasis machinery; or refold Aβ monomers into more unstable conformations, thus explaining the reduced secreted levels of Aβ in the media.

Compelling evidence suggests that Aβ toxicity is due to specific oligomeric conformations (or "strains") assembled during the aggregation kinetic of Aβ [155,201]. Therefore, any approach able to interfere with the formation of toxic oligomeric strains of Aβ is a successful strategy for future disease-modifying therapies. In order to test whether Hsp60 had any effect on Aβ-driven cytotoxicity, we used SH-SY5Y cells as a neuronal *in vitro* model for testing changes in cytotoxicity of both naturally secreted and preformed oligomers. The finding that Hsp60 significantly reduced Aβ-driven cytotoxicity suggests a possible detoxifying effect of Hsp60 on toxic strains. I speculate that this detoxifying effect of Hsp60 could be through a mechanism of refolding of these Aβ oligomers toward less toxic conformations. This mechanism of action of Hsp60 is supported by the biophysical investigation of the effect of Hsp60 on preformed Aβ using bis-ANS and PK assays, which

showed that Aβ oligomers are qualitatively (PK assay) and quantitatively (bis-ANS assay) different upon treatment with Hsp60.

Investigations on the effect of Aβ oligomers pre-treated with Hsp60 on synaptic plasticity (long-term potentiation) and binding to synapses strongly suggest that Hsp60-treated Aβ oligomers impair significantly less synaptic plasticity and long-term potentiation and could be due to a reduced binding affinity to synapses as showed by flow-cytometry results. This latter finding is in agreement with the proposed effect of Hsp60 to refold Aβ oligomers into different conformations and suggests Hsp60 as a viable candidate for possible therapies aimed to prevent Aβ-derived memory impairments.

Overall, data obtained implies that Hsp60 targets both misfolded monomers and pre-formed oligomers of Aβ. This protein-protein interaction leads to an irreversible inhibition of Aβ aggregation kinetic and a reduction of the downstream Aβ-induced synaptic toxicity. Therefore, Hsp60 can be proposed as an attractive backbone for any active AD therapy centered on targeting Aβ oligomer toxicity.

To further validate the protective role of Hsp60 against Aβ toxicity, the protective effect of Hsp60 on Aβ neurotoxicity should be also investigated *in vivo*. To propose Hsp60 as a potential future therapy relevant to AD, it will be important to characterize whether Hsp60 reverts some of the known phenotypes caused by Aβ toxicity, such as memory impairment [59,217,218]. Testing the behavioral changes of pre-treated Aβ oligomers with or without Hsp60 will provide a strong support for proposing Hsp60 as a potential therapeutic candidate for AD.

In order to test the translational potential of Hsp60 several approaches can be proposed. A first approach could involve the upregulation of endogenous levels of Hsp60. This can be done either through gene therapy, by delivering Hsp60-cDNA through AAV-vectors [219], or by using natural compounds with known up-regulating effects on endogenous Hsp60 levels, such as rikkunshito [220]. As Hsp60 has been shown to cross-talk with the immune system and to be involved in both apoptosis and oncogenesis [140],

another approach could involve the design of small compounds that mimic the protein binding site of Hsp60. This approach could contribute to preventing possible side effects linked to the uncontrolled up-regulation of Hsp60 *in vivo*. Based on our immunoprecipitation data and PK assay results, Hsp60 binds to pre-formed Aβo and the resulting Hsp60-Aβ complex is both resistant to denaturing WB conditions and to PK digestion (discussed in chapter 4). Therefore, this Hsp60-Aβ complex could be isolated and further analyzed by mass spectrometry (MS) and the resulting MS fragmentation could be used as a template for designing a library of small compounds that can be tested for pharmacokinetic and pharmacodynamic both *in vitro* and *in vivo* on suitable models of APP overexpression and downstream Aβ neurotoxicity.

Another possible future direction for this project would be to investigate possible relationships between Hsp60 levels and the main risk factor responsible for the onset of sporadic AD, Apo Eε4, as the role in the onset of sporadic AD is poorly understood. An intriguing hypothesis lays on the recent discovery of a link between Apo E and clusterin or apolipoprotein J [133], an extracellular chaperone known to be involved in cell survival and stress response and whose mechanism of action seems to be antagonized by a direct binding to Hsp60 [134]. Interestingly, increased levels of clusterin have been associated with AD pathology and particularly with levels of APOE and increased secreted levels of tau and Aβ. Therefore, it would be interesting to test the hypothesis that the genetic variant Apo Eε4 has a role in influencing the chaperone machinery leading to a pathologic accumulation of Aβ peptides, which are known to be involved in AD onset. The rationale that could support this hypothesis is the known interaction between ApoE, clusterin and Hsp60 [133,134]. A possible experimental approach could be to determine Hsp60 levels in transgenic mice expressing the human ApoE3, ApoE4 and ApoE2 variants and investigate if changes in Hsp60 and clusterin have an effect on Aβ accumulation and down-stream toxicity.

While more research is needed to propose Hsp60 as a valid therapeutic candidate for Aβ-driven pathology, this project contributed to the understanding of critical mechanisms involving Hsp60 and novel strategies against Aβ synaptic toxicity, which have not been reported before. The significant effect of Hsp60 on toxic Aβ conformations strongly supports the concept that targeting Hsp60 is a viable molecular target for future innovative therapies for AD centered on negating Aβ oligomer toxicity. Given the knowledge that Hsp60, could also target other misfolded proteins, and that oligomers of different amyloid proteins share similar structural conformation and toxicity [76,113,115,133,212], these studies will contribute to further studies extending beyond the immediate borders of Aβ oligomer toxicity. Experiments aimed at expanding the interaction between Hsp60 and other synaptotoxic oligomers profile will foster an emerging area of amyloid protein neurobiology focused on targeting disease-relevant amyloid conformations.

Appendix A - Supplementary material for Chapter 3

Supplementary Table 1. Optimization of cell transfection

Lipofectamine 2000 (µL)	0	7	9	12	-
µg of transfected plasmid (pCMV6-Empty/ hHsp60)	0	1	3	5	7
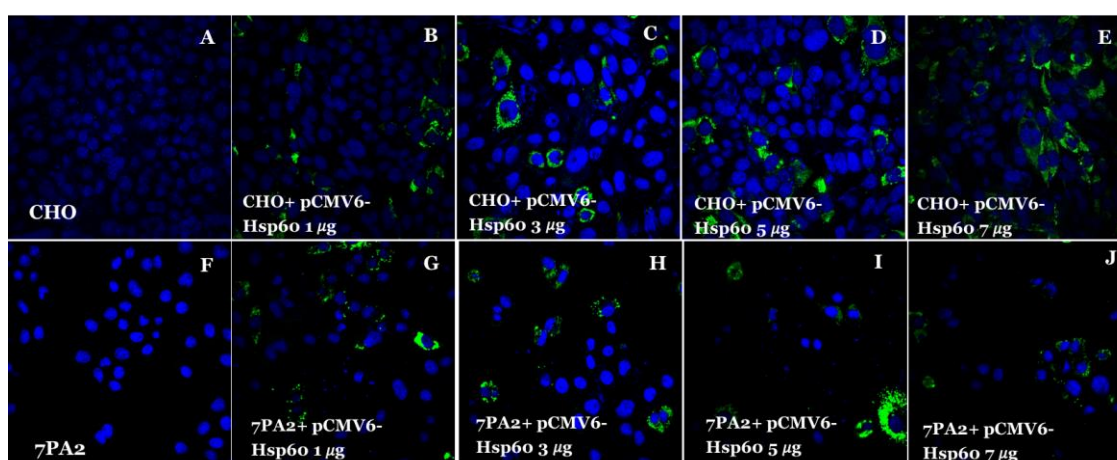
Supplementary Figure A.1. Validation of the protocol of plasmid transfection.

A-E. Representative ICC of CHO cells transfected with increasing quantity of pCMV6-Hsp60 plasmid, from none (A) to 7 µg (E). F-J. Representative ICC of 7PA2 cells transfected with increasing quantity of pCMV6-Hsp60 plasmid, from none (F) to 7 µg (J). For all ICC, DDK antibody was used as primary antibody and Alexa-Fluor 488 was used as secondary antibody, DAPI was used to counterstain nuclei.
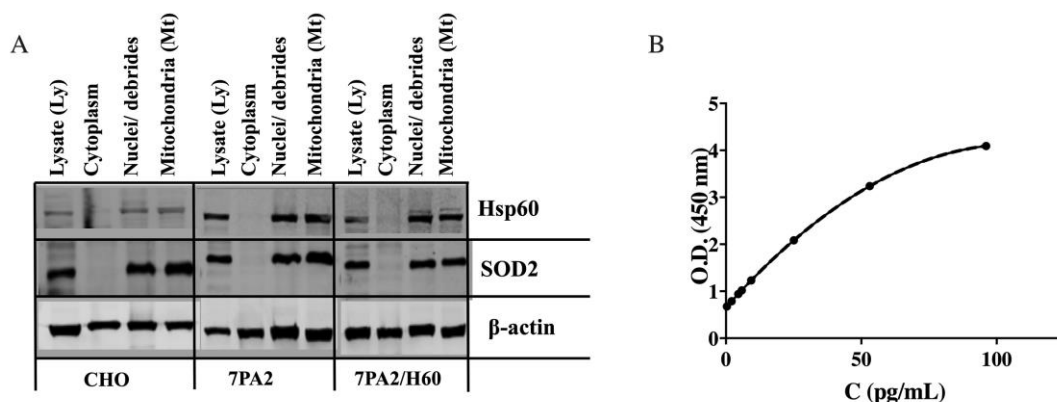
Supplementary Figure A.2. Optimization of sub-cellular fractionation protocols

A. Representative western blotting of total cell lysates (Ly), cytoplasm, nuclei/debrides and mitochondria (Mt) from CHO, 7PA2 and 7PA2/H60 cells, showing that mitochondria are positive to Hsp60 and SOD2, a specific marker of mitochondria. B. Representative standard curve of Aβ used to quantify Aβ levels in the culture media collected from 7PA2 and 7PA2/H60 cells.
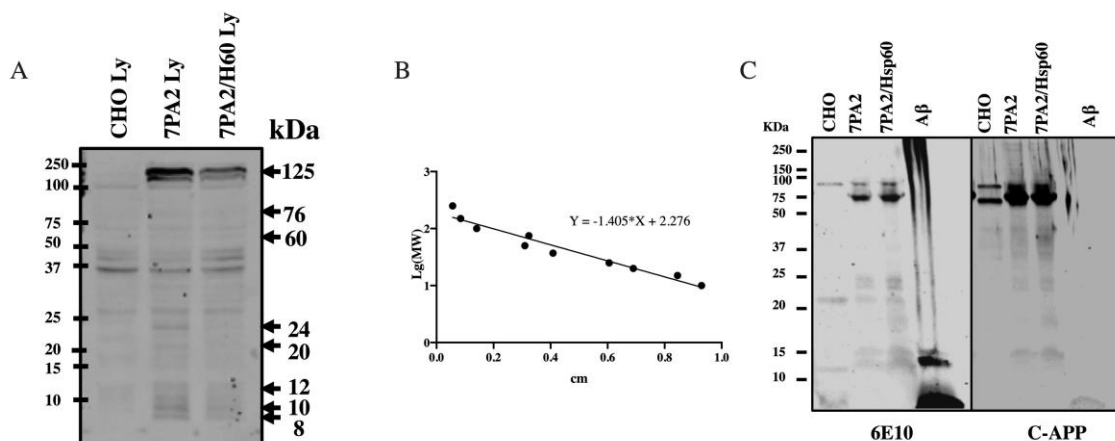
Supplementary Figure A.3. Analysis of low molecular weight bands 6E10 positive.

(A) Representative western blotting of total cell lysates (Ly) probed with the anti-amyloid antibody 6E10, showing multitude of bands detected (representative bands are indicated by black arrows) that can be either relative to APP protein or to Aβ at different stages of aggregation. (B) Representative standard curve for the molecular weight analysis of the 6E10 positive bands, specific for Aβ forms, shown in A. (C) representative comparison of blots of total cell lysates of CHO, 7PA2, 7PA2/H60 detected with the anti-amyloid 6E10 (left blot) and anti c-terminus APP antibody c-APP (right blot), used to detect APP fragments that are not amyloid beta. showing the different band detections between the two antibodies.
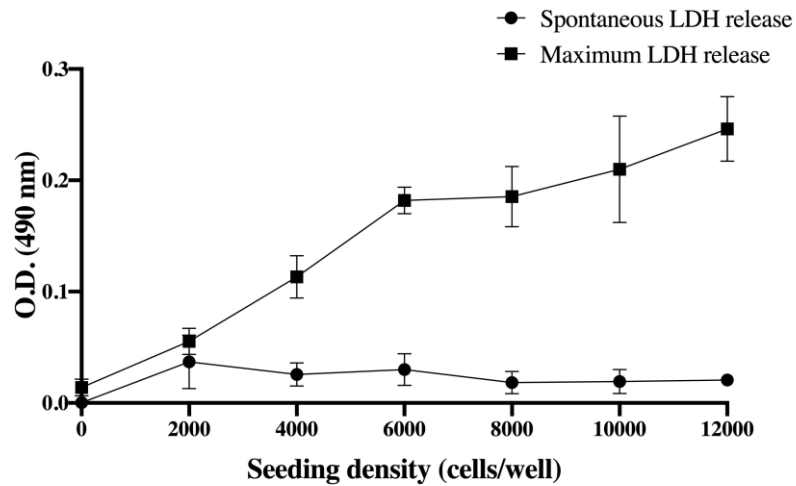
Supplementary Figure A.4. Optimization of LDH assay protocol.

LDH assay of increasing seeding density of SH-SY5Y cells either not treated (spontaneous LDH release) or treated with Triton-X 100, a cytotoxic agent (maximum LDH release) to quantify the amount of LDH release that is either spontaneous or maximum. Data expressed as the average ± SEM of optical density (O.D.) used to detect LDH levels in the culture media per number of cells per well. The increasing O. D. observed in the maximum LDH release curve is indicative of the increasing cell death that is proportional to the increasing number of cells.

Appendix B – Supplementary material for Chapter 4

Supplementary Table 2. Two-Way ANOVA analysis for bis-ANS Assay shown in figure 1.d.

Tukey's mult. comp. test	Mean Diff.	95.00 % CI of diff.	Sign. ?	Adj. P	Mean 1	Mean 2	Mean Diff.	SE of diff.	N1	N2	q	DF
Row 1: Time 0												
Aβo vs. Aβo + Hsp60	- 14.25	-60.04 to 31.54	ns	0.8186	98.91	113.2	- 14.25	16.32	11	11	1.235	19.44
Aβo vs. Hsp60	25.52	-13.12 to 64.15	ns	0.2521	98.91	73.39	25.52	12.91	11	11	2.795	11.38
Aβo vs. Vehicle	35.38	-3.233 to 74.00	ns	0.076	98.91	63.52	35.38	12.88	11	9	3.883	11.29
Aβo + Hsp60 vs. Hsp60	39.76	7.041 to 72.49	*	0.0164	113.2	73.39	39.76	11.01	11	11	5.106	11.94
Aβo + Hsp60 vs. Vehicle	49.63	16.94 to 82.33	**	0.0035	113.2	63.52	49.63	10.99	11	9	6.389	11.8

Hsp60 vs. Vehicle	9.867	-3.089 to 22.82	ns	0.1745	73.39	63.52	9.867	4.581	11	9	3.046	17.88
Row 2: Time 2 Hrs												
Aβo vs. Aβo + Hsp60	-19.64	-51.89 to 12.60	ns	0.3464	87.94	107.6	-19.64	11.5	11	11	2.415	19.68
Aβo vs. Hsp60	18.94	-7.592 to 45.48	ns	0.1957	87.94	69	18.94	8.759	11	11	3.059	10.57
Aβo vs. Vehicle	26.22	-0.6476 to 53.08	ns	0.0565	87.94	61.73	26.22	9.028	11	9	4.107	11.82
Aβo + Hsp60 vs. Hsp60	38.58	15.20 to 61.97	**	0.0021	107.6	69	38.58	7.74	11	11	7.05	10.74
Aβo + Hsp60 vs. Vehicle	45.86	22.07 to 69.65	***	0.0005	107.6	61.73	45.86	8.043	11	9	8.063	12.32

Hsp60 vs. Vehicle	7.274	-1.586 to 16.13	ns	0.1236	69	61.73	7.274	3.01	11	9	3.418	12.73
Row 3: Time 4 Hrs												
Aβo vs. Aβo + Hsp60	-16.96	-46.04 to 12.11	ns	0.3819	86.18	103.1	-16.96	10.36	11	11	2.316	19.33
Aβo vs. Hsp60	16.59	-8.128 to 41.31	ns	0.2413	86.18	69.59	16.59	8.272	11	11	2.836	11.5
Aβo vs. Vehicle	24.81	-0.01700 to 49.64	ns	0.0502	86.18	61.37	24.81	8.348	11	9	4.203	11.86
Aβo + Hsp60 vs. Hsp60	33.55	12.93 to 54.17	**	0.002	103.1	69.59	33.55	6.959	11	11	6.818	12.18
Aβo + Hsp60 vs. Vehicle	41.77	21.01 to 62.54	***	0.0003	103.1	61.37	41.77	7.049	11	9	8.38	12.67

Hsp60 vs. Vehicle	8.22	-1.148 to 17.59	ns	0.0969	69.59	61.37	8.22	3.298	11	9	3.525	17.11
Row 4: Time 6 Hrs												
Aβo vs. Aβo + Hsp60	-37.72	-60.87 to -14.57	**	0.0048	65.21	102.9	-37.72	6.845	7	7	7.792	6.48
Aβo vs. Hsp60	-5.665	-24.66 to 13.33	ns	0.7553	65.21	70.88	-5.665	5.671	7	7	1.413	6.711
Aβo vs. Vehicle	8.217	3.564 to 12.87	**	0.0023	65.21	56.99	8.217	1.443	7	6	8.055	7.758
Aβo + Hsp60 vs. Hsp60	32.05	6.123 to 57.98	*	0.0149	102.9	70.88	32.05	8.684	7	7	5.22	11.56
Aβo + Hsp60 vs. Vehicle	45.93	22.72 to 69.15	**	0.0019	102.9	56.99	45.93	6.733	7	6	9.649	6.074

Hsp60 vs. Vehicle	13.88	-5.171 to 32.94	ns	0.154	70.88	56.99	13.88	5.535	7	6	3.547	6.109
Row 5: Time 8 Hrs											
Aβo vs. Aβo + Hsp60	-23.3	-42.93 to -3.658	*	0.0168	73.86	97.15	-23.3	6.978	11	11	4.722	18.81
Aβo vs. Hsp60	-0.9927	-24.92 to 22.93	ns	0.9994	73.86	74.85	-0.9927	8.377	11	11	0.1676	16.25
Aβo vs. Vehicle	12.81	-1.213 to 26.84	ns	0.0793	73.86	61.04	12.81	4.876	11	9	3.717	15.24
Aβo + Hsp60 vs. Hsp60	22.3	-3.255 to 47.86	ns	0.1003	97.15	74.85	22.3	9.077	11	11	3.475	18.73
Aβo + Hsp60 vs. Vehicle	36.11	18.57 to 53.64	***	0.0002	97.15	61.04	36.11	6	11	9	8.511	13.42

124

Hsp60 vs. Vehicle	13.81	-8.682 to 36.30	ns	0.3105	74.85	61.04	13.81	7.582	11	9	2.575	12.08
Row 6: Time 24 Hrs												
Aβo vs. Aβo + Hsp60	-22.18	-38.13 to -6.232	**	0.0052	69.45	91.64	-22.18	5.597	11	11	5.604	16.61
Aβo vs. Hsp60	-5.176	-25.61 to 15.26	ns	0.881	69.45	74.63	-5.176	7.032	11	11	1.041	14.03
Aβo vs. Vehicle	9.451	-1.458 to 20.36	ns	0.1032	69.45	60	9.451	3.859	11	9	3.463	17.97
Aβo + Hsp60 vs. Hsp60	17.01	-5.473 to 39.49	ns	0.1796	91.64	74.63	17.01	7.975	11	11	3.016	18.5
Aβo + Hsp60 vs. Vehicle	31.63	16.09 to 47.18	***	0.0002	91.64	60	31.63	5.389	11	9	8.301	14.88

Hsp60 vs. Vehicle	14.63	-5.542 to 34.79	ns	0.195	74.63	60	14.63	6.867	11	9	3.012	12.94
* Alpha = 0.05												
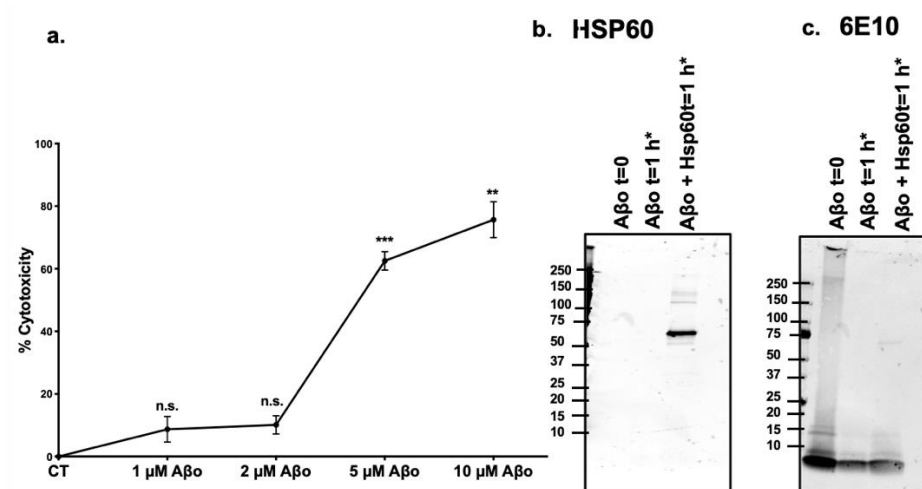
Supplementary Figure B.1. Cytotoxicity curve and quality control of doses for SH-Sy5Y cell treatments.

A. LDH assay of SH-SY5Y cells treated for 24 h, 37ºC, 5% CO_2 with increasing concentrations of pre-formed Aβo (1-10 μM, n=3), showing that 5 μM and 10 μM are significantly toxic concentrations. One-way ANOVA with Dunnett's multiple comparison analysis was used to determine the statistical significance between Aβo treatments compared to control (CT vs. 1μM Aβo n.s., p= 0.0950; CT vs. 2μM Aβo n.s., p= 0.0574; CT vs. 5μM Aβo, ***p= 0.0017; CT vs. 10 μM Aβo, **p=0.00421; DF=2; F (1.413, 2.826) = 703.7). Data plotted as mean of cytotoxicity percentage ± SEM. B. Representative western blotting of pre-formed Aβo not incubated (first line) or incubated 1 h at 37 ∘C either alone (second line) or with Hsp60 in 1:25 ratio (third line) using the anti-amyloid 6E10 antibody to detect Aβo. C. Representative western using anti-Hsp60 antibody to detect Hsp60 levels in the blot shown in (B).

A. Ex vivo treatments:
  a. Vehicle
  b. Aβ oligomers (o)
  c. Purified Aβo-Hsp60 treated
  d. Hsp60

B. Recordings:
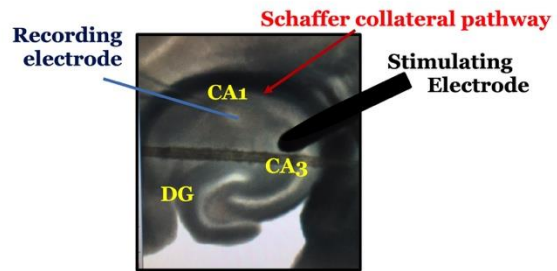
Hight frequency stimulation (HFS) paradigm:
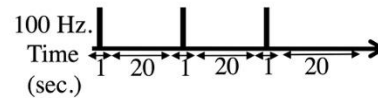
C. Data analysis

Supplementary Figure B.2. Experimental design for *ex vivo* electrophysiology recordings.

A. Diagram of the experimental protocol used to test changes in long-term potentiation of ex vivo brain slices of WT mice treated with vehicle (a.), Aβo (b.), Aβo + Hsp60 (c.) or Hsp60 (d.). B. Representative diagram of the electrophysiological recordings of the Schaffer collateral pathway projecting from the CA3 to the CA1 regions of the hippocampus. LTP was determined using the high frequency stimulation paradigm, consisting in delivering a train of 3 100 Hz stimulations of 1 s separated by 20s intervals. C. Data analysis of the traces was obtained by the analysis of the average of the slopes of fEPSP recorded pre- and post- HFS stimulation.
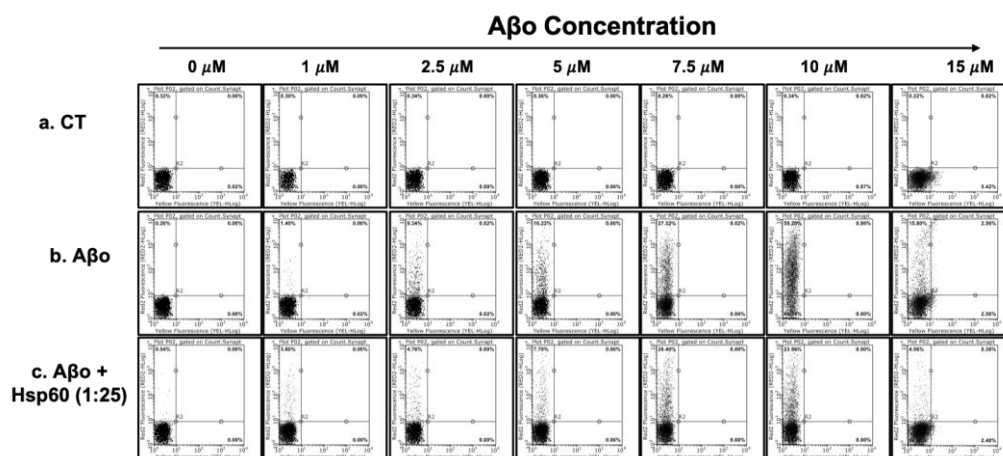
Supplementary Figure B.3. Representative flow cytometry plots of synaptosome binding studies.

Representative flow cytometry plots of isolated hippocampal synaptosomes treated either with vehicle (**a**.) or increasing concentrations of pre-formed Aβo either not treated (**b**.) or pre-treated with Hsp60 (**c**.), showing reduced binding to synaptosomes upon Aβo treatment with Hsp60. Plots represents the percentage of red fluorescence bound to the gated synaptosomes. The top-left quadrant expresses the levels of Aβ-Alexa647 bound to the gated synaptosomes.

References

[1]   Masters CL, Bateman R, Blennow K, Rowe CC, Sperling RA, Cummings JL (2015) Alzheimer's disease. *Nat. Rev. Dis. Prim.* **1**,.

[2]   Strassnig M, Ganguli M (2005) About a Peculiar Disease of the Cerebral Cortex : Alzheimer ' s Original Case Translation from the original publication of Alois Alzheimer : Über eine eigenartige Erkrankung der Hirnrinde (1907). *Psychiatry* **2**, 30–33.

[3]   Selkoe DJ (2011) Alzheimer's Disease. *Cold Spring Harb. Perspect. Biol.* **3**, a004457-75.

[4]   Holtzman DM, Morris JC, Goate AM (2011) Alzheimer ' s Disease : The Challenge of the Second Century. *Sci. Transl. Med.* **3**, 1–35.

[5]   Association A (2019) 2019 Alzheimer's Disease Facts and Figures. *Alzheimer's Dement.* **15**, 321–387.

[6]   Reitz C, Mayeux R (2014) Alzheimer disease: Epidemiology, diagnostic criteria, risk factors and biomarkers. *Biochem. Pharmacol.* **88**, 640–651.

[7]   Hebert LE, Beckett LA, Scherr PA, Evans DA (2001) Annual incidence of Alzheimer disease in the United States projected to the years 2000 through 2050. *Alzheimer Dis. Assoc. Disord.*

[8]   Selkoe DJ, Hardy J (2016) The amyloid hypothesis of Alzheimer's disease at 25 years. *EMBO Mol. Med.* **8**, 595–608.

[9]   Prince M, Bryce R, Albanese E, Wimo A, Ribeiro W, Ferri CP (2013) The global prevalence of dementia: A systematic review and metaanalysis. *Alzheimer's Dement.*

[10] Querfurth HW, LaFerla FM (2010) Alzheimer's disease. *N. Engl. J. Med.* 329–344.

[11] Dávila E, Targa G, Ávila J, Soriano E, Pascual M (2018) Differential accumulation of Tau phosphorylated at residues Thr231, Ser262 and Thr205 in hippocampal interneurons and its modulation by Tau mutations (VLW) and amyloid-β peptide. *Neurobiol. Dis.*

[12] Masters CL, Selkoe DJ (2012) Biochemistry of amyloid β-protein and amyloid deposits in Alzheimer disease. *Cold Spring Harb. Perspect. Med.* **2**, 1–24.

[13] Sperling RA, Aisen PS, Beckett LA, Bennett DA, Craft S, Fagan AM, Iwatsubo T, Jack CR, Kaye J, Montine TJ, Park DC, Reiman EM, Rowe CC, Siemers E, Stern Y, Yaffe K, Carrillo MC, Thies B, Morrison-Bogorad M, Wagster M V., Phelps CH (2011) Toward defining the preclinical stages of Alzheimer's disease: Recommendations from the National Institute on Aging-Alzheimer's Association workgroups on diagnostic guidelines for Alzheimer's disease. *Alzheimer's Dement.* **7**, 280–292.

[14] Veitch DP, Weiner MW, Aisen PS, Beckett LA, Cairns NJ, Green RC, Harvey D, Jack CR, Jagust W, Morris JC, Petersen RC, Saykin AJ, Shaw LM, Toga AW, Trojanowski JQ (2018) Understanding disease progression and improving Alzheimer's disease clinical trials: Recent highlights from the Alzheimer's Disease Neuroimaging Initiative Dallas. *Alzheimer's Dement.* **In press**, 1–47.

[15] Briley D, Ghirardi V, Woltjer R, Renck A, Zolochevska O, Taglialatela G, Micci MA (2016) Preserved neurogenesis in non-demented individuals with AD neuropathology. *Sci. Rep.* **6**, 1–10.

[16] Zolochevska O, Taglialatela T (2016) Non-Demented Individuals with Alzheimer's Disease Neuropathology: Resistance to Cognitive Decline May Reveal New Treatment Strategies. *Curr. Pharm. Des.* **22**, 4063–4068.

[17] Zolochevska O, Bjorklund N, Woltjer R, Wiktorowicz JE, Taglialatela G (2018) Postsynaptic Proteome of Non-Demented Individuals with Alzheimer's Disease Neuropathology. *J. Alzheimer's Dis.* **65**, 1–24.

[18] Bjorklund NL, Reese LC, Sadagoparamanujam VM, Ghirardi V, Woltjer RL, Taglialatela G (2012) Absence of amyloid β oligomers at the postsynapse and regulated synaptic Zn2+in cognitively intact aged individuals with Alzheimer's disease neuropathology. *Mol. Neurodegener.* **7**, 1–13.

[19] Lue L-F, Kuo YM, Roher AE, Brachova L, Shen Y, Sue L, Beach T, Kurth janice H, Rydel RE, Rogers J (1999) Soluble Amyloid $_L^N$ Peptide Concentration as a Predictor of Synaptic Change in Alzheimer's Disease Lih-Fen. *Am. J. Pathol.* **155**, 853–862.

[20] Alzheimer's Association (2016) 2016 Alzheimer's disease facts and figures. *Alzheimer's Dement.* **12**, 459–509.

[21] Musiek ES, Holtzman DM (2015) Three dimensions of the amyloid hypothesis: Time, space and "wingmen." *Nat. Neurosci.* **18**, 800–806.

[22] Casavant MJ (2002) Goodman and Gilman's The Pharmacological Basis of Therapeutics. *JAMA J. Am. Med. Assoc.*

[23] Schneider LS, Sano M (2009) Current Alzheimer's disease clinical trials: Methods and placebo outcomes. *Alzheimer's Dement.*

[24] Cummings J, Aisen PS, Dubois B, Frölich L, Jack CR, Jones RW, Morris JC,

Raskin J, Dowsett SA, Scheltens P (2016) Drug development in Alzheimer's disease: The path to 2025. *Alzheimer's Res. Ther.* **8**, 1–12.

[25]   Szeto J, Lewis S (2016) Current Treatment Options for Alzheimer's Disease and Parkinson's Disease Dementia. *Curr. Neuropharmacol.*

[26]   De Strooper B (2010) Proteases and Proteolysis in Alzheimer Disease: A Multifactorial View on the Disease Process. *Physiol. Rev.*

[27]   Taylor RC, Dillin A (2011) Aging as an event of proteostasis collapse. *Cold Spring Harb. Perspect. Biol.*

[28]   Lu T, Aron L, Zullo J, Pan Y, Kim H, Chen Y, Yang TH, Kim HM, Drake D, Liu XS, Bennett DA, Colaiácovo MP, Yankner BA (2014) REST and stress resistance in ageing and Alzheimer's disease. *Nature*.

[29]   Weiner MW, Veitch DP, Aisen PS, Beckett LA, Nigel J, Cedarbaum J, Green RC, Harvey D, Jack CR, Luthman J, Morris JC, Petersen RC, Saykin AJ, Shaw L, Shen L, Schwarz A, Toga AW, Trojanowski JQ, Francisco S, Francisco S, Francisco S, Francisco S, Francisco S, Diego S, Jolla L, Louis S, Development EC, Idec B, Clinic M, Development C, Medicine G, Creation P (2015) 2014 Update of the Alzheimer's Disease Neuroimaging Initiative: A review of papers published since its inception. **11**, e1-120.

[30]   Duthie A, Chew D, Soiza RL (2011) Non-psychiatric comorbidity associated with Alzheimer's disease. *Qjm* **104**, 913–920.

[31]   Michaud M, Balardy L, Moulis G, Gaudin C, Peyrot C, Vellas B, Cesari M, Nourhashemi F (2013) Proinflammatory cytokines, aging, and age-related diseases. *J. Am. Med. Dir. Assoc.* **14**, 877–882.

[32]   Herrup K (2010) Re-imagining Alzheimer's disease – an age-based hypothesis Karl. **30**, 16755–16762.

[33]   Ries HM, Nussbaum-Krammer C (2016) Shape matters: the complex relationship between aggregation and toxicity in protein-misfolding diseases. *Essays Biochem.*

[34]   Molinuevo JL, Ayton S, Batrla R, Bednar MM, Bittner T, Cummings J, Fagan AM, Hampel H, Mielke MM, Mikulskis A, O'Bryant S, Scheltens P, Sevigny J, Shaw LM, Soares HD, Tong G, Trojanowski JQ, Zetterberg H, Blennow K (2018) Current state of Alzheimer's fluid biomarkers. *Acta Neuropathol.* **136**, 821–853.

[35]   Reddy PH, McWeeney S (2006) Mapping cellular transcriptosomes in autopsied Alzheimer's disease subjects and relevant animal models. *Neurobiol. Aging*.

[36]   Dong HK, Gim JA, Yeo SH, Kim HS (2017) Integrated late onset Alzheimer's disease (LOAD) susceptibility genes: Cholesterol metabolism and trafficking perspectives. *Gene* **597**, 10–16.

[37]   Smith M (2017) Genetics of Alzheimer's disease. In *Dementia, Fifth Edition*.

[38]   Hardy J, Allsop D (1991) Amyloid deposition as the central event in the aetiology of Alzheimer's disease. *Trends Pharmacol. Sci.* **12**, 383–388.

[39]   Head E, Powell D, Gold BT, Schmitt FA (2012) Alzheimer's Disease in Down Syndrome. *Eur. J. Neurodegener. Dis.* **1**, 353–364.

[40]   Bertram L, Tanzi RE (2012) The genetics of Alzheimer's disease. *Prog. Mol. Biol. Transl. Sci.*

[41]   Bruni AC, Conidi ME, Bernardi L (2014) Genetics in degenerative dementia: Current status and applicability. *Alzheimer Dis. Assoc. Disord.*

[42]   Jarrett JT, Lansburry PT (1993) Seeding "one dimensional cristallization" of

amyloid: a pathogenic mechanism in Alzheimer's disease and scrapie? *Cell* **73**, 1055–1058.

[43] Jansen I, Savage J, Watanabe K, Bryois J, Williams D, Steinberg S, Sealock J, Karlsson I, Hagg S, Athanasiu L, Voyle N, Proitsi P, Witoelar A, Stringer S, Aarsland D, Almdahl I, Andersen F, Bergh S, Bettella F, Bjornsson S, Braekhus A, Brathen G, Leeuw C de, Desikan R, Djurovic S, Dumitrescu L, Fladby T, Homan T, Jonsson P, Kiddle S, Rongve A, Saltvedt I, Sando S, Selbak G, Skene N, Snaedal J, Stordal E, Ulstein I, Wang Y, White L, Hjerling-Leffler J, Sullivan P, Flier W van der, Dobson R, Davis L, Stefansson H, Stefansson K, Pedersen N, Ripke S, Andreassen O, Posthuma D (2019) Genome-wide meta-analysis identifies new loci and functional pathways influencing Alzheimer's disease risk. *Nat. Genet.* **51**, 404–413.

[44] Weller RO, Subash M, Preston SD, Mazanti I, Carare RO (2008) Perivascular drainage of amyloid-β peptides from the brain and its failure in cerebral amyloid angiopathy and Alzheimer's disease. In *Brain Pathology*.

[45] Rabinovici GD (2019) Late-onset Alzheimer Disease. *Contin. lifelong Learn. Neurol.* **25**, 14–33.

[46] Lott IT, Dierssen M (2010) Cognitive deficits and associated neurological complications in individuals with Down's syndrome. *Lancet Neurol.*

[47] Hickman RA, Faustin A, Wisniewski T (2016) Alzheimer Disease and Its Growing Epidemic: Risk Factors, Biomarkers, and the Urgent Need for Therapeutics. *Neurol. Clin.* **34**, 941–953.

[48] Reddy PH, Beal MF (2008) Amyloid beta, mitochondrial dysfunction and synaptic

damage: implications for cognitive decline in aging and Alzheimer's disease. *Trends Mol. Med.* **14**, 45–53.

[49]   Nuzzo D, Picone P, Baldassano S, Caruana L, Messina E, Gammazza A, Cappello F, Mulè F, Carlo M (2015) Insulin Resistance as Common Molecular Denominator Linking Obesity to Alzheimer's Disease. *Curr. Alzheimer Res.* **12**, 723–735.

[50]   Li JQ, Tan L, Wang HF, Tan MS, Tan L, Xu W, Zhao QF, Wang J, Jiang T, Yu JT (2016) Risk factors for predicting progression from mild cognitive impairment to Alzheimer's disease: A systematic review and meta-analysis of cohort studies. *J. Neurol. Neurosurg. Psychiatry* **87**, 476–484.

[51]   Mielke M, Vemuri P, Rocca W (2014) Clinical epidemiology of Alzheimer ' s disease : assessing sex and gender differences. *Clin. Epidemiol.* 37–48.

[52]   Braak H, Del Tredici K (2011) The pathological process underlying Alzheimer's disease in individuals under thirty. *Acta Neuropathol.* **121**, 171–181.

[53]   Frautschy SA, Cole GM (2010) Why pleiotropic interventions are needed for alzheimer's disease. In *Molecular Neurobiology*.

[54]   Mattson MP (2004) Pathways towards and away from Alzheimer's disease. *Nature*.

[55]   Butterfield S, Hejjaoui M, Fauvet B, Awad L, Lashuel HA (2012) Chemical strategies for controlling protein folding and elucidating the molecular mechanisms of amyloid formation and toxicity. *J. Mol. Biol.* **421**, 204–236.

[56]   Soto C (2003) Unfolding the role of protein misfolding in neurodegenerative diseases. *Nat. Rev. Neurosci.*

[57]   Soto C, Estrada LD (2008) Protein misfolding and neurodegeneration. *Arch.*

Neurol.

[58] Necula M, Kayed R, Milton S, Glabe CG (2007) Small molecule inhibitors of aggregation indicate that amyloid ?? oligomerization and fibrillization pathways are independent and distinct. *J. Biol. Chem.* **282**, 10311–10324.

[59] Selkoe DJ (2008) Soluble oligomers of the amyloid beta-protein impar synaptic plasticity and behavior. *Behav. brain Res.* **192**, 106–113.

[60] Langer F, Eisele YS, Fritschi SK, Staufenbiel M, Walker LC, Jucker M (2011) Soluble Aβ seeds are potent inducers of cerebral β-amyloid deposition. *J. Neurosci.* **31**, 14488–14495.

[61] Weidemann A, König G, Bunke D, Fischer P, Salbaum JM, Masters CL, Beyreuther K (1989) Identification, biogenesis, and localization of precursors of Alzheimer's disease A4 amyloid protein. *Cell*.

[62] Kang J, Lemaire HG, Unterbeck A, Salbaum JM, Masters CL, Grzeschik KH, Multhaup G, Beyreuther K, Müller-Hill B (1987) The precursor of Alzheimer's disease amyloid A4 protein resembles a cell-surface receptor. *Nature*.

[63] Walsh DM, Selkoe DJ (2007) Aβ oligomers - A decade of discovery. *J. Neurochem.*

[64] Haass C, Kaether C, Thinakaran G, Sisodia S (2012) Trafficking and Proteolytic Processing of APP.pdf. *Cold Spring Harb. Perspect. Med.* 1–26.

[65] Haass C (2004) Take five - BACE and the γ-secretase quartet conduct Alzheimer's amyloid β-peptide generation. *EMBO J.*

[66] Mitraki A (2010) *Protein aggregation: From inclusion bodies to amyloid and biomaterials*, Elsevier Inc.

[67] Breydo L, Uversky VN (2015) Structural, morphological, and functional diversity of amyloid oligomers. *FEBS Lett.* **589**, 2640–2648.

[68] Bodani RU, Sengupta U, Castillo-Carranza DL, Guerrero-Muñoz MJ, Gerson JE, Rudra J, Kayed R (2015) Antibody against Small Aggregated Peptide Specifically Recognizes Toxic Aβ-42 Oligomers in Alzheimer's Disease. *ACS Chem. Neurosci.* **6**, 1981–1989.

[69] Suzuki N, Iwatsubo T, Odaka A, Ishibashi Y, Kitada C, Ihara Y (1994) High tissue content of soluble beta 1-40 is linked to cerebral amyloid angiopathy. *Am. J. Pathol.* **145**, 452–60.

[70] Kumar S, Walter J (2011) Aging (Albany NY) 2011 Kumar S. **3**, 1–10.

[71] Marcus Fändrich, Matthias Schmidt and NG (2011) Recent progress in understanding Alzheimer's β-amyloid structures. *Trends Biochem Sci* **36**, 338–345.

[72] Hsia AY, Masliah E, McConlogue L, Yu G-Q, Tatsuno G, Hu K, Kholodenko D, Malenka RC, Nicoll RA, Mucke L (1999) Plaque-independent disruption of neural circuits in Alzheimer's disease mouse models. *Proc. Natl. Acad. Sci.* **96**, 3228–3233.

[73] Kayed R, Canto I, Breydo L, Rasool S, Lukacsovich T, Wu J, Albay R, Pensalfini A, Yeung S, Head E, Marsh JL, Glabe C (2010) Conformation dependent monoclonal antibodies distinguish different replicating strains or conformers of prefibrillar Aβ oligomers. *Mol. Neurodegener.* **5**, 57.

[74] Kayed R, Lasagna-Reeves CA (2013) Molecular Mechanisms of Amyloid Oligomers Toxicity. *J. Alzheimer's Dis.* **33**, s67–s78.

[75] Tomic JL, Pensalfini A, Head E, Glabe CG (2009) United Kingdom: HSE issues Buncefield overflow switch alert. *Neurobiol. Dis.* **35**, 352–358.

[76] Kayed R, Head E, Thompson JL, McIntire TM, Milton SC, Cotman CW, Glabel CG (2003) Common structure of soluble amyloid oligomers implies common mechanism of pathogenesis. *Science (80-.).* **300**, 486–489.

[77] Knowles TPJ, Vendruscolo M, Dobson CM (2014) The amyloid state and its association with protein misfolding diseases. *Nat. Rev. Mol. Cell Biol.*

[78] Kahler A, Sticht H, Horn AHC (2013) Conformational Stability of Fibrillar Amyloid-Beta Oligomers via Protofilament Pair Formation - A Systematic Computational Study. *PLoS One* **8**,.

[79] Puzzo D, Arancio O (2013) Amyloid-b Peptide: Dr. Jekyll or Mr. Hyde? *J. Alzheimer's Dis.* **33**, 1–14.

[80] Puzzo D, Privitera L, Palmeri A (2012) Hormetic effect of amyloid-beta peptide in synaptic plasticity and memory. *Neurobiol. Aging* **33**, 1484.e15-1484.e24.

[81] Benilova I, Karran E, De Strooper B (2012) The toxic Aβ oligomer and Alzheimer's disease: An emperor in need of clothes. *Nat. Neurosci.* **15**, 349–357.

[82] Braak H, Del Tredici K (2011) Alzheimer's pathogenesis: Is there neuron-to-neuron propagation? *Acta Neuropathol.* **121**, 589–595.

[83] Prusiner SB (1998) Prions. *Proc. Natl. Acad. Sci.* **95**, 13363–13383.

[84] Geschwind MD (2015) *Prion Diseases*.

[85] Walker LC (2018) Prion-like Mechanisms in Alzheimer Disease Lary. *Handb Clin Neurol.* **153**, 303–319.

[86] Ashe KH, Aguzzi A (2013) Prions, prionoids and pathogenic proteins in

Alzheimer disease. *Prion* **7**, 55–59.

[87]   Cai Q, Tammineni P (2017) Mitochondrial Aspects of Synaptic Dysfunction in
Alzheimer's Disease. *J. Alzheimer's Dis.* **57**, 1087–1103.

[88]   Lustbader JW, Cirilli M, Lin C, Xu HW, Takuma K, Wang N, Caspersen C, Chen
X, Pollak S, Chaney M, Trinchese F, Liu S, Gunn-Moore F, Lue LF, Walker DG,
Kappasamy P, Zewier ZL, Arancio O, Stern D, Yan SS Du, Wu H (2004) ABAD
Directly Links Aβ to Mitochondrial Toxicity in Alzheimer's Disease. *Science (80-.
).*

[89]   Manczak M, Mao P, Calkins MJ, Cornea A, Reddy AP, Murphy MP, Szeto HH,
Park B, Reddy PH (2010) Mitochondria-targeted antioxidants protect against
amyloid-β toxicity in Alzheimer's disease neurons. *J. Alzheimer's Dis.*

[90]   Crimins JL, Pooler A, Polydoro M, Luebke JI, Spires-Jones TL (2013) The
intersection of amyloid beta and tau in glutamatergic synaptic dysfunction and
collapse in Alzheimer's disease. *Ageing Res. Rev.*

[91]   Spires-Jones TL, Hyman BT (2014) The Intersection of Amyloid Beta and Tau at
Synapses in Alzheimer's Disease. *Neuron.*

[92]   Spillantini MG, Goedert M (2013) Tau pathology and neurodegeneration. *Lancet
Neurol.*

[93]   Ballatore C, Lee VMY, Trojanowski JQ (2007) Tau-mediated neurodegeneration
in Alzheimer's disease and related disorders. *Nat. Rev. Neurosci.*

[94]   Iqbal K, Del C. Alonso A, Chen S, Chohan MO, El-Akkad E, Gong CX, Khatoon
S, Li B, Liu F, Rahman A, Tanimukai H, Grundke-Iqbal I (2005) Tau pathology in
Alzheimer disease and other tauopathies. *Biochim. Biophys. Acta - Mol. Basis Dis.*

[95]   Khan SH, Kumar R (2017) Trehalose induced conformational changes in the amyloid-β peptide. *Pathol. Res. Pract.* **213**, 643–648.

[96]   Gerson JE, Kayed R (2013) Formation and propagation of tau oligomeric seeds. **4**, 1–10.

[97]   Kaufman SK, Sanders DW, Thomas TL, Ruchinskas A, Vaquer-alicea J, Sharma AM, Miller TM, Diamond MI (2017) HHS Public Access. **92**, 796–812.

[98]   Kaufman SK, Del K, Talitha T, Heiko LT, Marc B (2018) Tau seeding activity begins in the transentorhinal / entorhinal regions and anticipates phospho - tau pathology in Alzheimer ' s disease and PART . *Acta Neuropathol.* **136**, 57–67.

[99]   Bakota L, Brandt R (2016) Tau Biology and Tau-Directed Therapies for Alzheimer's Disease. *Drugs* **76**, 301–313.

[100]   Kester MI, Teunissen CE, Sutphen C, Herries EM, Ladenson JH, Xiong C, Scheltens P, Van Der Flier WM, Morris JC, Holtzman DM, Fagan AM (2015) Cerebrospinal fluid VILIP-1 and YKL-40, candidate biomarkers to diagnose, predict and monitor Alzheimer's disease in a memory clinic cohort. *Alzheimer's Res. Ther.* **7**, 1–9.

[101]   Fá M, Puzzo D, Piacentini R, Staniszewski A, Zhang H, Baltrons MA, Li Puma DD, Chatterjee I, Li J, Saeed F, Berman HL, Ripoli C, Gulisano W, Gonzalez J, Tian H, Costa JA, Lopez P, Davidowitz E, Yu WH, Haroutunian V, Brown LM, Palmeri A, Sigurdsson EM, Duff KE, Teich AF, Honig LS, Sierks M, Moe JG, D'Adamio L, Grassi C, Kanaan NM, Fraser PE, Arancio O (2016) Extracellular Tau Oligomers Produce An Immediate Impairment of LTP and Memory. *Sci. Rep.* **6**, 19393.

[102] Tripathi T, Kalita P (2019) Synergistic Effect of Amyloid-β and Tau Disrupts Neural Circuits. *ACS Chem. Neurosci.* acschemneuro.9b00037.

[103] Farlow MR, Salloway S, Tariot PN, Yardley J, Moline ML, Wang Q, Brand-Schieber E, Zou H, Hsu T, Satlin A (2010) Effectiveness and tolerability of high-dose (23 mg/d) versus standard-dose (10 mg/d) donepezil in moderate to severe Alzheimer's disease: A 24-week, randomized, double-blind study. *Clin. Ther.*

[104] Alam S, Lingenfelter KS, Bender AM, Lindsley CW (2017) Classics in Chemical Neuroscience: Memantine. *ACS Chem. Neurosci.* **8**, 1823–1829.

[105] Johnson JW, Kotermanski SE (2006) Mechanism of action of memantine. *Curr. Opin. Pharmacol.* **6**, 61–67.

[106] Rammes G, Rupprecht R, Ferrari U, Zieglgänsberger W, Parsons CG (2001) The N-methyl-D-aspartate receptor channel blockers memantine, MRZ 2/579 and other amino-alkyl-cyclohexanes antagonise 5-HT3 receptor currents in cultured HEK-293 and N1E-115 cell systems in a non-competitive manner. *Neurosci. Lett.* **306**, 81–84.

[107] Ritter A, Cummings J (2015) Fluid biomarkers in clinical trials of Alzheimer's disease therapeutics. *Front. Neurol.* **6**,.

[108] Golde BTE, Dekosky ST, Galasko D (2018) Alzheimer's disease: The right drug, the right time. **362**, 1250–1252.

[109] Asea AA, Brown IR (2008) *Heat Shock Proteins and the brain: Implications for Neurodegenerative diseases and Neuroprotection*, Springer Netherlands.

[110] Kaushik S, Cuervo AM (2015) Proteostasis and aging. *Nat. Med.*

[111] Kim YE, Hipp MS, Bracher A, Hayer-Hartl M, Ulrich Hartl F (2013) *Molecular*

Chaperone Functions in Protein Folding and Proteostasis.

[112] Douglas PM, Dillin A (2010) Protein homeostasis and aging in neurodegeneration. *J. Cell Biol.*

[113] Macario AJL, Cappello F, Zummo G, Conway De MacArio E (2010) Chaperonopathies of senescence and the scrambling of interactions between the chaperoning and the immune systems. *Ann. N. Y. Acad. Sci.* **1197**, 85–93.

[114] Richter K, Haslbeck M, Buchner J (2010) The Heat Shock Response: Life on the Verge of Death. *Mol. Cell* **40**, 253–266.

[115] Horwich AL, Buchner J, Smock RG, Gierasch LM, Saibil HR (2012) Chaperones and protein folding. *Compr. Biophys.* **3**, 212–237.

[116] Clare DK, Saibil HR (2013) ATP-driven molecular chaperone machines. *Biopolymers* **99**, 846–859.

[117] Skjærven L, Cuellar J, Martinez A, Valpuesta JM (2015) Dynamics, flexibility, and allostery in molecular chaperonins. *FEBS Lett.* **589**, 2522–2532.

[118] Hartl F (2002) Molecular Chaperones in the Cytosol: from Nascent Chainto Folded Protein. *Science (80-.).* **295**, 1852.

[119] Liberek K, Lewandowska A, Ziętkiewicz S (2008) Chaperones in control of protein disaggregation. *EMBO J.* **27**, 328–335.

[120] Chaudhuri TK, Farr GW, Fenton WA, Rospert S, Horwich AL (2001) GroEL/GroES-mediated folding of a protein too large to be encapsulated. *Cell*.

[121] Díaz-Villanueva JF, Díaz-Molina R, García-González V (2015) Protein folding and mechanisms of proteostasis. *Int. J. Mol. Sci.* **16**, 17193–17230.

[122] Uversky VN, Gillespie JR, Fink AL (2000) Why are "natively unfolded" proteins

unstructured under physiologic conditions? *Proteins Struct. Funct. Genet.*

[123] Uversky VN (2002) What does it mean to be natively unfolded? *Eur. J. Biochem.*

[124] Hoffmann A, Bukau B, Kramer G (2010) Structure and function of the molecular chaperone Trigger Factor. *Biochim. Biophys. Acta - Mol. Cell Res.*

[125] TOMPA P (2004) The role of structural disorder in the function of RNA and protein chaperones. *FASEB J.*

[126] Kovacs D, Tompa P (2012) Diverse functional manifestations of intrinsic structural disorder in molecular chaperones. *Biochem. Soc. T.*

[127] Uversky VN (2013) Intrinsically Disordered Proteins. In *Brenner's Encyclopedia of Genetics: Second Edition*.

[128] Dunker AK, Brown CJ, Obradovic Z (2002) Identification and functions of usefully disordered proteins. *Adv. Protein Chem.*

[129] Xu Z, Horwich AL, Sigler PB (1997) The crystal structure of the asymmetric GroEL-GroES-(ADP)7 chaperonin complex. *Nature.*

[130] Nisemblat S, Parnas A, Yaniv O, Azem A, Frolow F (2014) Crystallization and structure determination of a symmetrical "football" complex of the mammalian mitochondrial Hsp60-Hsp10 chaperonins. *Acta Crystallogr. Sect. FStructural Biol. Commun.* **70**, 116–119.

[131] Braig K, Otwinowski Z, Hegde R, Boisvert DC, Joachimiak A, Horwich AL, Sigler PB (1994) The crystal structure of the bacterial chaperonln GroEL at 2.8 Å. *Nature*.

[132] Hayer-Hartl M, Bracher A, Hartl FU (2016) The GroEL-GroES Chaperonin Machine: A Nano-Cage for Protein Folding. *Trends Biochem. Sci.*

[133] Okamoto T, Ishida R, Yamamoto H, Tanabe-Ishida M, Haga A, Takahashi H, Takahashi K, Goto D, Grave E, Itoh H (2015) Functional structure and physiological functions of mammalian wild-type HSP60. *Arch. Biochem. Biophys.* **586**, 10–19.

[134] Ishida R, Okamoto T, Motojima F, Kubota H, Takahashi H, Tanabe M, Oka T, Kitamura A, Kinjo M, Yoshida M, Otaka M, Grave E, Itoh H (2018) Physicochemical properties of the mammalian molecular chaperone HSP60. *Int. J. Mol. Sci.* **19**,.

[135] Ellis RJ (2003) Protein Folding: Importance of the Anfinsen Cage. *Curr. Biol.* **13**, 881–883.

[136] Barral JM, Broadley SA, Schaffar G, Hartl FU (2004) Roles of molecular chaperones in protein misfolding diseases. *Semin. Cell Dev. Biol.* **15**, 17–29.

[137] Bigotti MG, Clarke AR (2008) Chaperonins: The hunt for the Group II mechanism. *Arch. Biochem. Biophys.*

[138] Vilasi S, Carrotta R, Mangione MR, Campanella C, Librizzi F, Randazzo L, Martorana V, Gammazza AM, Ortore MG, Vilasi A, Pocsfalvi G, Burgio G, Corona D, Piccionello AP, Zummo G, Bulone D, De Macario EC, Macario AJL, San Biagio PL, Cappello F (2014) Human Hsp60 with its mitochondrial import signal occurs in solution as heptamers and tetradecamers remarkably stable over a wide range of concentrations. *PLoS One* **9**,.

[139] Cheng MY, Hartl F-U, Martin J, Pollock RA, Kalousek F, Neuper W, Hallberg EM, Hallberg RL, Horwich AL (1989) Mitochondrial heat-shock protein hsp60 is essential for assembly of proteins imported into yeast mitochondria. *Nature* **337**,

620.

[140] Cappello F, Conway De Macario E, Marasà L, Zummo G, Macario AJL (2008) Hsp60 expression, new locations, functions and perspectives for cancer diagnosis and therapy. *Cancer Biol. Ther.*

[141] Balchin D, Hayer-Hartl M, Hartl FU (2016) In vivo aspects of protein folding and quality control. *Science (80-.).* **353**,.

[142] Brown IR (2007) Heat shock proteins and protection of the nervous system. In *Annals of the New York Academy of Sciences*.

[143] Kurtishi A, Rosen B, Patil KS, Alves GW, Møller SG (2018) Cellular Proteostasis in Neurodegeneration.

[144] Veereshwarayya V, Kumar P, Rosen KM, Mestril R, Querfurth HW (2006) Differential effects of mitochondrial heat shock protein 60 and related molecular chaperones to prevent intracellular β-amyloid-induced inhibition of complex IV and limit apoptosis. *J. Biol. Chem.* **281**, 29468–29478.

[145] Jeng W, Lee S, Sung N, Lee J, Tsai FTF (2015) Molecular chaperones: guardians of the proteome in normal and disease states. *F1000Research* **4**, 1–11.

[146] Muchowski PJ (2010) Protein Folding and the Role of Chaperone Proteins in Neurodegenerative Disease. *Encycl. Neurosci.* 1163–1166.

[147] Walls KC, Coskun P, Gallegos-Perez JL, Zadourian N, Freude K, Rasool S, Blurton-Jones M, Green KN, LaFerla FM (2012) Swedish Alzheimer mutation induces mitochondrial dysfunction mediated by HSP60 mislocalization of Amyloid Precursor Protein (APP) and beta-amyloid. *J. Biol. Chem.* **287**, 30317–30327.

[148] Muschol M, Wang L, Uversky VN, Binder EB, Fontaine SN, Blair LJ, O'Leary JC, Cotman C, Zhang B, Scaglione KM, Kayed R, Nordhues BA, Berchtold N, Klengel T, Paulson HL, Golde TE, Dickey CA, Hill SE, Li P, Breydo L (2013) Accelerated neurodegeneration through chaperone-mediated oligomerization of tau. *J. Clin. Invest.* **123**, 4158–4169.

[149] Morley JF, Brignull HR, Weyers JJ, Morimoto RI (2002) The threshold for polyglutamine-expansion protein aggregation and cellular toxicity is dynamic and influenced by aging in Caenorhabditis elegans. *Proc. Natl. Acad. Sci.*

[150] World Health Organization (2017) *Dementia factsheet*.

[151] Cavallucci V, D'Amelio M, Cecconi F (2012) Aβ toxicity in Alzheimer's disease. *Mol. Neurobiol.* **45**, 366–378.

[152] Stoveken BJ (2013) Tau Pathology as a Cause and Consequence of the UPR. *J. Neurosci.* **33**, 14285–14287.

[153] Dineley KT, Kayed R, Neugebauer V, Fu Y, Zhang W, Reese LC, Taglialatela G (2010) Amyloid-β oligomers impair fear conditioned memory in a calcineurin-dependent fashion in mice. *J. Neurosci. Res.* **88**, 2923–2932.

[154] Uversky VN (2011) Flexible nets of malleable guardians: Intrinsically disordered chaperones in neurodegenerative diseases. *Chem. Rev.* **111**, 1134–1166.

[155] Liu P, Reed MN, Kotilinek LA, Grant MKO, Forster CL, Qiang W, Shapiro SL, Reichl JH, Chiang ACA, Jankowsky JL, Wilmot CM, Cleary JP, Zahs KR, Ashe KH (2015) Quaternary structure defines a large class of amyloid-β oligomers neutralized by sequestration. **11**, 1760–1771.

[156] Cohen SIA, Arosio P, Presto J, Kurudenkandy FR, Biverstål H, Dolfe L, Dunning

C, Yang X, Frohm B, Vendruscolo M, Johansson J, Dobson CM, Fisahn A, Knowles TPJ, Linse S (2015) A molecular chaperone breaks the catalytic cycle that generates toxic Aβ oligomers. *Nat. Struct. Mol. Biol.* **22**, 207–213.

[157] Fezoui Y, Hartley DM, Harper JD, Khurana R, Walsh DM, Condron MM, Selkoe DJ, Lansbury J, Fink AL, Teplow DB (2000) An improved method of preparing the amyloid β-protein for fibrillogenesis and neurotoxicity experiments. *Amyloid*.

[158] Carrotta R, Di Carlo M, Manno M, Montana G, Picone P, Romancino D, San Biagio PL (2006) Toxicity of recombinant beta-amyloid prefibrillar oligomers on the morphogenesis of the sea urchin Paracentrotus lividus. *FASEB J.*

[159] HOLDE KE Van, JOHNSON WC, HO PS (2006) *Principles of Physical Biochemistry,*.

[160] Lakowicz JR (2006) *Principles of fluorescence spectroscopy*.

[161] Canale C, Seghezza S, Vilasi S, Carrotta R, Bulone D, Diaspro A, San Biagio PL, Dante S (2013) Different effects of Alzheimer's peptide Aβ(1-40) oligomers and fibrils on supported lipid membranes. *Biophys. Chem.*

[162] Corsale C, Carrotta R, Mangione MR, Vilasi S, Provenzano A, Cavallaro G, Bulone D, San Biagio PL (2012) Entrapment of Aβ1-40peptide in unstructured aggregates. *J. Phys. Condens. Matter* **24**,.

[163] Wolfe LS, Calabrese MF, Nath A, Blaho D V., Miranker AD, Xiong Y (2010) Protein-induced photophysical changes to the amyloid indicator dye thioflavin T. *Proc. Natl. Acad. Sci.* **107**, 16863–16868.

[164] Biancalana M, Koide S (2010) Molecular mechanism of Thioflavin-T binding to amyloid fibrils. *Biochim. Biophys. Acta - Proteins Proteomics* **1804**, 1405–1412.

[165] Naiki H, Higuchi K, Hosokawa M, Takeda T (1989) Fluorometric determination of amyloid fibrils in vitro using the fluorescent dye, thioflavine T. *Anal. Biochem.* **177**, 244–249.

[166] Mangione MR, Vilasi S, Marino C, Librizzi F, Canale C, Spigolon D, Bucchieri F, Fucarino A, Passantino R, Cappello F, Bulone D, San Biagio PL (2016) Hsp60, amateur chaperone in amyloid-beta fibrillogenesis. *Biochim. Biophys. Acta - Gen. Subj.* **1860**, 2474–2483.

[167] Hellstrand E, Boland B, Walsh DM, Linse S (2010) Amyloid β-protein aggregation produces highly reproducible kinetic data and occurs by a two-phase process. *ACS Chem. Neurosci.*

[168] Dunstan DE, Hamilton-Brown P, Asimakis P, Ducker W, Bertolini J (2009) Shear flow promotes amyloid-β fibrilization. *Protein Eng. Des. Sel.*

[169] Hamilton-Brown P, Bekard I, Ducker WA, Dunstan DE (2008) How does shear affect a?? fibrillogenesis? *J. Phys. Chem. B*.

[170] Garvey M, Morgado I (2013) Peptide concentration alters intermediate species in amyloid β fibrillation kinetics. *Biochem. Biophys. Res. Commun.*

[171] Klement K, Wieligmann K, Meinhardt J, Hortschansky P, Richter W, Fändrich M (2007) Effect of Different Salt Ions on the Propensity of Aggregation and on the Structure of Alzheimer's Aβ(1-40) Amyloid Fibrils. *J. Mol. Biol.*

[172] Yagi-Utsumi M, Dobson CM (2015) Conformational Effects of the A21G Flemish Mutation on the Aggregation of Amyloid β Peptide. *Biol. Pharm. Bull.*

[173] Luiken JA, Bolhuis PG (2015) Primary Nucleation Kinetics of Short Fibril-Forming Amyloidogenic Peptides. *J. Phys. Chem. B* **119**, 12568–12579.

[174] Fezoui Y, Teplow DB (2002) Kinetic studies of amyloid β-protein fibril assembly. Differential effects of α-helix stabilization. *J. Biol. Chem.*

[175] Meisl G, Michaels TCT, Linse S, Knowles TPJ (2018) Kinetic analysis of amyloid formation. In *Methods in Molecular Biology*.

[176] Spigolon D (2017) Biophysical investigation on therapeutic proteins (Chaperonins , Hsp60 and CCT / TRiC) involved in human diseases.

[177] Moores B, Drolle E, Attwood SJ, Simons J, Leonenko Z (2011) Effect of surfaces on amyloid fibril formation. *PLoS One* **6**, 1–8.

[178] Wang Z, Zhou C, Wang C, Wan L, Fang X, Bai C (2003) AFM and STM study of β -amyloid aggregation on graphite. *Ultramicroscopy* **97**, 73–79.

[179] Pfister G, Stroh CM, Perschinka H, Kind M, Knoflach M, Hinterdorfer P, Wick G (2005) Detection of HSP60 on the membrane surface of stressed human endothelial cells by atomic force and confocal microscopy. *J. Cell Sci.* **118**, 1587–1594.

[180] Ricci C, Ortore MG, Vilasi S, Carrotta R, Mangione MR, Bulone D, Librizzi F, Spinozzi F, Burgio G, Amenitsch H, San Biagio PL (2016) Stability and disassembly properties of human naïve Hsp60 and bacterial GroEL chaperonins. *Biophys. Chem.* **208**, 68–75.

[181] Itoh H, Kobayashi R, Wakui H, Komatsuda A, Ohtani H, Miura AB, Otaka M, Masamune O, Andoh H, Koyama K, Sato Y, Tashima Y (1995) Mammalian 60-kDa stress protein (chaperonin homolog): Identification, biochemical properties, and localization. *J. Biol. Chem.* **270**, 13429–13435.

[182] Saibil H (2013) Chaperone machines for protein folding, unfolding and

disaggregation. *Nat. Rev. Mol. Cell Biol.* **14**, 630–642.

[183] Welzel AT, Maggio JE, Shankar GM, Walker DE, Ostaszewski BL, Li S, Klyubin I, Rowan MJ, Seubert P, Walsh DM, Selkoe DJ (2014) Secreted amyloid β-proteins in a cell culture model include N-terminally extended peptides that impair synaptic plasticity. *Biochemistry* **53**, 3908–3921.

[184] Walsh DM, Klyubin I, Fadeeva J V., Cullen WK, Anwyl R, Wolfe MS, Rowan MJ, Selkoe DJ (2002) Naturally secreted oligomers of amyloid β protein potently inhibit hippocampal long-term potentiation in vivo. *Nature* **416**, 535–539.

[185] Kittelberger KA, Piazza F, Tesco G, Reijmers LG (2012) Natural amyloid-beta oligomers acutely impair the formation of a contextual fear memory in mice. *PLoS One* **7**, 1–7.

[186] Life technologies, Lipofectamine® 2000 Reagent, Last updated 2013, Accessed on 2013.

[187] Meli G, Lecci A, Manca A, Krako N, Albertini V, Benussi L, Ghidoni R, Cattaneo A (2014) Conformational targeting of intracellular A' 2 oligomers demonstrates their pathological oligomerization inside the endoplasmic reticulum. *Nat. Commun.* **5**, 1–17.

[188] Thermo fisher (2013) PierceTM BCA Protein Assay Kit. **0747**, 1–7.

[189] Scientific T (2007) BCA TM Protein Assay Kit. *BCA Protein Assay Kit*.

[190] Capello F, Conaway de Macario E, Marasa L, Zummo G, J.L. Macario A (2008) Hsp60 expression, new locations, funcitons, and perspectives for cancer diagnosis and therapy. *Cancer Biol. Ther.* **7**, 801–809.

[191] Reese LC, Laezza F, Woltjer R, Taglialatela G (2011) Dysregulated

phosphorylation of Ca2+/calmodulin-dependent protein kinase II-α in the hippocampus of subjects with mild cognitive impairment and Alzheimer's disease. *J. Neurochem.* **119**, 791–804.

[192] Lambert MP, Velasco PT, Chang L, Viola KL, Fernandez S, Lacor PN, Khuon D, Gong Y, Bigio EH, Shaw P, De Felice FG, Krafft GA, Klein WL (2007) Monoclonal antibodies that target pathological assemblies of Aβ. *J. Neurochem.*

[193] Tillement L, Lecanu L, Papadopoulos V (2011) Alzheimer's disease: Effects of β-amyloid on mitochondria. *Mitochondrion*.

[194] Townsend M, Shankar GM, Mehta T, Walsh DM, Selkoe DJ (2006) Effects of secreted oligomers of amyloid β-protein on hippocampal synaptic plasticity: A potent role for trimers. *J. Physiol.* **572**, 477–492.

[195] Mangione MR, Vilasi S, Marino C, Librizzi F, Canale C, Spigolon D, Bucchieri F, Fucarino A, Passantino R, Cappello F, Bulone D, San Biagio PL (2016) Hsp60, amateur chaperone in amyloid-beta fibrillogenesis. *Biochim. Biophys. Acta - Gen. Subj.* **1860**,.

[196] Lo Cascio F, Kayed R (2018) Azure C Targets and Modulates Toxic Tau Oligomers. *ACS Chem. Neurosci.* **9**, 1317–1326.

[197] Thermo-Scientific (2016) Pierce LDH Cytotoxicity Assay Kit. *User's Guid.*

[198] Comerota MM, Krishnan B, Taglialatela G (2017) Near infrared light decreases synaptic vulnerability to amyloid beta oligomers. *Sci. Rep.* **7**, 1–11.

[199] Reese LC, Zhang W, Dineley KT, Kayed R, Taglialatela G (2008) SELECTIVE INDUCTION OF CALCINEURIN ACTIVITY AND SIGNALING BY OLIGOMERIC AMYLOID BETA. *Aging Cell* **7**, 824–835.

[200] Krishnan B, Kayed R, Taglialatela G (2018) Elevated phospholipase D isoform 1 in Alzheimer's disease patients' hippocampus: Relevance to synaptic dysfunction and memory deficits. *Alzheimer's Dement. Transl. Res. Clin. Interv.* **4**, 89–102.

[201] Bao F, Wicklund L, Lacor PN, Klein WL, Nordberg A, Marutle A (2012) Different β-amyloid oligomer assemblies in Alzheimer brains correlate with age of disease onset and impaired cholinergic activity. *Neurobiol. Aging* **33**, 825.e1-825.e13.

[202] Liu P, Paulson JB, Forster CL, Shapiro SL, Ashe KH, Zahs KR (2015) Characterization of a Novel Mouse Model of Alzheimer's Disease—Amyloid Pathology and Unique β-Amyloid Oligomer Profile. *PLoS One* **10**, e0126317.

[203] Hatami A, Albay R, Monjazeb S, Milton S, Glabe C (2014) Monoclonal antibodies against Aβ42 fibrils distinguish multiple aggregation state polymorphisms in vitro and in Alzheimer disease brain. *J. Biol. Chem.* **289**, 32131–32143.

[204] Sakono M, Zako T, Yohda M, Maeda M (2012) Amyloid oligomer detection by immobilized molecular chaperone. *Biochem. Eng. J.* **61**, 28–33.

[205] Prangkio P, Yusko EC, Sept D, Yang J, Mayer M (2012) Multivariate Analyses of Amyloid-Beta Oligomer Populations Indicate a Connection between Pore Formation and Cytotoxicity. *PLoS One* **7**,.

[206] Kayed R, Pensalfini A, Margol L, Sokolov Y, Sarsoza F, Head E, Hall J, Glabe C (2009) Annular protofibrils area structurally and functionally distinct type of amyloid oligomer. *J. Biol. Chem.* **284**, 4230–4237.

[207] Kim JH, Anwyl R, Suh YH, Djamgoz MB, Rowan MJ (2001) Use-dependent effects of amyloidogenic fragments of (beta)-amyloid precursor protein on

synaptic plasticity in rat hippocampus in vivo. *J. Neurosci.* **21**, 1327–33.

[208] Lambert MP, Barlow AK, Chromy BA, Edwards C, Freed R, Liosatos M, Morgan TE, Rozovsky I, Trommer B, Viola KL, Wals P, Zhang C, Finch CE, Krafft GA, Klein WL (1998) Diffusible, nonfibrillar ligands derived from A 1-42 are potent central nervous system neurotoxins. *Proc. Natl. Acad. Sci.* **95**, 6448–6453.

[209] Repalli J, Meruelo D (2015) Screening strategies to identify HSP70 modulators to treat Alzheimer's disease. *Drug Des. Devel. Ther.* **9**, 321–331.

[210] Lackie RE, Maciejewski A, Ostapchenko VG, Marques-Lopes J, Choy WY, Duennwald ML, Prado VF, Prado MAM (2017) The Hsp70/Hsp90 chaperone machinery in neurodegenerative diseases. *Front. Neurosci.* **11**, 1–23.

[211] Saidi LJ, Polydoro M, Kay KR, Sanchez L, Mandelkow EM, Hyman BT, Spires-Jones TL (2015) Carboxy terminus heat shock protein 70 interacting protein reduces tau-associated degenerative changes. *J. Alzheimer's Dis.* **44**, 937–947.

[212] Fändrich M, Schmidt M, Grigorieff N (2011) Recent progress in understanding Alzheimer's β-amyloid structures. *Trends Biochem. Sci.*

[213] Cortez L, Sim V (2014) The therapeutic potential of chemical chaperones in protein folding diseases. *Prion* **8**, 1–6.

[214] Tanaka M, Machida Y, Niu S, Ikeda T, Jana NR, Doi H, Kurosawa M, Nekooki M, Nukina N (2004) Trehalose alleviates polyglutamine-mediated pathology in a mouse model of Huntington disease. *Nat. Med.*

[215] Cox D, Selig E, Griffin MDW, Carver JA, Ecroyd H (2016) Small Heat-shock Proteins Prevent α-synuclein aggregation via transient interactions and their efficacy is affected by the rate of aggregation. *J. Biol. Chem.*

[216] Mattoo RUH, Goloubinoff P (2014) Molecular chaperones are nanomachines that catalytically unfold misfolded and alternatively folded proteins. *Cell. Mol. Life Sci.* **71**, 3311–3325.

[217] Fitzjohn SM, Kuenzi F, Morton RA, Rosahl TW, Lewis H, Smith D, Seabrook GR, Collingridge GL (2010) A study of long-term potentiation in transgenic mice over-expressing mutant forms of both amyloid precursor protein and presenilin-1. *Mol. Brain* **3**,.

[218] Lacor PN (2004) Synaptic Targeting by Alzheimer's-Related Amyloid   Oligomers. *J. Neurosci.* **24**, 10191–10200.

[219] Hocquemiller M, Giersch L, Audrain M, Parker S, Cartier N (2016) Adeno-Associated Virus-Based Gene Therapy for CNS Diseases. *Hum. Gene Ther.* **27**, 478–496.

[220] Otaka M, Tamaki K, Shibuya T, Sakamoto N, Yamamoto S, Odashima M, Itoh H, Watanabe S (2012) Traditional herbal medicine, Rikkunshito, induces HSP60 and enhances cytoprotection of small intestinal mucosal cells as a nontoxic chaperone inducer. *Evidence-based Complement. Altern. Med.* **2012**,.

Curriculum Vita

Claudia Marino   Date: 02/24/2019

PRESENT POSITION AND ADDRESS:

Pre-doctoral fellow
University of Texas Medical Branch at Galveston
Department of Neuroscience, Cell Biology & Anatomy (NCBA)
10.148 Medical Research Building
301 University Blvd.
Galveston, TX 77555-1045
Email: clmarino@utmb.edu

BIOGRAPHICAL:

Birth and place: 10/02/86, Palermo IT
Citizenship: Italian
Home Address: 515, 1st Street, Casa Caribe, Apt 347.
Galveston, TX 77550
Phone: (409) 443-9986

EDUCATION:

09/2014 to present   ***Ph.D. Neuroscience   (GPA 4/4)***
Neuroscience Graduate Program
(Combined Program with the University of Palermo, IT)
Department of Neurology, UTMB
Mentor: Dr. Giulio Taglialatela

01/2014- 03/2017   ***Ph.D. Neuroscience (100/100)***
Department of Experimental Biomedicine and Clinical
Neuroscience
University of Palermo, Italy
Advisors: Dr. Giulio Taglialatela (UTMB), Dr. Giovanni Zummo
and Dr. Pier Luigi San Biagio (Biophysics Institute, CNR, IT)

11/2004-03/2013   ***Master of Science in Pharmacy, Cum Laude***
Dipartimento di Scienze e Tecnologie Biologiche, Chimiche e
Farmaceutiche "STEBICEF"
University of Palermo, Italy

Advisors: Dr. Silvestre Buscemi, Dr. Antonio Palumbo Piccionello and Dr. Maria R. Mangione (Biophysics Institute, CNR, IT)

CERTIFICATIONS:

06/2013 to present   Licensed to practice as a Pharmacist in Italy, Palermo, IT

09/2014 to present   Certified in Biosafety Level 2 (BSL2) and animal biosafety level 1 (ABSL1), UTMB, TX

PROFESSIONAL AND TEACHING EXPERIENCE:

Professional:

01/2014 to present   **Graduate Assistant**. University of Texas Medical Branch at Galveston, Department of Neurology & University of Palermo, BioNec Department, Palermo (IT). Project:" Molecular interaction between Amyloid Beta Peptide: Relevance to Alzheimer's Disease". <u>Collaboration:</u> Biophysics Institute, National Research Council. Palermo (IT).
<u>Mentors</u>: Dr. Giulio Taglialatela, Dr. Pier Luigi San Biagio and Dr. Giovanni Zummo.

09/2013- 12/ 2013   **Undergraduate fellow**. Biophysics Institute, National Research Council, Palermo (IT). Qualitative and quantitative analysis of biological samples (HPLC, SPME-GC-MS, Gel Electrophoresis and Western Blot); chemical and physical analysis with spectroscopic techniques, headspace analysis with electronic nose; preparation of biological samples and organic compounds extraction from food matrices. <u>Supervisors</u>: Dr. Pier Luigi San Biagio and Dr. Maria R. Mangione.

04/2013 – 08/2013   **Volunteer Training**. Biophysics Institute, National Research Council, Palermo (IT). Spectroscopic analysis of proteins; qualitative analysis of aggregation kinetics of proteins with probes (ThT essay) and Circular Dichroism; HPLC and SDS-PAGE analysis of proteins (Aβ1-40, BSA). <u>Supervisors</u>: Dr. Pier Luigi San Biagio and Dr. Maria R. Mangione.

09/2011- 03/2013   **Research Assistant.** Master's Degree thesis:" Synthesis and interaction between fluorinated oxadiazols and amyloid beta peptide". University of Palermo, Department of Science, Biological, Chemical and Pharmaceutical Techniques (Stebicef). Palermo, Italy. <u>Mentors:</u> Dr. Silvestre Buscemi, Dr. Antonio Palumbo Piccionello and Dr. Maria R. Mangione. <u>Collaboration:</u> Biophysics Institute, National Research Council. Palermo, Italy.

RESEARCH SUPPORT
10/01/2017-08/31/18 Jeane B. Kempner Scholarship
11/2015-10/2016   Zelda Zinn Casper Endowed Scholarship

TEACHING RESPONSIBILITIES
Teaching Experience:

01/12/18-04/13/18   Small group facilitator. Teaching in Molecular biology and Genetics class. The University of Texas Medical Branch, Galveston Texas.

03/09/16-04/29/16   Laboratory Teaching Assistant. Neuroscience of Human Behavior, medical school class. The University of Texas Medical Branch, Galveston Texas.

Training and Supervision of Undergraduate, Graduate and Medical Students
06/2018-08/2018   Mentoring research activity of Julie Capece during the Neuroscience Summer Undergraduate Research program (NSURP).
04/2013- 06/2013   Mentoring research activity of Union College students (Schenectady – NY 12308) during a research activity period in biophysics studies. National Research Council, IBF UOS Palermo, Italy. Student: Rebekah Williams and Taera Kim.

Technical Skills and Experience:

Biophysics/Chemistry: Circular Dichroism, UV-VIS spectroscopy, Chromatography (TLC, HPLC, LC, GC/MS), organic synthesis, liquid/liquid separation, protein purification, conformation and aggregation assays (ThT, proteinase K, bis-ANS).

Molecular biology: ELISA, LDH, MTS, BCA assays, Western blotting, SDS-PAGE electrophoresis, cell culture, plasmid transfection, immunocytochemistry, IP, immunofluorescence, confocal imaging, animal behavior, mouse handling and brain dissections, ex-vivo electrophysiology (field recordings).

Computer skills: Office, GraphPad, ImageJ, GIMP, MSGRACE. Operative Systems used: Linux (Fedora, Ubuntu), Windows, MacOS.

MEMBERSHIPS IN SCIENTIFIC SOCIETIES:

International:

05/2014 to present	Student Member, Society for Neuroscience
09/2016 to present	Sigma Xi, UTMB chapter

Local:

09/2017 to present	Honored member of The National Society of Leadership and Success
09/2014 to present	Student Member, Society for Neuroscience Galveston Chapter

HONORS AND AWARDS:

12/2018	Recipient of James E. Beall Memorial Award.
10/2018	Excellence in Student Research for Basic Science and Neuroscience Research category, 22nd Annual Forum on Aging. The University of Texas Medical Branch. Galveston, TX.
07/2018	Recipient of the award "Neurodegeneration and Disease", 3rd Annual Neuroscience Graduate Program Student Symposium. The University of Texas Medical Branch.
11/2017	Recipient of James E. Beall Memorial Award.
09/2017	Recipient of Jeane B. Kempner Scholarship.
06/2017	Recipient of Best Overall Oral Presentation Award, 2nd Annual Neuroscience Graduate Program Student Symposium. The University of Texas Medical Branch. Galveston, TX.
06/2017	Recipient of Student's Choice Award, 2nd Annual Neuroscience Graduate Program Student Symposium. Galveston, TX.
12/2016	Recipient of Dennis Bowman Memorial Scholarship, The University of Texas Medical Branch. Galveston, TX.
10/2016	Excellence in Student Research for Neuroscience, 20th Annual Forum on Aging. The University of Texas Medical Branch. Galveston, TX.
06/2016	Chair of the "Third Year Graduate Students" session of the Neuroscience Graduate Student Symposium. Galveston, TX.
06/2016	Best Oral Presentation: Second Year, The University of Texas Medical Branch, Neuroscience Graduate Program Symposium. Galveston, TX.
06/2016	Service Excellence Award, The University of Texas Medical Branch, Neuroscience Graduate Program Symposium. Galveston, TX.
04/2016	Excellence in Translational Science Award, 57th Annual National Student Research Forum. Galveston, TX.
02/2016	Chair of the "Bioscience" session of the XI Conference of Italian Researchers in the world, Houston, TX.
11/2015	Recipient of Zelda Zinn Casper Endowed Scholarship.
11/2015	Recipient of Arthur V. Simmang Scholarship Fund.
11/2014	Excellence in Student Research for Neuroscience, 18th Annual Forum on Aging, The University of Texas Medical Branch at Galveston. Galveston, TX.

COMMUNITY SERVICE AND ACTIVITIES:

04/10/2018	Volunteer at Brain fair organized by SfN, Galveston Chapter, UTMB
09/2017	Volunteer for the Rugby relief organization created to help after Harvey Hurricane
10/12/2016	Volunteer at Brain fair organized by SfN, Galveston Chapter, UTMB
09/2016 to 08/2017	President, Neuroscience Student Organization, UTMB
09/2015 -08/2016	Vice President (same as student representative), Neuroscience Graduate Program club, UTMB
08/2014 to present	Student Member, UTMB Neuroscience Graduate Program Club

BIBLIOGRAPHY:
Publications

1. *Submitted*. **Marino C**., et al. (2019) Hsp60 protects against Amyloid β oligomer synaptic toxicity via modification of toxic oligomer conformation. ACS Chem. Neurosci.
2. *Submitted*. Caruso Bavisotto C., Scalia F., Pitruzzella A., Górska-Ponikowska M., **Marino C**., et al. (2018) Hsp60 in modifications of nervous system homeostasis and neurodegeneration. Heat Shock Proteins, Springer Ed.
3. Mangione MR, Vilasi S, **Marino C.**, et al. (2016) Hsp60, amateur chaperon in amyloid-beta fibrillogenesis. BBA- General subjects 1860 (11): 2474-2483.
4. Mangione MR, Palumbo Piccionello A., **Marino C.** et al. (2015) Photo-inhibition of Aβ fibrillation mediated by a newly designed fluorinated oxadiazole. *RSC Adv.*, **5,** 16540-16548.

Abstracts:

1. February 2019 - "Modulation of neurotoxic amyloid beta oligomers: A role for Hsp60." Marino C. et al. Meeting: South Texas Alzheimer's Conference San Antonio, TX.
2. November 2018 - "Modulation of neurotoxic amyloid beta oligomers: A role for Hsp60." **Marino C.** et al. Meeting: CSSI 2018. Alexandria. Virginia.
3. November 2018 – "Modulation of neurotoxic amyloid beta oligomers: A role for Hsp60." **Marino C.** et al. Meeting: Neuroscience 2018. San Diego. California.
4. October 2018- "Modulation of neurotoxic amyloid beta oligomers: A role for Hsp60." **Marino C.** et al. Meeting: 22nd Annual forum on Aging, Galveston. Texas.
5. December 2017 – "The role of Hsp60 in amyloid beta toxicity: Relevance to Alzheimer's disease**. Marino C.** et al." Meeting: NCBA Annual Retreat. Galveston. Texas.
6. April 2017 - "APP/Aβ- Hsp60 functional interaction: Relevance to Alzheimer's Disease. **Marino C.** et al". Meeting: Meeting: 58th Annual National Student Research Forum. Galveston, Texas.

7. March 2017- **-** "APP/Aβ- Hsp60 functional interaction: Relevance to Alzheimer's Disease. **Marino C.**, et al". Meeting: Galveston Symposium on Alzheimer's Disease and Related Disorders: Basic, Translational & Clinical advances. Galveston. Texas.

8. December 2016 **-** "APP/Aβ- Hsp60 functional interaction: Relevance to Alzheimer's Disease. **Marino C.**, et al". Meeting: 20th Annual Forum on Aging. The University of Texas Medical Branch.

9. November 2016 - "APP/Aβ - Hsp60 functional interaction: Relevance to Alzheimer's Disease. **Marino C.**, et al". Meeting: Society for Neuroscience 46th Annual Meeting. San Diego, California.

10. April 2016– "Hsp60 as a protective factor against amyloid beta misfolding. **Marino C.**, et al". Meeting: 57th Annual National Student Research Forum. Galveston, Texas.

11. March 2016 – "Hsp60 as a protective factor against amyloid beta misfolding. **Marino C.**, et al". Meeting: The 2016 Clinical & Translational Research Forum. UTMB Galveston, Texas.

12. February 2016 – "Hsp60 as a protective factor against amyloid beta misfolding. **Marino C.**, et al". Meeting: XI Conference of Italian Researchers in the World, Houston, Texas.

13. October 2015 – "Hsp60 as a protective factor against amyloid beta misfolding. **Marino C.**, et al". Meeting: 19th Annual Forum on Aging. UTMB Galveston, Texas.

14. October 2015 – "Hsp60 as a protective factor against amyloid beta misfolding". **Marino C.**, et al.". Meeting: Neuroscience 2015. Chicago, Illinois.

15. September 2015 – "Hsp60 as a protective factor against amyloid Beta misfolding. **Marino, C**. et al". Meeting: The 9th Annual Research Symposium on Alzheimer's Disease & Related Dementias. Houston (TX).

16. April 2015 – "Hsp60 as a novel inhibitor of amyloid beta misfolding. **Marino C.**, et al.". Meeting: National Student Research Forum. 56th Annual Meeting. Galveston, Texas.

17. February 2015 – "Hsp60 as a novel inhibitor of amyloid beta misfolding. **Marino C.**, et al.". Meeting: 59th Annual Meeting of Biophysical Society. Baltimore, Maryland.

18. December 2014 – "The inhibitory effect of hsp60 on amyloid beta aggregation: a biophysical study. **Marino C**. et al. Meeting: 19th Annual Forum on Aging, UTMB. Galveston, Texas.

19. September 2014 – "Hsp60 effect on the Aβ amyloid peptide fibrillogenesis. Mangione M.R., **Marino C.**, et al.". Meeting: XXII Congresso Nazionale SIBPA. Palermo, Italy.

20. November 2014 – "The inhibitory effect of hsp60 on amyloid beta aggregation: a biophysical study. **Marino C**. et al. Meeting: Neuroscience 2014. Washington DC.

21. July 2014 - "Effect of chaperones with intrinsically disordered regions (IDRs) on the fibrillogenesis of Aβ amyloid peptide. Vilasi S., Mangione M.R., Passantino R., **Marino C**. et al. (2014)" Meeting: The 2014 Gordon Conference on Intrinsically Disordered Proteins. Easton, MA.

22. May 2014 - "Synthesis of a new 1,2,4-oxadiazole and evaluation of its ability to inhibits

abeta-peptide aaggregation. **Marino C**. et al. Meeting: 29th International Conference of ADI, San Juan.

23. June 27th -28th, 2013 - "Studi biofisici dell'interazione di ossadiazoli fluorurati col peptide Beta Amiloide. **Marino C**. et al." Meeting: "Biotecnologie: ricerca di base, interdisciplinare, traslazionale in ambito biomedico". Palermo, Italy.

Permanent address: 515 1st. Street, Apt.347, 77550 Galveston, TX (USA)

This dissertation was typed by Claudia Marino.